TRANSPORTATION RESEARCH RECORD 871

Segmental and System Bridge Construction; Concrete Box Girder and Steel Design

TRANSPORTATION RESEARCH BOARD

NATIONAL RESEARCH COUNCIL

NATIONAL ACADEMY OF SCIENCES
WASHINGTON, D.C. 1982

Transportation Research Record 871
Price $11.40
Edited for TRB by Scott C. Herman

modes
1 highway transportation
2 public transit
3 rail transportation

subject areas
25 structures design and performance
33 construction

Library of Congress Cataloging in Publication Data
National Research Council. Transportation Research Board.
Segmental and system bridge construction–concrete box girder and steel design.

(Transportation research record; 871)
Reports presented at the 61st annual meeting of the Transportation Research Board.
1. Bridges, Concrete–Design and construction–Addresses, essays, lectures. 2. Bridges, Iron and steel–Design and construction–Addresses, essays, lectures. I. National Research Council (U.S.). Transportation Research Board. II. Series.
TE7.H5 no. 871 [TG335] 380.5s [624'.4] 83-2218
ISBN 0-309-03400-0 ISSN 0361-1981

Sponsorship of the Papers in This Transportation Research Record

GROUP 2–DESIGN AND CONSTRUCTION OF TRANSPORTATION FACILITIES
R.V. LeClerc, consultant, Olympia, Washington, chairman

Structures Section
LeRoy T. Oehler, Michigan Department of Transportation, chairman

Committee on General Structures
Heinz P. Koretsky, Pennsylvania Department of Transportation, chairman
John M. Kulicki, Modjeski & Masters, secretary
Dan S. Bechly, Neal H. Bettigole, William E. Brakensiek, Martin P. Burke, Jr., Paul F. Csagoly, Jack H. Emanuel, Dah Fwu Fine, Donald J. Flemming, G.G. Goble, J. Leroy Hulsey, William A. Kline, Celal N. Kostem, John M. Kruegler, Clellon Lewis Loveall, Richard M. McClure, Marianne Mueller, Gordon R. Pennington, Charles G. Schilling, Arun Shirole, Wendell M. Smith, Marcello H. Soto, Robert F. Victor

Committee on Concrete Bridges
John M. Hanson, Wiss, Janney & Elstner & Associates, chairman
T. Alberdi, Jr., Craig A. Ballinger, Robert C. Cassano, W. Gene Corley, C.S. Gloyd, James J. Hill, Ti Huang, Cornie L. Hulsbos, Roy A. Imbsen, Hubert Janssen, Heinz P. Koretzky, H.G. Kriegel, John M. Kulicki, R. Shankar Nair, Edward G. Nawy, Walter Podolny, Jr., Adrianus VanKampen, Julius F.J. Volgyi, Jr., Donald J. Ward, W. Jack Wilkes

Construction Section
David S. Gedney, DeLeuw Cather & Company, chairman

Committee on Construction of Bridges and Structures
Robert M. Barnoff, Pennsylvania State University, chairman
John K. Bright, D. Stephen Brown, Thomas H. Ellis, George A. Harper, Wayne Henneberger, Marvin H. Hilton, Frank J. Kempf, Andrew Lally, John P. Rutter, William H. Shaw, Sydney W. Smith, Michael M. Sprinkel, Man-Chung Tang, J.R. Wilder, Thomas G. Williamson, Kenneth C. Wilson

William G. Gunderman and Lawrence F. Spaine, Transportation Research Board staff

Sponsorship is indicated by a footnote at the end of each report. The organizational units, officers, and members are as of December 31, 1981.

Contents

Authors of the Papers in This Record

Albrecht, Pedro, Department of Civil Engineering, University of Maryland, College Park, MD 20742

Beal, David B., Engineering Research and Development Bureau, New York State Department of Transportation, 1220 Washington Avenue, State Campus, Albany, NY 12232

Bell, G. Duane, Highway and Treated Wood Products Division, Wheeler Division, St. Regis Paper Company, P.O. Box 26499, 3340 Republic Avenue, St. Louis Park, MN 55426

Bon, Vu Dinh, California Department of Transportation, 1120 N Street, Sacramento, CA 95814

Bouwkamp, Jack G., Department of Civil Engineering, University of California, Berkeley, Berkeley, CA 94720

Davis, Raymond E., California Department of Transportation, 1120 N Street, Sacramento, CA 95814

FitzSimons, Neal, Engineering Counsel, 10408 Montgomery Avenue, Kensington, MD 20895

Gamble, William L., Civil Engineering Department, University of Illinois, 2209 Civil Engineering Building, 208 North Romine Street, Urbana, IL 61801

Hays, Clifford O., Jr., Department of Civil Engineering, University of Florida, Gainesville, FL 32611

Hill, James J., Minnesota Department of Transportation, Transportation Building, St. Paul, MN 55155

Lin, T.Y., T.Y. Lin International, 315 Bay Street, San Francisco, CA 94133

Lo, George K., T.Y. Lin International, 315 Bay Street, San Francisco, CA 94133

Lybas, John M., Department of Civil Engineering, University of Florida, Gainesville, FL 32611

Marshall, Vernon L., Civil Engineering Department, University of Illinois, 2209 Civil Engineering Building, 208 North Romine Street, Urbana, IL 61801

Olson, Kenneth A., Highway and Treated Wood Products Division, Wheeler Division, St. Regis Paper Company, P.O. Box 26499, 3340 Republic Avenue, St. Louis Park, MN 55426

Redfield, Charles, T.Y. Lin International, 315 Bay Street, San Francisco, CA 94133

Russell, Henry G., Structural Development Department, Construction Technology Laboratories, Portland Cement Association, 5420 Old Orchard Road, Skokie, IL 60077

Scholer, Charles F., School of Civil Engineering, Purdue University, West Lafayette, IN 47907

Scordelis, Alex C., Department of Civil Engineering, University of California, Berkeley, Berkeley, CA 94720

Seible, Frieder, Department of Civil Engineering, University of California, Berkeley, Berkeley, CA 94720

Seim, Chuck, T.Y. Lin International, 315 Bay Street, San Francisco, CA 94133

Semans, Frank M., California Department of Transportation, 1120 N Street, Sacramento, CA 95814

Shirole′, Arunprakash M., Department of Public Works, 203 City Hall, Minneapolis, MN 55415

Shiu, Kwok-Nam, Structural Experimental Section, Construction Technology Laboratories, Portland Cement Association, 5420 Old Orchard Road, Skokie, IL 60077

Slavis, Charles, Portland Cement Association, 5420 Old Orchard Road, Skokie, IL 60077

Tai, James C., T.Y. Lin International, 315 Bay Street, San Francisco, CA 94133

Tang, Man-Chung, DRC Consultants, Inc., 500 Fifth Avenue, New York, NY 10036

Wasti, S. Tanvir, Department of Civil Engineering, Middle East Technical University, Ankara, Turkey

I-205 Over Columbia River Bridge: Geometric Control for Cast-in-Place and Precast Segmental Box-Girder Construction

JAMES C. TAI AND GEORGE K. LO

Precast or cast-in-place segmental cantilevered construction forms a relatively new generation in U.S. bridge construction. One of the largest-scale projects of this kind is the I-205 Columbia River Bridge in Portland, Oregon, which was started in 1979 and is due for completion in 1982. The project consists of two parallel bridges, each 75 ft wide. Its final contract for the main superstructure (length of 5770 ft) was awarded to a joint venture of S. J. Groves and Guy F. Atkinson. Responding to the Oregon Department of Transportation's policy of value engineering, the longer 480-, 600-, and 480-ft spans were changed from precast to in-place construction by using traveling wagons; the shorter 240-, 300-, and 360-ft spans remained precast. This unique setup afforded a special opportunity for comparing the two construction methods and for coordinating design and geometric control with construction. Included in this paper is an outline of geometric control for both cast-in-place and match-cast segments; methods for predicting deflections, which consider shrinkage and creep; and a brief description of computer programs for cantilevered construction. Also included are a description of the coordination between designer and field personnel in order to achieve quality and accuracy in construction, a comparison of actual constructed elevations with predicted elevations, and, finally, a discussion regarding implications for future segmental construction.

In cantilever construction, the structure usually undergoes two phases. During construction, cantilever arms progress outward, and segments are gradually added until the ends of the designed cantilevers are reached. For the final bridge, a continuous structure is achieved when the cantilever ends are either hinged or integrated into the cantilever construction from the adjacent pier (Figure 1).

Figure 1. Segmental construction.

During construction, the cantilevers are usually free from restraint at their cantilever ends and are fixed, or partly restrained, at their pier supports. Because this type of construction involves stage loading, which in turn involves time-dependent deflections and strain changes, camber control during the erecting or casting of the segments is absolutely essential for the successful completion of the structure.

Basically, determination of forces, stresses, and deflections of the cantilevers follows beam theory. Although the calculations themselves are fairly simple, their accuracy depends on the recognition of all influences that are responsible for the deflection of the structure. Especially important are inelastic strains, which must not be neglected.

This paper describes the methods used in simplified analyses of cantilever deflections. Correlation between calculated values and actual field measurements is also given.

ELASTIC AND PLASTIC DEFORMATION CHARACTERISTICS OF BRIDGES

Cantilever construction of segmental bridges progresses along a predetermined pattern, which recognizes the stages of the contruction or erection of the segments comprising the cantilever. Typically, the construction cycle will vary from three to seven days per segment, depending on field conditions. After all the segments are in place, the ends of opposing cantilevers are joined and the bridge structure becomes continuous.

The deflections of the cantilever during the various stages of construction and the deflections of the final structure are affected by the following conditions:

1. Cantilevered structure: dead load of segments, weight of traveler or hoist, weight of form and construction equipment, prestressing forces, and pier deflections due to unbalanced loading; and
2. Final structure: dead load of the connecting segment; removal of traveler or hoist; closure pour form; prestressing forces; topping, railing, curbs, and utilities; and removal of shoring, temporary supports, etc.

Cantilevered Structure

Cantilevered structures should take into account the following conditions:

1. Dead load: The dead weight on the bridge is the most significant item that produces deflection. If the bridge was left to deflect without compensating prestressing forces, it would be difficult to control its deflection and associated stresses during and after construction. Hence, posttensioning is essential and must be fully used.

2. Traveler: In cast-in-place segmental cantilever construction, a new segment is cantilevered from the previously constructed segment; hence, special travelers with movable forms that cantilever out to support the new segment are required. The effect of their weight must be considered. For precast segmental construction, hoisting equipment for lifting new segments is required, and its weight must be considered in the deflection of the precast cantilever structure. A common traveler weighs 90-135 tons (including forms) and a hoist weighs approximately 35 tons.

3. Form and construction load: Weights of steel or wood forms and a working platform must be included for cast-in-place construction. In precast segmental construction, a working platform attached to the hoisting equipment will be required because it will affect the deflection.

4. Posttensioning: In the longitudinal direction (along the top flange), posttensioning will counteract the dead-load deflection to a great extent. It is not economically feasible to supply enough posttensioning to totally offset the dead-load deflection for a long span cantilever. Generally, about 70-80 percent of the dead-load deflection will be counteracted by incremental posttensioning forces in the first half of the cantilever and about 50 percent in the last half. This leaves the dead load not assumed by posttensioning to deflect the cantilever downward. Because the posttensioning forces will gradually relax, the loss of prestress must also be taken into account, as it will produce a further deflection of the cantilever. Such losses are well known for both normal weight or lightweight construction and can be predicted successfully in the computation of deflections.

5. Pier deflection: Because the bridge is connected to its vertical supporting member or pier, the deflection due to pier deformation (both axial and rotation) may affect the cantilever end appreciably. An appropriate adjustment is required in cast-in-place construction, especially for long, slender piers.

6. Foundation rotation: Sometimes, cantilever construction is built with unbalanced segments at the two sides. This produces a certain degree of rotation at the pier and its foundation, and the ensuing angle change at the foundation and pier head may induce an appreciable amount of deflection at the cantilever ends. This effect is significant, particularly in cast-in-place construction and in elevations where the setting of forms must be adjusted.

Continuous Framed Structure

Continuous framed structures should take into account the following conditions:

1. Dead load: The dead weight of the connecting segment is shared by the two adjacent cantilevers before its hardening. The deflection due to this closure pour and the related forms must be determined and included in the camber design.

2. Travelers: Travelers are usually removed prior to the closure pour. The upward deflection that results from the removal of the weight has to be considered.

3. Forms and bracing: The deflection due to the weight of forms and the action of the bracing system that distributes the weight toward each end of the cantilever must be a part of the deflection computation.

4. Topping, railing, curb, and utilities: Topping, railing, curb, and utilities must be accounted for in the deflection calculations. The construction schedule for the above must be predetermined for purposes of camber calculations, since it will make a substantial difference whether or not these loads are applied after the bridge becomes a continuous frame.

5. Removal of shoring and supports: The deflections due to removal of the shoring, temporary supports, etc., will affect the bridge deflections and stresses. Staged removal or removal at the final stage is to be decided before the camber design and precast work can be planned.

MAGNITUDE OF DEFLECTIONS

The magnitude of the deflection will be influenced by the following conditions:

1. Cantilevered structure: free cantilever system, sectional properties, modulus of elasticity, prestressing losses, concrete creep and shrinkage, and loading cycle and loading age; and

2. Final continuous framed structure: continuous framed system, closure sectional property, modulus of elasticity, prestressing losses, creep and shrinkage, and ratio of dead load to prestressing balancing forces.

Cantilevered Structure

Cantilevered structure deflections are influenced by the following properties:

1. System: The cantilever is built in the earlier stage of bridge construction by using segmental cantilever techniques before the adjacent cantilevers are linked with either a hinge or an integrated closure, which will then form a continuous framed structure. As the result of the change in continuity, the deflection characteristics in the system prior to the connection are different from those in the connected system. Time dependency of load application is important. For example, the railing or curb loading may be added onto the bridge before or after the continuity pour in some precast segmental construction. Their deflections will be influenced by the system and the curing age of the concrete. The correspondent magnitude of the deflection will differ on the order of two to three times.

2. Sectional properties: The cross-sectional properties of the bridge superstructure--namely the moment of inertia of the section, its shear area, and torsional properties--will directly relate to its deflection. Proper span-depth ratios and dimensions for the bottom slab, which resist compression forces, are also essential to the performance and deflection characteristics of the structure. Sectional properties at the closure, either a hinge or integrated pour, will have an influence on the deflection behavior as well.

3. Modulus of elasticity: Because the modulus of elasticity for concrete varies with age, aggregate, and mix, its prediction must be verified with actual field conditions in order to make control of the camber possible. The approximate time-dependent function can be defined in accordance with recent research and committee recommendations. The 28-day concrete modulus of elasticity can be expressed by the American Concrete Institute (ACI) formula (in 8.5.1) for both lightweight and normal weight concrete:

$$Ec = W^{1.5} \cdot 33 \cdot \sqrt{f_c'} \quad (1)$$

4. Prestress losses: Tendon forces are subject

to losses due to creep and shrinkage of concrete, elastic shortening of successive stressing, and relaxation of steel. For a cantilever system, the prestressing losses will not only influence stresses but also the cantilever deflection. All of these are time-dependent variables and can be expressed as time-dependent logarithmic functions.

5. Creep: The proper ultimate creep factor must be assessed before initial prediction for construction camber design. The effect of creep (1,2) must be checked with measured deflections in actual creep testing in order to obtain correct camber elevations for construction. In the camber design of the I-205 Columbia River Bridge in Portland, Oregon, ultimate creep values of 2.0 and 1.5 were assumed for cast-in-place and precast construction, respectively.

6. Loading cycle and age of concrete: Because the creep patterns are affected by the age of the concrete at loading and the duration of the load, the segment cycle, which dominates the prestressing operation cycle, will influence the long-term deflection of the bridge. This will also affect the stress and strain redistribution after the system changes. In the I-205 Columbia River Bridge, a working cycle of seven days was considered for cast-in-place construction and a two-day cycle was considered for precast construction.

Continuous Framed Structure

For continuous framed structures, the following items are additional considerations to the items mentioned for cantilevered structures:

1. Modulus of elasticity: The change in the modulus of elasticity will not influence deflections in the final structure significantly; however, it will produce changes in strains and stresses in association with time change.

2. Prestressing losses: At this stage, losses of the prestress forces will not influence deflections significantly, since the sensitive point--the tip of the cantilever--has been changed from a free end to the point of a continuous frame.

3. Creep and shrinkage: As the structural system changes from a simple determinate structure to an indeterminate structure, the strains and stresses associated with concrete creep and shrinkage will cause some change and redistribution of the stresses in the continuous systems after the connection of the cantilevers. Although the resulting deflection change is relatively small, the stress change should not be neglected.

4. Ratio of dead load to prestress balancing forces: As the ratio of the dead-load force and prestress balancing force increases, the stress redistribution after the continuity pour will also be increased. Although stress redistribution is significant, the associated deflections are not due to structural continuity.

BASIC THEORY FOR DEFLECTION COMPUTATION

For cantilever construction, the deflection on the bridge is basically the problem of a determinate structure. Deflections can be determined by the use of the moment-area method:

$$\text{Delta} = \Sigma\,(M \cdot X)/(Ec \cdot I) \qquad (2)$$

where

Delta = deflection of the cantilever;
M = moment due to dead load, construction load, and prestressing balancing load;
X = distances at each referenced point;
Ec = time-dependent concrete modulus of elasticity; and
I = cantilever segmental section properties (moment of inertia).

For analyzing the deflections and stresses of continuous bridges, various computer programs that use finite-element or stiffness-matrix methods can be used. The equivalent method for determining the long-term effects in the final continuous structure can be found in several papers (1-5). In this paper, only the deflection due to the cantilever will be discussed, and a simplified camber design will be described.

Design Parameters

The following are design parameters for evaluating segmental deflections.

Variable Modulus of Elasticity

The modulus of elasticity of concrete is defined by formulas in ACI 318-77 as follows:

$$Ec = W^{1.5} \times 33 \times \sqrt{f'_c} \text{ at 28 days} \qquad (3)$$

Time-dependent Ec can be described by an expression that is linear in the log scale and represents time-dependent characteristics. The Ec value in old concrete can be on the order of 20-30 percent higher (6) than in its initial 28 days. Proper assumptions can be made to define a curve that represents time-dependent Ec values for use in the computer program.

Loss of Prestress Force

The moment-area method is dependent on bending moments of dead load, construction load, and prestress balancing forces. The dead and construction loads are not time-dependent quantities, but the prestress balancing force and its effects are a time-dependent quantity, as these forces are added in conjunction with additional segments. The prestressing forces also vary due to relaxation of steel, creep, and shrinkage in concrete. For simplicity in predicting prestressing losses in a structure with a 50-year lifespan, it may be assumed that 15 percent (on average) of the initial force will be lost. The expression can be described as follows:

$$Fs = Fsi\,[1 - 0.0352\,\text{Log}\,(t - 1)] \qquad (4)$$

where Fs is the steel stress at t days after initially being stressed to Fsi, Fsi is the initial prestressing steel stresses, and there is a log base of 10.

Creep of Concrete

Concrete creep characteristics can be determined through laboratory testing procedures and estimated from values recommended by the Prestressed Concrete Institute (2) and Post Tensioning Institute (1). The ratio of the ultimate creep strain to initial elastic strain is defined as the ultimate concrete creep factor Cu. Its value is influenced by environment, percentage of steel, concrete age, duration of loading, concrete mix and aggregate, method of curing used (7), etc. Laboratory test values (in accordance with ASTM C512) will vary from 1.5 to 3.5. However, taking into consideration all external effects, the Cu value may reduce to 1.25 or 2.5 in most bridge construction.

For example, let Cu = 2.5 in a 50-year structure. Assuming that it is loaded at seven days, the

following formula can be used for analysis:

$$Ct = 0.235 \times Cu \times \text{Log}(t + 1) \times [1 - 0.224 \times \text{Log}(T/7)] \quad (5)$$

where

Ct = creep coefficient at different time stages,
Cu = ultimate creep coefficient,
t = time after loading applied (days), and
T = days when load is applied (7 days < T < 1 year).

The above formula should be modified to best fit actual concrete properties for individual projects. The ultimate creep value Cu must be verified with actual test data.

Shrinkage of Concrete

Due to its axial deformation characteristic, shrinkage of the concrete will not significantly affect the deflections and stresses of the structure during the cantilever construction. It will, however, cause strain and stress changes in the later stages of the continuous structure. The axial deformations are restrained by supporting piers; thus, stress redistribution will be induced into the system.

The following formula (6) can be assumed for axial deformation of the concrete:

$$Esh = 12.5 \times 10^{-6} \times (90 - H) \quad (6)$$

where H is the relative humidity (in percent) and Esh is the shrinkage strain (use 0.0005 for H = 50). Furthermore, shrinkage will vary with time and will reach 100 percent at 50 years, as shown in the following formula:

$$(Esh)\,t = 12.5 \times 10^{-6} \times (90 - H) \times 0.235 \times \text{Log}(t + 1) \quad (7)$$

where t is time at the point of concern (in days).

Basic Deflection Formulas

For basic deflection formulas, let us assume the following:

1. At each segmental stage between each increment of loads and prestressing forces, the superposition method is applied (4). Concrete modulus of elasticity (Ec) changes with time.
2. For each increment, the section will have a curvature change due to the dead load and prestressing force. The expression can be written as follows:

$$\theta_t = \theta_{mt} + \theta_{pt} \quad (8)$$

where

θ_t = total curvature,
θ_{mt} = curvature that is induced by dead load and construction load, and
θ_{pt} = curvature that is induced by prestressing forces.

Thus,

$$\theta_{mt} = (1 + C_t) \times [M/(E_t \times 1)] \quad (9)$$

where C_t is the creep coefficient at different time stages. For θ_{pt}, the rate-of-creep method is used, i.e.,

$$\theta_{pt} = [(-P_i \times e)/(E_t \times 1)] + (P_i - P_t) \times [e/(E_t \times 1)] - [(P_i + P_t)/2] \times C_t \times [e/(E_t \times 1)] \quad (10)$$

where P_i is the initial prestressing forces and P_t is the prestressing forces after losses at the time of t. Therefore,

$$\theta_t = (M - P_t \times e) \times [1/(E_t \times 1)] + \{M - [(P_i + P_t)/2] \times e\} \times [C_t/(E_t \times 1)] \quad (11)$$

3. For axial deformation only, the following is used:

$$E = \{P_t + [(P_i + P_t)/2] \times C_t\} \times [1/(E_t \times A)] + Esh \quad (12)$$

where A is the cross-sectional area and Esh is the strain change due to shrinkage.

4. Shear deformation in cantilever girder was neglected.

Based on the above assumptions, the elastic deformations will be calculated by use of the beam theory. The moment-area method or stiffness-matrix method can accurately predict elastic deformations. However, in the above formulas, the moment is a time-dependent quantity and subject to variation of stage prestressing. This is also coupled with variable sectional properties. An electronic calculator or computer program that traces all the variable and relative displacements will ultimately give the deflections for each section at each construction stage. The program flowchart is illustrated in Figure 2.

Tabulation

The deflection for each stage can be tabulated and

Figure 2. Program flowchart.

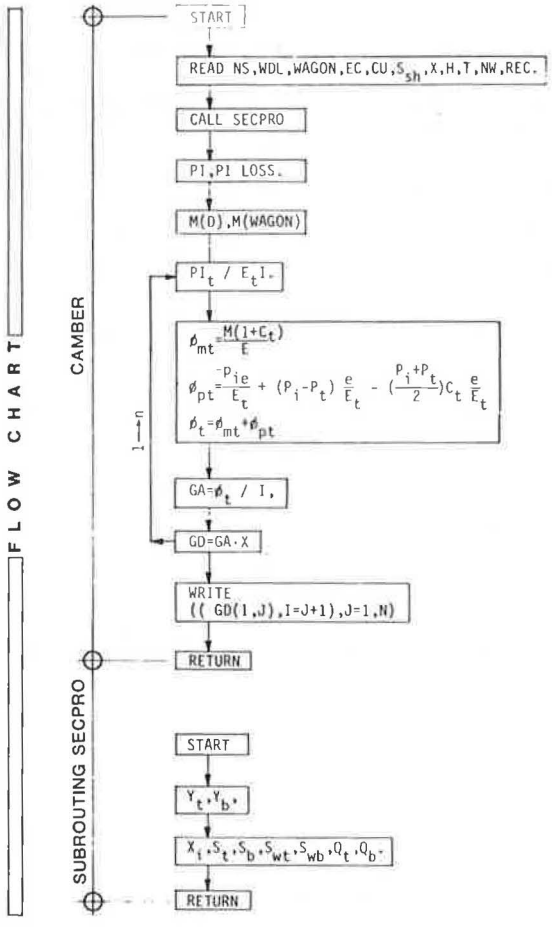

Figure 3. Tabulation of bridge deflection and camber.

ESTIMATE OF VERTICAL DEFLECTIONS IN INCH

RIGHT SPAN

INCREMENTAL DEFLECTIONS AT CONSTRUCTION STAGE

2	3	4	5	6	7	8	9	10
-.00								
-.01	-.02							
-.01	-.03	-.06						
-.00	-.02	-.04	-.08					
-.00	-.02	-.04	-.08	-.13				
.00	.01	.02	.03	.03	.04			
.00	.02	.03	.05	.08	.10	.12		
.01	.02	.05	.08	.12	.16	.20	.23	
.00	.01	.02	.04	.06	.07	.08	.08	.07

DEFLECTION AS THE RESULT OF SEGMENT 7 AND PRESTRESS

COMPLETE OF BRIDGE

.00	.00	.01	.01	.01	.01	.01	.01	.01

AFTER 50 YEARS (DUE TO CREEP)

.01	.02	.04	.06	.09	.12	.14	.15	.15

CAMBER TO COMPENSATE DEFLECTION DURING CONSTRUCTION IF TOTAL CAMBER EQUALS

2	3	4	5	6	7	8	9	10
-.01	-.02	-.02	.05	.16	.37	.41	.33	.08

THEN CAMBER ELEVATIONS DURING CONSTRUCTION WILL BECOME

-.00								
.00	-.00							
.01	.03	.04						
.01	.04	.09	.13					
.02	.06	.13	.21	.29				
.02	.05	.11	.18	.26	.34			
.01	.04	.08	.13	.19	.24	.29		
.01	.02	.03	.05	.07	.08	.09	.09	
.00	.00	.01	.01	.01	.01	.01	.01	.01

CAMBER VALUE AFTER SEGMENT 7 CONSTRUCTION

COMPLETE OF BRIDGE

.00	.00	.00	-.00	-.00	-.00	-.00	-.00	-.00

Figure 4. Traveler for cast-in-place construction.

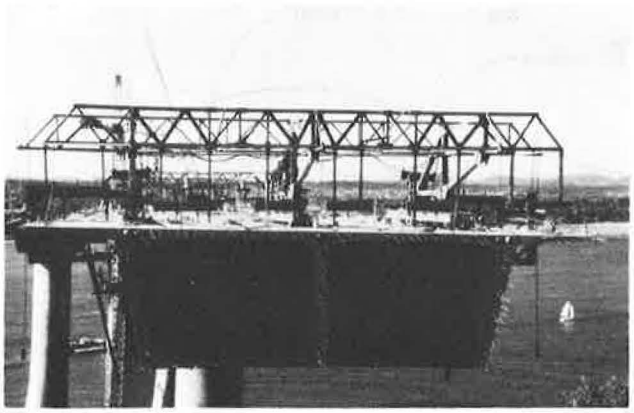

summarized. For compensating deflections, the camber can be obtained at a particular joint by adding all of the deflections found in one column. Figure 3 shows tabulated deflections for each construction stage at different segment joints. Camber calculation and camber design were based on the assumption that the deflection would be compensated 100 percent. For example, at the construction stage of segment 10, the camber value will be the summation of the deflections found under column 10, which is the total algebraic summation of 0.07 and 0.01 (total 0.08).

CAMBER CONTROL IN CAST-IN-PLACE CONSTRUCTION

The camber values for a cantilever can be determined by providing an opposite amount of deformations at each segment joint, such as the following:

1. Cantilever construction deflection due to dead load, construction load, and prestressing force;
2. Closure weight and forms and continuity prestressing force;
3. Topping, railing, curb, and utility;
4. Removal of traveler; and
5. Long-term deflection adjustment, if any.

Note that the deflection due to unbalanced moments at the pier and foundation must be considered in the field before the new form elevation is set. It must be recognized that, at the final balanced condition, this effect must also be compensated.

Cantilever traveling forms, as shown in Figure 4, have been used in most bridge construction of this type. In the I-205 Columbia River Bridge (north channel), the traveler was designed to have a total weight of 135 tons, including formwork. The maximum weight for a segment is 350 tons and the maximum length is 16 ft 3 in.

The camber for construction is tabulated and illustrated in the diagrams shown in Figures 5 and 6. On the upper table of Figure 5, the values shown in heavy diagonal boxes are the design camber readings for new segments. The new form at joint N is set at elevation EL. N (Figure 6). After concreting and prestressing, the elevation will drop to EL. Nn. The contractor must modify the forwarding form elevation if consecutive elevations are not consistent with those predicted.

Constructed elevations on a completed 300-ft cantilever have been examined and compared with the proposed cambers. The elevations at the cantilever segment joints were within 0.5 in from the designed elevations.

During the construction of segments, elevations at each segment can be surveyed and compared with the predicted elevation. If the deflection change between each segmental cycle was not compatible with the predicted change, either the design assumption or the material properties needs to be examined and adjusted.

CAMBER CONTROL IN PRECAST SEGMENTAL CONSTRUCTION

For precast segmental construction, the casting techniques can be put into two categories.

Long-Line Casting

For long-line casting, the bridge is cast in a bed with the entire bridge length as if it were built on shoring. The camber design is the same as the camber diagram for cast-in-place construction.

Short-Line Match Casting

For short-line match casting, the segment will be cast one segment at a time and cast against a previously finished segment. Figure 7 illustrates casting techniques in the I-205 project (note that the previous segment is used as the match-cast form and is seated on an adjustable table). The correct relative angle change between each adjacent segment becomes the governing factor in the successful control of deflections. Unlike in long-lined casting, only two segments are being adjusted at a time, and any error in one segment will affect the profile of the rest of the cast work and the qualities of its assembly. The procedure for deflection control when match casting is as follows.

Figure 5. Camber design values and diagram.

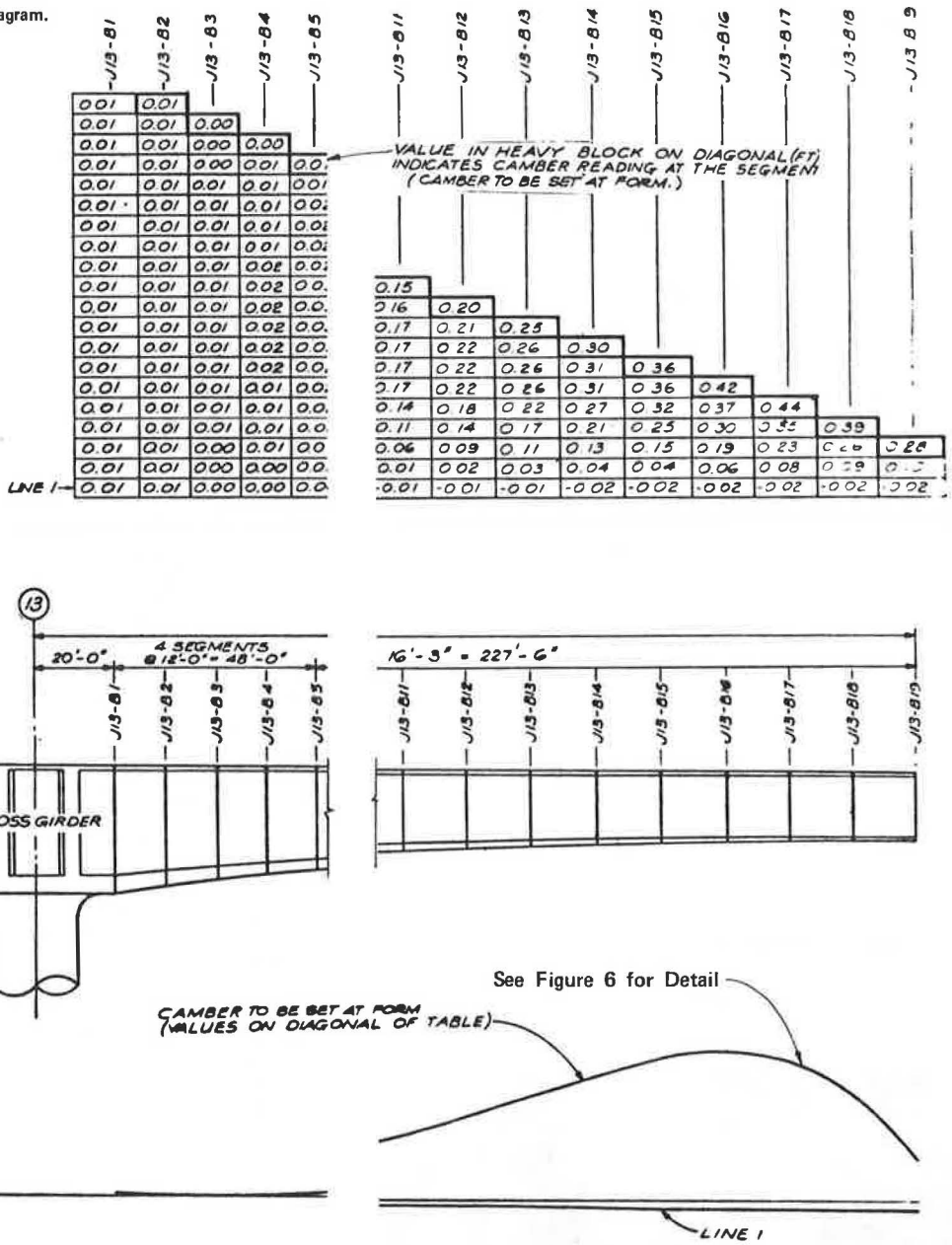

Figure 6. Bridge camber construction history.

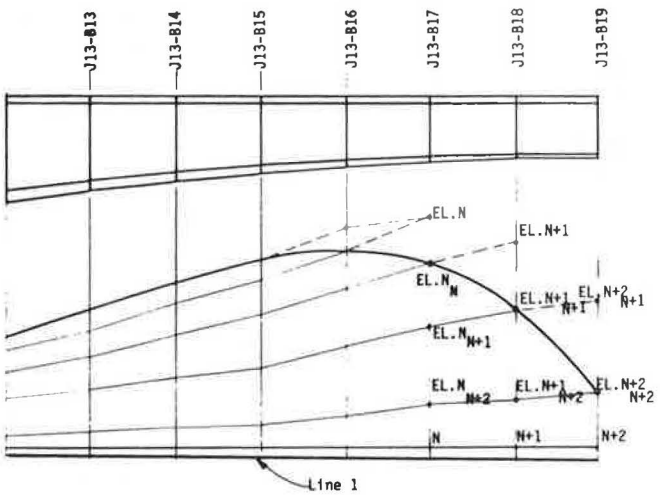

For precast segmental construction, the camber shall be built accurately into the precast segment without the convenience of field adjustment found in cast-in-place construction. To avoid shimming in the field, adjustments are usually made in the precasting yard to correct relative angles. In order to compensate for deflection, the segments are cast with their camber, which requires a relative angle change. The angle between two chords that represent the two top surfaces of the segment indicates the angle change. Because it is a problem of space geometry, the relative angle may not necessarily lie in a vertical plane. It is also true that the angle change related to the bridge may not lie in a horizontal plane. A dihedral angle between two random surfaces can be derived through known formulas, and their angle can be obtained through vector computations.

The following is an example of angle change calculations. Assume two surfaces in a space, where one surface passes through three known points. A

Figure 7. Match-cast operation.

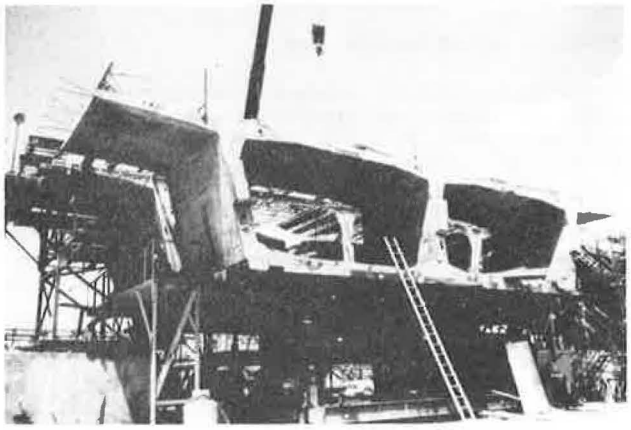

Figure 8. Two random surfaces and their dihedral angle.

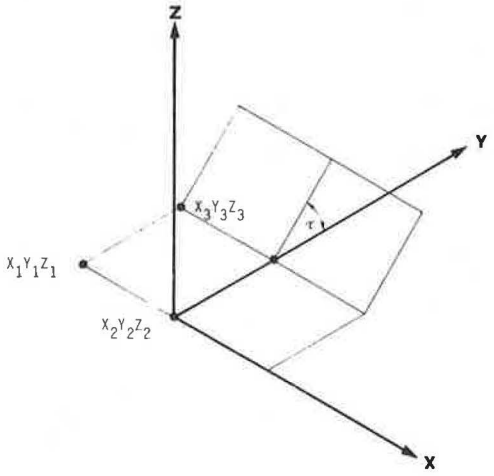

plane shown in Figure 8 can be defined as follows:

$$\begin{vmatrix} X & Y & Z & 1 \\ X_1 & Y_1 & Z_1 & 1 \\ X_2 & Y_2 & Z_2 & 1 \\ X_3 & Y_3 & Z_3 & 1 \end{vmatrix} = 0 \tag{13}$$

$$\begin{vmatrix} Y_1 & Z_1 & 1 \\ Y_2 & Z_2 & 1 \\ Y_3 & Z_3 & 1 \end{vmatrix} X + \begin{vmatrix} Z_1 & X_1 & 1 \\ Z_2 & X_2 & 1 \\ Z_3 & X_3 & 1 \end{vmatrix} Y + \begin{vmatrix} X_1 & Y_1 & 1 \\ X_2 & Y_2 & 1 \\ X_3 & Y_3 & 1 \end{vmatrix} Z = \begin{vmatrix} X_1 & Y_1 & Z_1 \\ X_2 & Y_2 & Z_2 \\ X_3 & Y_3 & Z_3 \end{vmatrix} \tag{14}$$

$$A_1 \cdot X + B_1 \cdot Y + C_1 \cdot Z = D_1 \tag{15}$$

Thus, solve determinant of A_1, B_1, C_1, D_1.

We can find the fourth point elevation Z if we knew X_4 and Y_4, or we can verify the calculated Z_4 with actual elevation. Two planes can be used to establish two equations that consist of A, B, C, and D. Their angle change of τ can be solved for a dihedral angle between two planes as follows:

$$\text{Cos}\tau = [(A_1 \cdot A_2) + (B_1 \cdot B_2) + (C_1 \cdot C_2)]/(\sqrt{A_1^2 + B_1^2 + C_1^2} \cdot \sqrt{A_2^2 + B_2^2 + C_2^2}) \tag{16}$$

Figure 9. Cast procedure of precast segments.

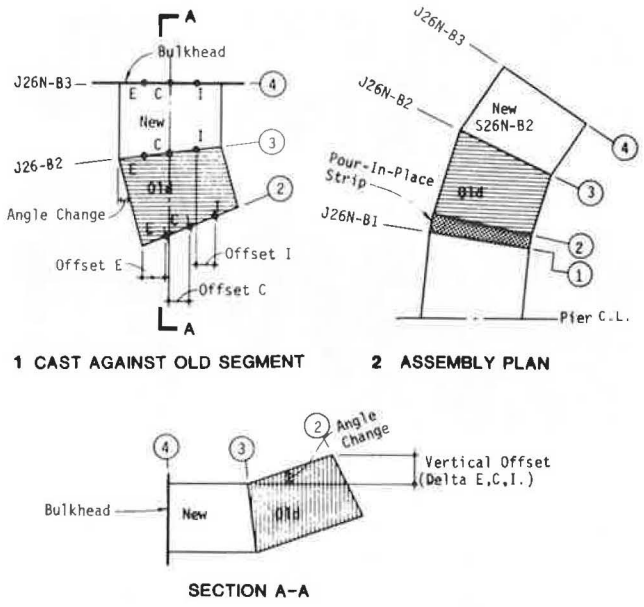

Figure 10. Precast segment is hoisted up to its key-in position

Scaler:

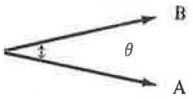

$A \cdot B = /A/ \cdot /B/ \cdot \text{Cos}\ \theta$

Thus, the relative angle change for each adjacent segment is established. Based on bridge grade profile and curve data, segment geometry can be established by superimposing the above data with design cambers. Then the angle change between segments can be determined in accordance with the above-outlined procedures. After the relative angle between two segments has been determined, the horizontal and vertical offset can be calculated based on the chord lengths. The diagram in Figure 9 illustrates the casting procedure. Then, segments shipped from the casting yard are hoisted into position, as shown in Figures 10 and 11.

By examining the structural record of a 180-ft precast segmental construction, it is found that the variations between the predicted and actual surveyed elevations are on the order of 0.25 in for most joints and 0.75 in at two particular joints (Figure 12). It is also noted that the above-mentioned cantilever construction was done without the use of shimming.

Figure 11. Hoisting equipment moves new segment into correct position.

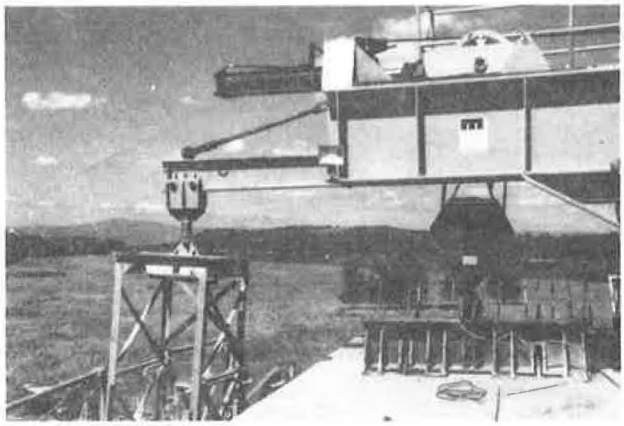

Figure 12. Design camber versus as-built elevation.

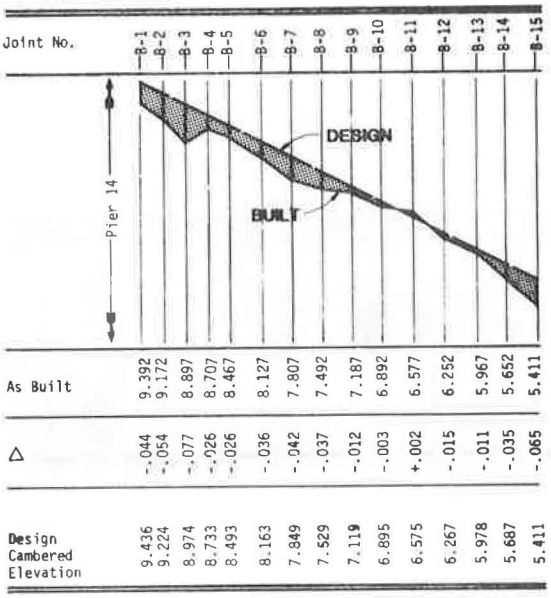

In precast segmental construction, it is difficult to construct a twisting angle between two adjacent segments, which is necessary to accommodate a superelevation change. It involves twisting of the web or bottom slab from the plane of the previous segment. It also causes a gap at the segment joint, which complicates the concreting. In the I-205 project, a slight tilting of one of the supports of the old segment at the casting bed was used to achieve the necessary superelevation angle change.

CONCLUSION AND RECOMMENDATIONS

With proper control, segmental cantilevered construction, either cast-in-place or precast, can be built accurately in elevation and plane geometry. Camber or deflection prediction involves many parameters, which are either time dependent or independent. In construction, a simplified analysis of deflection prediction is desirable. The methods outlined in this paper have demonstrated the practicality of a simple approach to deflection control, and the results have proved to be satisfactory.

From the experience of several projects, and the I-205 project in particular, the simplified method of deflection prediction can be used for both cast-in-place and precast cantilever segmental constructions. The correct elevation in cast-in-place construction relies on the correct setting of forms, while in precast segmental construction the correct elevation depends on accurate casting techniques. Success in both types of construction will depend on good camber prediction.

ACKNOWLEDGMENT

Thanks are due John Clark of the University of Washington, Seattle, for his help in developing the precast match-cast control techniques.

REFERENCES

1. Post-Tensioned Box Girder Bridge Manual. Post Tensioning Institute, Phoenix, 1978.
2. Precast Segmental Box Girder Bridge Manual. Prestressed Concrete Institute, Chicago, 1978.
3. T.Y. Lin and N. Burnes. Design of Prestressed Concrete Structures, 3rd ed. Wiley, New York, 1978.
4. Deflections of Prestressed Concrete Members. Journal of the American Concrete Institute, Dec. 1963.
5. CEB-FIP Model Code for Concrete Structures. Comite Euro-International du Beton-Federation Internationale de la Precontrainte, Paris, 1978.
6. Deflections of Concrete Structures. American Concrete Institute, Detroit, Special Publ. 43, April 1974.
7. M. Polivka. Lightweight Concrete for the Ruck-A-Chucky Bridge. T.Y. Lin International, San Francisco, July 7, 1977.

Publication of this paper sponsored by Committee on Concrete Bridges and Committee on Construction of Bridges and Structures.

Current Practices in Systems Construction of Concrete Bridge Structures

JAMES J. HILL AND ARUNPRAKASH M. SHIROLE'

The current practices in systems construction of precast and cast-in-place concrete superstructures are reviewed. The paper covers a wide range of bridges from shorter single-span to longer multispan bridges. It discusses currently used standard sections, their economic and operational efficiencies, as well as their limitations. It describes effective use of systems techniques that can optimize costs related to formwork, on- or off-site labor, materials, equipment, time, transportation, and traffic detours. Systems techniques that can make superstructure rehabilitation alternatives for deficient bridges economically feasible are also given.

The construction practices for concrete bridge superstructures have undergone very significant and innovative changes during the past 20 years. The major thrust of these changes has been toward systems construction in order to accomplish overall savings of time and money while maintaining or improving the quality of construction.

Systems construction can be described as a clearly defined and well-coordinated sequence of construction activities to accomplish economically and operationally efficient construction. Applications of systems concepts to the construction of concrete bridge superstructures has resulted in the development of standardized sections, techniques, and procedures in precast as well as in cast-in-place concrete superstructures. The standardized sections include single, double, bulb, and quad tees; flat or voided-slab and rib-deck panels; single or multicell box girders; precast arch segments; and precast railings. Standardized techniques of methods include use of standardized sections in the construction of continuous spans, form-traveler, balanced cantilever, launching girder, incremental launching, and optimal scheduling. Standard procedures include standardization in design, specifications, and details; multiple-use forms; use of precast concrete or corrugated steel stay-in-place forms; and slip forming. Current practices in the systems construction of concrete bridge superstructures are discussed in the following sequence: basic systems concepts, precast concrete superstructures, and cast-in-place concrete superstructures.

BASIC SYSTEMS CONCEPTS

Basic systems concepts currently used in the construction of concrete bridge superstructures are discussed below.

Standardization

Standardization can be defined as a process of bringing repeatedly used similar components, steps, and operations into conformity with substantially uniform and well-established components, methods, procedures, or techniques. Use of standardization is beneficial when a number of dimensionally similar sections, details, or repeated construction operations are involved. Resulting benefits are stricter quality control, increased speed of construction, and reduced overall on-site labor, material, and equipment costs.

Use of standardization is limited to situations that have a large number of similar operations or sections of similar geometry. Other limitations include location-related constraints; availability of required skilled labor, materials, and equipment; as well as reduced flexibility in design. In certain situations, environmental, aesthetical, and other considerations may also limit the usable standardization options.

Optimization

Optimization can be defined as a process of organizing a group of interrelated components, activities, or operations into a system that is as economically and/or operationally efficient as possible. It provides the best compromise solution in terms of use of available resources and yields the best overall benefit/cost ratio possible.

The concept of optimization is being used widely in construction scheduling. Construction scheduling essentially consists of arranging the construction operations in such a sequence that the project is completed with optimal use of available resources and in the least amount of time. Frequent revision of schedules during construction keeps them current and facilitates prompt corrective actions.

PRECAST CONCRETE SUPERSTRUCTURES

Standardized Sections

Figure 1 shows the different types of currently used standard precast concrete sections. It also indicates the ranges of section depths, widths, span lengths, weights, and current costs. Precast concrete sections such as these are very widely used and have proved to be very competitive with rolled and built-up structural steel sections. Many states and fabricators have developed their own standard sections and have promoted their use. This has resulted in cheaper superstructure components and total bridge systems that require minimum material and on-site labor.

Use of standard sections has proved to be economically and operationally efficient where precast concrete plants are in the proximity and transportation as well as erection equipment are available at a reasonable cost. Current trends indicate increasing applications of segmental construction technology in the construction of precast concrete superstructures.

Standardized Techniques and Procedures

Standardized techniques and procedures that are currently used for the construction of precast concrete bridge superstructures include segmental construction, progressive placing, cable-stayed spans, and Benton Bogen (BEBO) concrete arch.

Segmental construction (1) is a construction that is put together segment by segment, then erected, glued together with epoxy, and finally posttensioned. Segmental posttensioned box-girder bridges, which originated in Europe, are being constructed in the United States in increasing numbers. Maximum spans in excess of 750 ft (230 m) (2,3) have been attained by using this technique. In a balanced-cantilever segmental system, construction proceeds by cantilevering segments from a pier in a balanced

Figure 1. Currently used standard precast concrete sections.

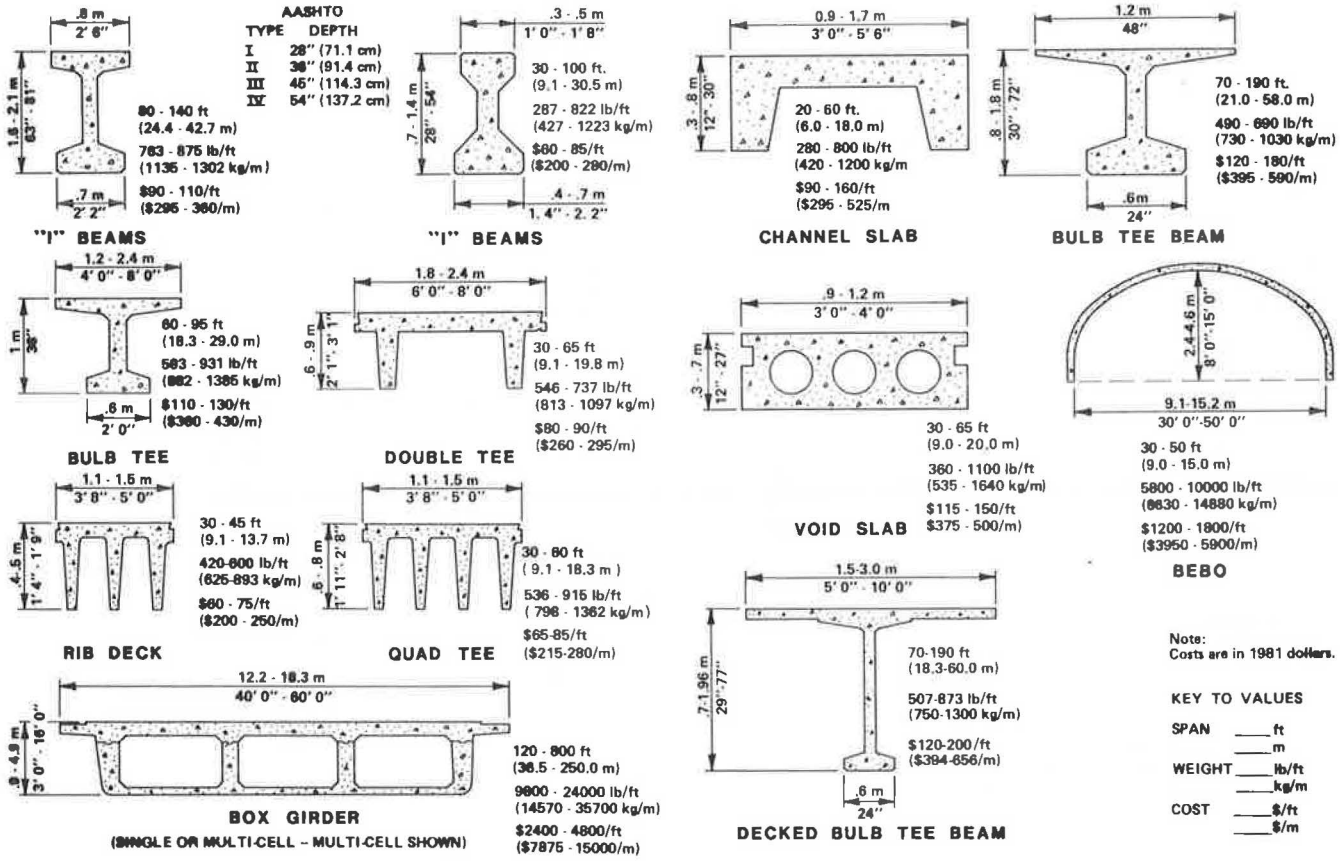

fashion on each side until midspan is reached from both sides, and then a closure section is poured. This procedure is repeated until the entire structure is completed. Where symmetrical sections cannot be erected simultaneously, a temporary bracing or falsework is necessary. Span lengths to 300 ft (92 m) have been common. Segmental technology offers the benefits of all seasons and, therefore, shorter-duration construction; partial or total elimination of falsework requirements; greater spans; and aesthetically pleasing, slender structures. One recent example of this type of construction is the Kishwaukee Bridge in Rockford, Illinois.

Progressive placing (1) consists of placing precast concrete sections cantilevered out progressively from a pier or abutment in a continuous manner from one abutment to the other. This method appears to be practical in span ranges from 100 to 160 ft (30-35 m), where the balanced-cantilever method is generally not economical. This system has the obvious limitation of cantilever stresses becoming excessive in relation to construction depth, and a temporary stay may be required.

The cable-stayed system uses temporary cables anchored to a prestressed concrete beam at the top of the tower bent to place the traveler and deck segment during erection. Additional temporary fore and back stays, which stretch long distances, support the bent during deck construction. Before the traveler is advanced for the next section, two prefabricated permanent stays are attached. Sliding hangers haul the stays up a guide cable to steel anchorages atop the tower columns. Once stays are positioned at the tower head, the lower ends of the cables are jacked into anchorages in the deck segments. Placed on opposite sides of a section, both stays are stressed simultaneously as the erection cables are eased. Spans of more than 1000 ft (305 m) have been constructed by using this method. This method is particularly suitable where the height of the structure precludes the use of lifting cranes from barges. The cable-stayed design has proved to be structurally more efficient and economical than a cantilever steel truss for spans between 600 and 1800 ft (183 and 549 m). The 981-ft (229-m) main-span Pasco-Kennewick Bridge in the State of Washington (a recent example of this technique) was estimated to cost $110/ft² ($1184/m²) against $150/ft² ($1614/m²) for steel.

The BEBO precast concrete arch uses counterarch deformation action of passive earth pressures to balance arch deformations. Precast concrete BEBO arch spans up to 60 ft (18 m) have been successfully constructed. A recent project in Edina, Minnesota, is an example of this technique.

These and other standardized techniques and procedures (4) for precast concrete superstructure construction offer many advantages. They include the following:

1. Considerable savings in construction costs and time,
2. Drastic reduction or total elimination of the need for falsework,
3. Reduction or elimination of problems related to concrete shrinkage,
4. Factory casting conditions allow better quality control and higher-strength concrete, and
5. Longer and more slender-looking spans (at lower costs) have become possible.

There are also limitations of these techniques and procedures. They include the following:

1. Need for heavy site-lifting equipment, such as cranes and gantries;
2. Need for close proximity of precasting plant to be cost effective;
3. Difficulties in maintaining control of horizontal and vertical alignment;
4. Trucks used to transport precast concrete sections are subject to load restrictions along their routes; and
5. Depending on the technique used, fabrication of special launching girders, trusses, or gantries is expensive (e.g., $900 000 launching truss fabricated for the $11.4 million Denny Creek Bridge in the State of Washington) (5).

Applications for Superstructure Rehabilitation

Use of precast concrete technology in partial or total rehabilitation of concrete bridge superstructures has become increasingly common in recent years. Plain or voided precast concrete deck modules, railing sections, and even precast concrete superstructures (complete with curb, sidewalk, and railings) are currently being used (6).

The precast deck modules being used have been basically nonstandard items than have dimensions that suit individual rehabilitation projects. These range from 5 to 8 in (12-20 cm) in thickness, 4 to 8 ft (1.25-2.5 m) in width, and up to 30 ft (9 m) in length. Mobile truck cranes that have lifting capacities of 10-15 tons (9.1-13.6 Mg) can generally handle the erection and placement of these modules. Precast modules are then fastened together by means of welded, epoxy, and/or cement-grouted connections. Where placement is to be over steel beams, modules are epoxy-glued to the top flanges and further attached by stud connectors and grout.

Types of precast railings commonly used are AASHTO Type J, which weigh about 400 lb/ft (600 kg/m) and typically cost from $25 to $35/ft ($82-$115/m). The precast concrete superstructures (complete with curb, sidewalk, and railings) are nonstandard and much heavier sections, which pose erection and placement difficulties.

The economic and operational efficiencies of using precast technology in superstructure rehabilitation have been quite significant. In addition to better quality construction, it can result in substantial reduction in time required for on-site rehabilitation work, often with portions of the structure under heavy urban traffic. With traffic-detour-related costs soaring high and with the energy crunch, current trends indicate increasing future use of precast concrete in superstructure rehabilitation.

CAST-IN-PLACE CONCRETE SUPERSTRUCTURES

Current practices in the construction of concrete superstructures indicate that, for the short to medium single-span range [20-130 ft (6-40 m)], cast-in-place concrete, for the most part, is being replaced by precast concrete systems. However, cast-in-place concrete systems are being used for multiple spans with continuous design and bridges with curves and flares (7). Innovative techniques in design and construction of cast-in-place structures are being developed to overcome the obvious disadvantages of greater on-site labor and construction time for falsework, forms, rebar placement, as well as placement and finishing of concrete. These innovations have been in terms of standardized construction techniques and procedures; standardization in design, specifications, and details; and scheduling of construction operations.

Standardized Techniques and Procedures

Standardized techniques and procedures that are currently used in the construction of cast-in-place concrete superstructures include the following: balance cantilever, span by span, and incremental launching.

The balanced-cantilever technique (1), although basically similar to the one used in the precast system, uses movable formwork supported from a previously erected segment or form-traveler, while the segment is formed, cast, and stressed. The Pasco-Kennewick Bridge in the State of Washington was constructed with this technique. Span lengths up to 300 ft (92 m) have been successfully and economically built by using this technique.

Span by span (1) is construction of the superstructure in one direction, one span at a time, by using a movable form carrier. The form carrier provides a type of factory operation at the job site; its advantage is that it permits versatile adjustments in the field. It is supported on piers or on the ground when possible. As each segment is cast, the reusable forms are released and the segment rolls forward by means of structural steel out-riggers on the outside of the form carrier. The carrier may be located above or below the deck, depending on space and span requirements. This type of construction is especially suitable for long viaduct-type structures, where repeated construction can afford economies. It was used in the construction of the Denny Creek Bridge in the State of Washington, where typical construction time for a 100-ft (30.5-m) span was five to eight calendar days.

Incremental launching (1) is a segmental construction technique. It involves superstructure segments, from 33 to 100 ft (10-30.5 m) in length, which are match-cast in place in stationary forms behind the abutment. After the concrete reaches sufficient strength, the new segment is posttensioned to the previously cast segment. The assembly of units is then jacked forward, horizontally and vertically, over teflon and stainless-steel bearings on top of the piers. Straight or simple curved superstructure alignments are possible with spans up to 200 ft (61 m). Construction of spans up to 300 ft (92 m) are possible with this technique if temporary falsework is used. The incremental-launching technique is particularly suitable where the terrain and use of heavy crane equipment are difficult. Construction of the Wabash River Bridge in Covington, Indiana, was planned by using this technique.

Standardization in Design, Specifications, and Details

Although there is great potential for their application, systems concepts are not being applied commonly to design, specifications, and details. Current applications and their benefits are as follows:

1. Standardization of design components in order to simplify formwork and reduce labor, materials, and equipment costs, as well as overall construction time;
2. Standardization and optimization of rebar details (i.e., sizes and spacings) to simplify placing and effect savings in placement time and costs;
3. Design that reduces the number of joints or eliminate time-consuming and costly expansion joints;
4. Design that uses commonly available equipment and locally available materials;
5. Use of objective and realistic tolerances in the specifications;
6. Use of standardized details to simplify placement of materials and save on-site labor, equipment time, and cost;

7. Design that uses prefabricated forms if possible; and
8. Use of specifications and specialized materials that can result in time savings and improve the quality of construction (e.g., superplasticizers that help reduce water content and simplify placement and finishing of concrete).

Scheduling of Construction Operations

The systems concept of optimization is widely used in the scheduling of operations in cast-in-place concrete construction. Objectives in the use of optimization techniques are reduction of on-site labor, materials, and equipment costs, as well as savings in overall construction time.

Construction scheduling essentially consists of arranging several construction operations in such a sequence that the project is completed in the least possible time while using the available resources in the best possible way. Incorporated in such a schedule is a thorough understanding and knowledge of how long each construction operation would take; lead-time requirements for labor, materials, and equipment; time required to prepare and obtain approvals of shop drawings; and subsequent delivery of materials. Extensive use of the critical path method (CPM) and the program evaluation and review technique (PERT) of similar methods is currently being made for scheduling construction of cast-in-place superstructures.

Applications to Superstructure Rehabilitation

Use of systems concepts in cast-in-place concrete superstructure rehabilitation has currently been somewhat limited. Precast concrete form panels, corrugated-metal deck forms, and slipforming are commonly being used to accomplish reduction in time and costs related to falsework and formwork. Construction scheduling is the other area where systems concepts are effectively employed.

CONCLUSION

This paper has reviewed the current practices in system construction and rehabilitation of precast and cast-in-place concrete superstructures. On the basis of this review, the following conclusions can be made:

1. Use of standardized sections has been effective in reducing on-site construction labor costs and time while providing reliable measures of strict quality control. Current trends indicate future innovations in standardized sections to further reduce on-site labor costs and time.
2. Use of standardized techniques has made a simplified application of sophisticated techniques feasible and practical.
3. Use of standardized procedures has ensured optimal use of on-site labor, equipment, and materials.
4. Innovative use of systems concepts to rehabilitation of concrete superstructures is becoming more common. It has effected very valuable savings in construction time as well as traffic-detour-related and other costs, especially in urban areas.

REFERENCES

1. C.A. Ballinger, W. Poldony, Jr., and M.J. Abrahamson. A Report on the Design and Construction of Segmental Prestressed Concrete Bridges in Western Europe, 1977. FHWA, U.S. Department of Transportation, 1978.
2. G.H. Brameld. Segmental and Stage Construction of Prestressed Concrete Box-Girder Bridges. TRB, Transportation Research Record 665, 1978, pp. 192-199.
3. B.E. Diaz. The Technique of Glueing Precast Elements of the Rio-Niteroi Bridge. Material in Construction, Vol. 8, 1975, pp. 43-50.
4. Systems Building for Bridges. HRB, Special Rept. 132, 1971.
5. M.K. Hurd. Denny Creek Bridge: A Concrete Answer to Environmental Challenges. Concrete International, Nov. 1980, pp. 16-24.
6. M.M. Sprinkle. Systems Construction Techniques for Short-Span Concrete Bridges. TRB, Transportation Research Record 665, 1978, pp. 222-227.
7. R. Tokerud. Economical Structures for Low-Volume Roads. TRB, Transportation Research Record 665, 1978, pp. 214-221.

Publication of this paper sponsored by Committee on General Structures and Committee on Construction of Bridges and Structures.

System Construction of Medium-Span Bridges in Prestressed Concrete

MAN-CHUNG TANG

The system-construction method has been applied widely in the construction of medium-span bridges in the United States in recent years. The advantage of achieving efficiency through repetition of work becomes obvious. The most commonly used schemes are put into four groups: incremental launching, cantilevering, span by span, and stage construction. Both precast and cast-in-place applications are discussed.

Medium-span prestressed concrete bridges have undergone significant development in North America in the past decade. The developments can be grouped in three areas: (a) code modifications, (b) more advanced methods of analysis, and (c) innovative construction techniques.

There have been many changes and modifications in the design codes to accommodate and facilitate the use of modern prestressed concrete. They encouraged transverse posttensioning and eliminated costly intermediate diaphragms for box girders. Many codes also provide a more realistic assessment of prestressed losses and the time-dependent behavior of concrete.

More clearly defined and simpler methods of anal-

Figure 1. Schematic sequence of incremental launching of box girders.

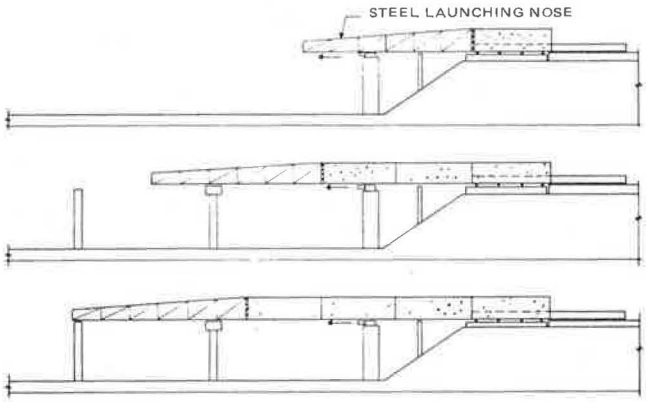

Figure 2. Incremental launching.

ysis are now available. More sophisticated computer programs have made it possible to analyze bridges that have complicated configurations and construction stages.

Many cast-in-place and precast methods have achieved further development to make them suitable for medium-span bridges. Besides classical cantilever construction, bridges have been built by span-by-span segmental construction, with overhead or underrunning trusses, by stage construction, by incremental launching, and by many other techniques.

GENERAL

Many new and efficient construction methods have been introduced to the U.S. building industry over the past decade for the construction of concrete bridges. Besides the cantilever method, which has made possible the construction of large spans such as the 790-ft Koror Bridge and the 640-ft Perrotts Ferry Bridge, other construction techniques for medium-span concrete bridges have been used very successfully. These new techniques have made construction of concrete bridges more efficient and, consequently, more competitive.

This paper reports only on those construction methods that are suitable for medium-span lengths, i.e., 120-350 ft. It also includes those methods that have not been used in the United States but have been applied successfully elsewhere in the world. In most cases, the efficiency is a product of repetition, i.e., system construction.

INCREMENTAL LAUNCHING

Although incremental launching was developed more than a decade ago, this method had been applied only once in the United States. This method was used on the Warren County Bridge in Indiana.

The principle of incremental launching is quite simple. It involves using a stationary casting bed at one end of the bridge. The girder is cast in segments of between 30 and 80 ft in length. After each segment has been cast and posttensioned, the girder is pushed out from the casting bed incrementally. To facilitate launching, or the pushing operation, sliding blocks are installed on top of the piers. These sliding blocks have a stainless-steel skin. Teflon-coated pads are fitted in between the girder soffit, and the sliding blocks thus reduce friction to as low as 1.5-2 percent of the vertical reaction. A launching nose, usually made of steel, is attached to the leading edge of the bridge girder to reduce the cantilever bending moment (Figures 1 and 2).

Depending on the size of the segments, each stage of construction can be completed in a oneto two-week cycle. For small bridge girders, the segments may be cast in one operation. For large bridge girders, the usual procedure is to cast the bottom slab first and then the webs and top slab in a second casting operation. Thus, the length of the casting bed is equal to the length of two segments, so that the bottom slab will be cast at the end of the casting bed simultaneously with the casting of the webs and top slab of the previous segment. This system is especially advantageous for union labor in the United States, where the work of various trades may not be interchanged; therefore, having two working locations can accommodate the even distribution of the labor forces.

The advantage of this method is that the casting bed, which is sometimes called the factory, is stationary. The major part of the work force is employed in repetitive work every working cycle and in the same location. In addition, the logistics of material transportation and accessibility is greatly simplified. One major drawback with this method occurs during the launching operation. Usually, the launching of each segment will last only about 3 h. However, one worker is required to be at each location where a sliding support is used. This will require additional workers, who are all needed at the same time, for a short period during the launching operation.

Because the bridge is cast at one end and advanced until it reaches the opposite abutment, certain geometric restrictions exist. Generally, only straight bridges or bridges with uniform curvature (a circular arc in either the horizontal or vertical direction) can be built by this method. This is not a serious restriction for a bridge structure. However, this method has to be incorporated into the design before the geometry of the bridge has been established. Because this construction method poses these restrictions in the geometry of the bridge, many highway engineers will not attempt to accommodate such a geometric layout. If the bridge is on a nonuniform curve, this construction method cannot be used. This is probably the major reason this method has not been used more widely in the United States.

SPAN-BY-SPAN CONSTRUCTION

In lieu of a stationary casting bed or factory at the abutment from where the bridge girder is sequen-

tially pushed from one abutment to the other, it is also possible to build the bridge span by span by using a casting factory that can span from pier to pier and cast the bridge girder either in segments within a span or cast a span in a single operation. There are many alternatives to this type of construction.

Elz Valley System

The Elz Valley system was first applied to the construction of the Elz Valley Bridge in West Germany (Figure 3). Although the early bridges built this way usually had spans of about 120 ft, it is possible to build this type of bridge with spans up to 200 ft. This construction method employs a steel form carriage that is one span in length and is designed to support the weight of the total span. The form carriage has a launching nose that can be used to move the carriage from span to span or, more correctly, from pier to pier. Instead of building spans from pier to pier with construction joints close to the piers, it is more economical to locate the construction joints at inflection points or, usually, just at the fifth point of the span. Expansion joints can also be located at these construction joints if they are required. Construction of the superstructure can be accomplished without interfering with ground traffic or navigation. It is, therefore, very suitable for high-level bridges where material supply from below is difficult or costly. Because the superstructure is continuously built from one end to the other, construction material can be supplied across the completed deck to the span under construction.

There are variations of this system. Instead of using a complete carriage as one unit, separate underdeck trusses have been found very economical (Figure 4). These are trusses that span from pier to pier and can also be moved forward.

Although this construction method was originally developed for solid girder bridges and for mushroom-type (variable-depth slab) superstructures, it has been applied to box girders in recent years (Figure 5). The result has been quite successful. The construction time for each span usually takes between two to three weeks after the crew has acquainted themselves with the construction method. For bridges that have longer spans or wider decks, the segments can be reduced to 50- to 70-ft lengths. This is economical, especially if the total length of the bridge is not great and, by subdividing the span into smaller segments, the required formwork will be less and the form will be used over a larger area, thereby reducing costs.

Eel River Method

If the total length of the bridge is not long and the investment in a span-by-span form carriage is not economically warranted, it is possible to use a variation of this span-by-span method, as in the case of the Eel River Bridge (Figure 6). The principle is the same as the Elz Valley method except, instead of a form carriage, falsework will be used

Figure 3. Elz Valley method.

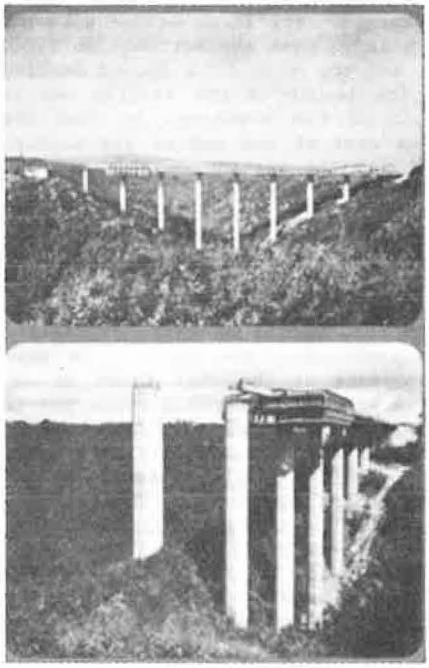

Figure 4. Span-by-span T-girder construction with below-deck erection trusses.

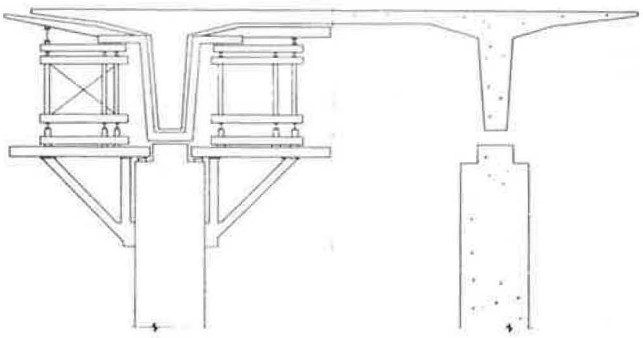

Figure 5. Span-by-span box-girder construction with below-deck erection trusses.

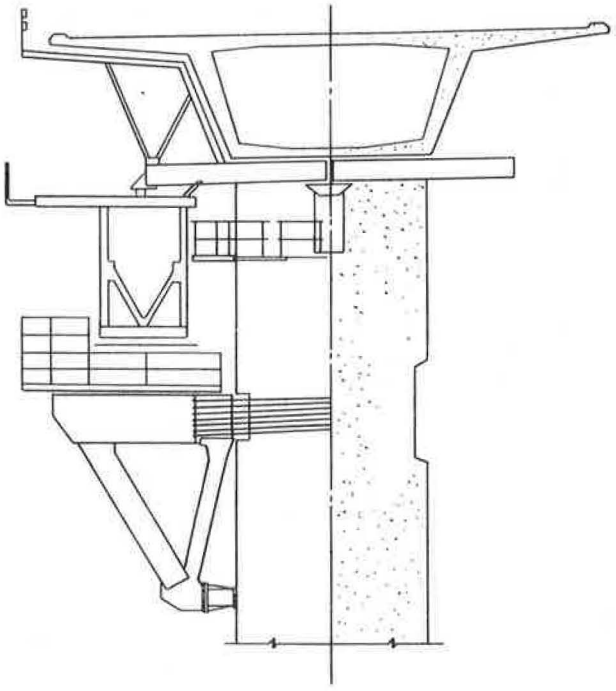

Figure 6. Eel River Bridge.

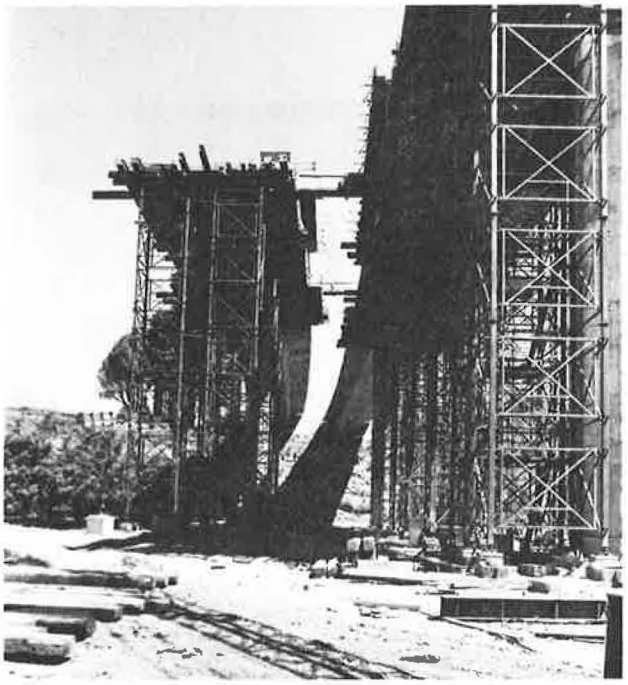

Figure 7. Seven Mile Bridge: span-by-span (over water) precast concrete box-girder construction with overhead trusses.

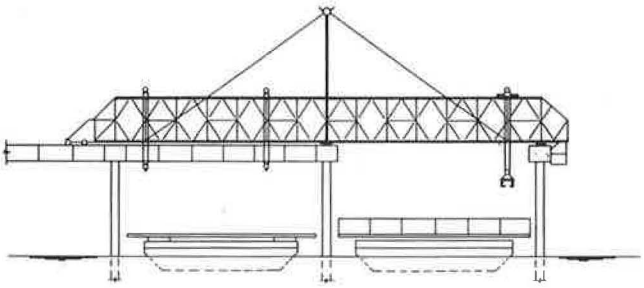

that is supported from the ground and provides a platform for the formwork of the superstructure. The falsework is about one span long, which is similar to the length of the form carriage. The bridge superstructure can then be divided into smaller segments (about 40 ft), as in the case of the Eel River Bridge. The formwork can be slid on top of the falsework platform. After each segment is completed, these forms can be simply lowered and slid into position for the next segment in a matter of 1-2 h. Again, due to the repetitious cycling of the work, the labor force becomes very efficient after a few cycles of operation.

Long Key Method

Precast segments were used in the construction of the Long Key Bridge, which is about 12 000 ft long and has typical spans of 118 ft. A steel truss is used to support the precast segments. These segments are transported to the job site from the precasting yard and then assembled on the steel truss. The completed span is then posttensioned together, and the steel truss is lowered and moved forward to the next span.

A variation of this method was used for the construction of the Seven Mile Bridge in Florida (Figure 7). This bridge has a total length of about 35 900 ft and typical spans of 135 ft. The segments are transported by barge to the bridge site and assembled on a barge-mounted truss. This barge is then placed between the piers. The pier segment is erected separately by means of an overhead truss. After the erection of the pier segment, the overhead truss is then used to raise the whole span. A closure pour is then made between the new span and the previous span while the new segments are supported by the overhead truss. The superstructure is then posttensioned after the closure-pour concrete has gained sufficient strength. The newly erected span is self-supporting after posttensioning; the supporting truss is then released and the cycle is repeated at the next span.

Two features have made this method very efficient. The first is the use of dry joints between the precast segments, i.e., without epoxy or any other bonding agent. This allows for easy assembly of the segments on the truss because, without any bonding agent between the joints, the segments are not sus- ceptible to deformations of the truss. The second feature is the use of internal-suspension-type ten- dons. These tendons are not bonded to the concrete structure but only suspended at the high point at the piers and the low point at locations inside the box girder. They are protected by grouting the plastic conduits for the tendons. These internal tendons will eliminate some tolerance problems in duct alignment that occur when tendons are embedded in the concrete section. When using a very high early-strength concrete for the closure pour, this erection method has achieved a construction speed of one span per day.

CANTILEVER CONSTRUCTION

For medium-span bridges, cantilever construction can be competitive by using overhead trusses or erection cranes. If an overhead launching truss is used, the bridge is usually constructed in a balanced-cantilever pattern from atop the piers and proceeds in one direction to the completion of the bridge. The truss will span from the finished part of the bridge to the next pier where the new cantilevers are to be started. Precast segments are transported to the end of the truss. The hoisting equipment at the truss will pick up this segment and transfer it across the open span to the ends of the cantilever, where it is tied to the previously erected segments by posttensioning. A closure pour will then be made in the middle of the following span. The launching truss is then advanced after the concrete at the closure pour has attained sufficient strength and posttensioning of the continuity tendons in completed. It is also possible to connect the cantilevers at the closure joint by means of local steel clamps so that the launching truss may be moved to the next span without having to wait until the closure pour is completed. However, certain precautions are necessary to avoid disturbance of the concrete closure pour when the concrete is still young. The first cantilever bridge in the United States that used an overhead truss is the Kishwaukee Bridge (Figure 8).

This method can also be used for cast-in-place cantilevers (Figure 9). The first use of this method was at the Siegtal Bridge in Germany. Instead of transporting the precast segments, the overhead truss is used to transfer form travelers from one pier to the next pier. It also serves as a walkway for personnel and for the transportation of construction materials.

Figure 8. Kishwaukee River Bridge: cantilever with overhead truss.

Figure 9. Cantilever construction method with launching truss.

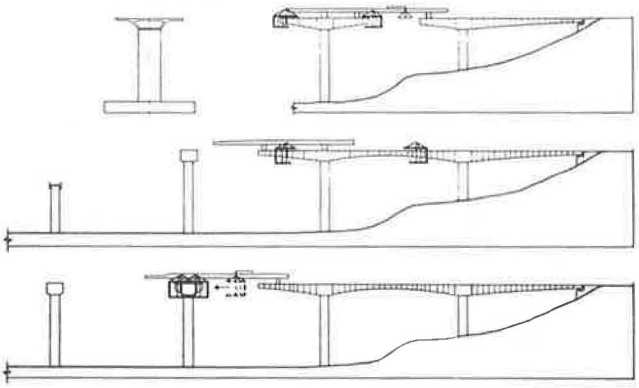

Two recent applications of this concept are the Vejle Fjord Bridge (Figure 10) in Denmark, which used cast-in-place construction, and the St. Catharine's Bridge in Canada, which used precast segments.

For the construction of the Linn Cove Bridge in North Carolina, another variation occurs. In order to avoid disturbing the local environment, no access roads are allowed to the intermediate piers. A stiffleg is used to reach to the next support from the finished portion of the bridge. A stiffleg crane is used to erect segments from the advancing edge of the bridge. Temporary supports are provided at the midspan so that the superstructure will cantilever only half of the span each time to the next pier. A closure pour is provided in each span to eliminate any tolerance problem within this span.

STAGE CONSTRUCTION

Stage construction is similar to span-by-span construction, except that the cross section of the bridge is subdivided into longitudinal slices.

One example of this type of construction is the Denny Creek Bridge in the State of Washington (Figure 11). The cross section of this bridge is subdivided into three parts. The first is a U-shaped section that consists of the bottom slab and the two webs. The second is the top slab between the webs, and the third part is the cantilever slab at both sides of the cross section. The first and second parts are cast in lengths of one span, while the

Figure 10. Vejle Fjord Bridge.

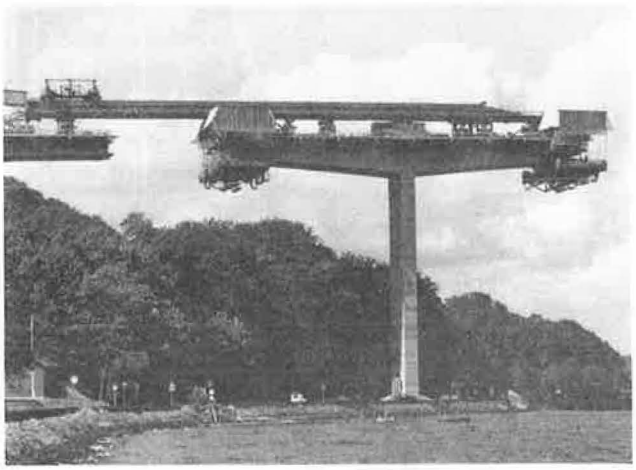

Figure 11. Span-by-span stage construction method (Denny Creek).

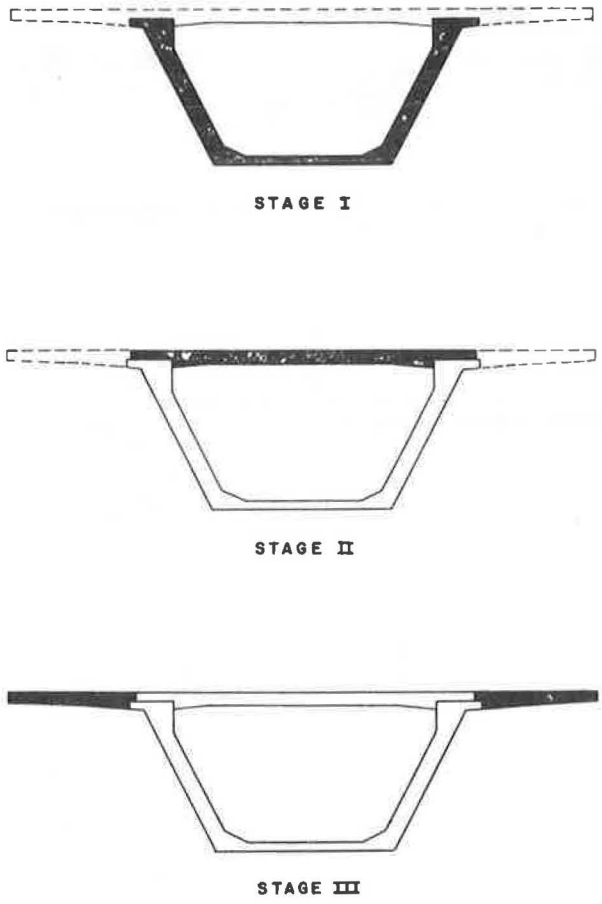

third part of the cross section can be divided again into two or more segments per span.

The bridge is designed in such a way that the first portion is cast by means of a launching truss supported by the piers, which is very similar to the span-by-span construction described previously. This U-shaped girder, after posttensioning, is self-supporting. It is also strong enough to support additional formwork for the middle part of the top slab plus the weight of the top slab. After the U-shaped girder is posttensioned, the supporting

Figure 12. Cantilever and stage construction combination (Kochertal Bridge).

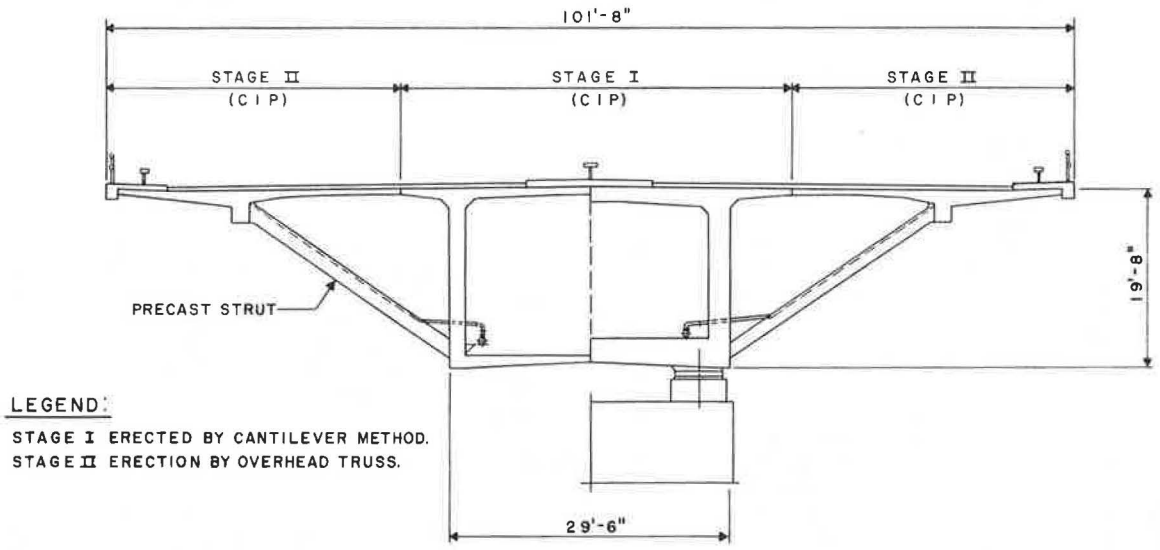

Figure 13. Cantilever and stage construction combination for casting wing slabs (phase 2).

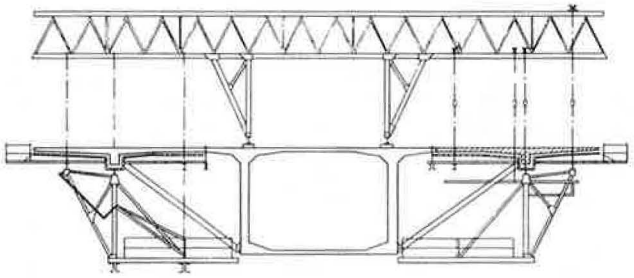

truss can be moved ahead for the construction of the next span. The third portion of the cross section, the wing slabs, are cast by using formwork supported by an afterrunner.

The advantage of this system is that the supporting truss that spans from pier to pier carries only the weight of the U-shaped girder, whereas with span-by-span construction the truss has to carry the total weight of the girder. The savings in the weight of the truss are manifold. Moreover, this method allows the construction work to be spread out into three separate stages; therefore, cycling of the labor force is more efficiently distributed.

Similar methods have been applied to other bridges in Europe. One method employs an underslung truss to support the total weight of the span but, during construction, it is separated into two stages: first, the bottom slab and a small part of the web, then, in a second stage, the remainder of the webs and the top slab in one piece. It is reported that an average two-week cycle was quickly achieved.

By using precast girders, span by span with cast-in-place top slabs could also be defined as stage construction. This is a very common construction method for shorter spans. However, by using box-shaped girders similar to the construction of the Dumbarton Bridge in San Francisco, the span of the bridge can be extended to 150-160 ft.

A combination method uses precast girders that have relatively smooth top surfaces erected on hammerhead piers. The top slab is cast by a stationary form at one end of the bridge and then pushed out segmentally, which is similar to the incremental-launching method. The top slab can then be connected either by shear studs that are cast into preformed holes in the slab or by welding together steel plates that are separately cast in the girder and the top slab, respectively. Depending on the size and geometry of the bridge, this combination method can be competitive. Other combinations, such as that of the Kochertal Bridge (Figures 12 and 13), can also be very efficient.

SUMMARY

The purpose of system construction is to apply the principle of mass production to achieve efficiency and economy by the cycling of repetitive operations. Standard American Association of State Highway and Transportation Officials (AASHTO) girders have been used widely in the United States. Post-tensioning has provided bridge engineers another excellent tool in developing new construction techniques. It is very encouraging to see that many contractors are receptive to this type of construction. As a matter of fact, many contractors have even developed some new construction ideas to achieve efficiency and economy by themselves.

Unlike long-span concrete bridges, which up to now could only be built practically by free cantilevering or cable-stayed free-cantilever methods, medium-span bridges can be built in a wide variety of ways. The various alternatives grouped under the subtitles of incremental launching, span by span, cantilevering, and stage construction are some basic examples of how those bridges can be built. With imagination, many more variations on these systems can be created.

Publication of this paper sponsored by Committee on Construction of Bridges and Structures.

Segmental Construction for Concrete and Steel Bridges That Incorporate Posttensioning

CHARLES REDFIELD, CHUCK SEIM, AND T.Y. LIN

An overview of recent segmental construction for concrete and steel bridges is presented. Particular emphasis is on bridges where posttensioning techniques have been used. Currently, segmental construction is perhaps the most predominately used method of systems construction for bridge structures. This paper describes the various types of segmental construction. The variables discussed are major materials employed, type or shape of segment used, structural systems incorporated, and construction methods employed.

This paper presents an overview of the recent segmental construction for concrete and steel bridges up to 1981 and places particular emphasis on those bridges where posttensioning techniques have been used. Currently, segmental construction is perhaps the most predominantly used method of that portion of what is called systems construction for bridge structures.

Systems construction of bridge structures may not have a strict definition, but it is generally believed that it includes repetitive use of designs, forms, plants, machinery, and equipment in the production and erection of bridge members. Segmental construction may be defined in different ways. In its narrower sense, segmental construction has come to refer only to bridges made of precast or cast-in-place concrete box sections. In its broader sense, any bridge construction that employs repetitive placement of segments in any material of whatever shape may be termed segmental construction. Many steel bridges of the box-girder type are erected in segments, and these bridges are certainly of the segmental type.

Because the main purpose of this paper is to describe the various types of segmental construction that have been or are being employed in this country and in other parts of the world, it will be interesting to describe the several variables involved in this construction, such as the following:

1. Major materials employed,
2. Type or shape of segments used,
3. Structural systems incorporated, and
4. Construction methods employed.

There can be various combinations of the above four variables. For example, a segmental bridge of steel construction can be built by using box-shaped segments to form a cable-stayed bridge built by the double-cantilever method of construction. We believe that with this approach, engineers will broaden their outlook of segmental construction and view it as consisting of different combinations of these variables applicable to various requirements for a project.

MAJOR STRUCTURAL MATERIALS

Most bridges that employ segmental-type construction are built by using concrete or structural steel. However, the segmental concept can also be applied to other materials, such as wood and masonry. Frequently, steel cables are either applied externally or internally to construct prestressed units or used as external supports to form cable-stayed structures. The combination of steel and concrete, which usually act together in composite action (with steel as the main carrying members and concrete for the bridge deck), is often used. Cable can be used to either posttension or pretension concrete decks. It can also be used to posttension the steel girders to reduce dead load moments that in turn reduce the weight of steel required. Thus, we can envision three major structural materials--concrete, structural steel, and steel cables--used alone or in combination for the purpose of achieving economical segmental construction.

TYPES OF SEGMENTS

Currently, the most popular type of segment is the transverse segmental type that normally comprises a box shape. The box shape has a special advantage in that it is a rugged section that can be easily transported and erected and forms a torsionally stiff section that adapts itself to both the positive and negative moments of the structural system employed. However, there are also some basic disadvantages for a box shape, as compared with other shapes, since it may require excessive material and labor. This is true for both concrete and steel box sections. As a result, boxes with orthotropic steel decks frequently have proved to be uneconomical. Concrete boxes may be uneconomical for short or medium spans or where the bottom soffit may not be required structurally. They also add weight and additional cost for labor, forming, transportation, and material.

Longitudinal precast segments, which use standard I-beams and T-beams and are precast and erected in parallel, have been another popular type of segmental construction for many years. They can be classified as longitudinal segments to distinguish them from the transverse segments described above. The immediate advantages in the use of such segments when constructed in elements of 120 ft are the simplicity of fabrication and the relative ease in transportation. Furthermore, in continuous systems they can be lengthened to 150 ft and perhaps beyond. These longitudinal sections are spaced sided by side with the concrete deck poured in place. This is often an expensive process, since such in-place concreting has not yet been highly mechanized. By using reinforced concrete decks, these segments are spaced somewhat close together. Then, by using transverse posttensioning of the deck, the spacing can be increased, thereby resulting in overall economy. Concrete T-beams of the longitudinal segmental type can simplify deck construction, but their spacing may be limited unless gaps are left between the T-beams.

Another longitudinal segmental type is the V-shape or inverted-Delta shape that was used for the Dumbarton Bridge. These V-beams are rugged and relatively stable for handling and can be joined to form longer spans. For example, the Dumbarton Bridge joined two 75-ft-long V-beams to form beams 150 ft long. When used for approach spans, their sloping sides blend well aesthetically with the longer main-span box girders (Figure 1).

Another interesting shape is the segmental waffle type. Precast waffle segments can be placed in a grid pattern on falsework supports to form bridges of varying width and curvature. Tendons are placed

between the webs of the units and the space is filled with concrete that has a topping. The Hegenberger Bridge in Oakland, for example, was made of waffle segments 10 ft by 15 ft by 6 ft 2 in; the walls were only 3 in thick. These were precast at the site in the form of inverted bathtubs (Figure 2). Tendons were then placed within the troughs between these segments and integrated with poured-in-place concrete.

Another segmental construction technique is illustrated by the Rio Colorado Bridge in Costa Rica (Figure 3). Precast channel-shaped plate elements are supported on cables draped between abutments. These cables were then posttensioned to form a rigid lower platform from which the entire superstructure, also composed of precast column and beam elements, was erected.

Wing-type segments were used for the San Francisco International Airport elevated roadway (Figure 4) and then again for six intersections in Bogota, Colombia (Figure 5). These wing-shell sections with transverse ribs were precast without match-casting and placed side by side on falsework with a 0.5-in gap in between. Epoxy is not used at the joint. Then in situ concrete is poured over the top to form the deck onto the spinal beam. Posttensioning is applied in the spinal beam to carry the load longitudinally, but the posttensioning forces are transmitted only through the in situ concrete. The wing elements are used to support the loads transversely. This is a very economical segmental construction when using concrete, but its span is probably limited to less than 200 ft. A combination of a steel spinal beam with composite concrete wings perhaps can prove to be a solution for longer spans.

Figure 1. Dumbarton Bridge.

Figure 2. Hegenberger Bridge.

Figure 3. Rio Colorado Bridge.

Figure 4. San Francisco International Airport elevated roadway.

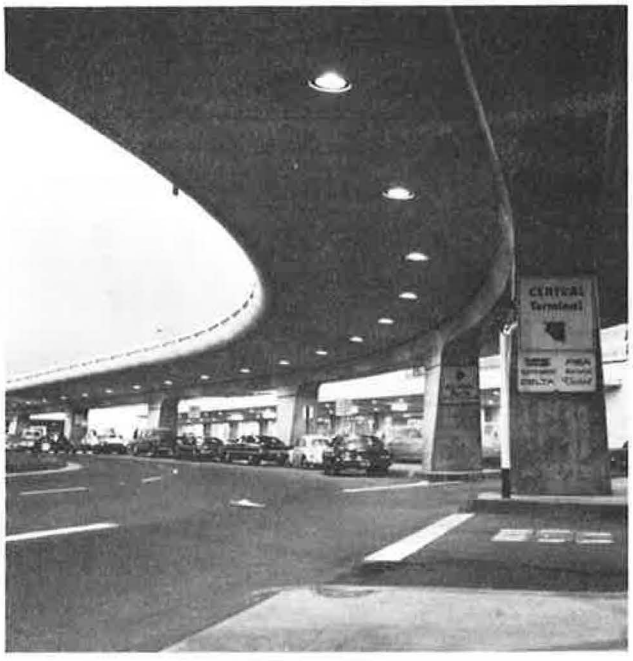

STRUCTURAL SYSTEMS

The third variable in segmental bridge construction lies in the basic structural systems employed. Currently, the balanced double cantilever is the most frequently used system (Figure 6). However, the single cantilever, which has the other end anchored by counterweight, has also been built. In any case, cantilever construction is a natural solution when steel cables are posttensioned along the top of the section. Although this has been used only for concrete construction, it is envisioned that it can be used for steel bridges that incorporate composite concrete decks.

The second predominate type of segmental bridge construction is the cable-stayed bridge. For example, the Pasco-Kennewick Bridge used precast transverse sections in a cable-stayed bridge (Figure 7), while the Kwong Fu Bridge in Taiwan employed precast longitudinal sections (Figure 8). Other segmental bridges of the cable-stayed type could be built with travelers in cantilevering fashion, as was planned for the Ruck-A-Chucky Bridge.

Span-by-span erection seems to be a method for shorter spans. These simple spans can be made partly continuous for live load, such as was done for the Long Key Bridge in Florida (Figure 9).

Another approach is the use of continuous spans by using segmental construction (as was used for the San Francisco Airport elevated roadway). Expansion joints are placed either over the supports or at the point of inflection for every few spans. The Rio Colorado Bridge is an example of a suspension bridge that uses segmental construction for the lower suspended chord, columns, and deck system.

CONSTRUCTION METHOD

The construction method is a prime consideration in both the design and erection of segmental bridges,

Figure 5. Bogota, Colombia, intersection.

Figure 6. Rio Higuamo Bridge, San Pedro de Meloris, Dominican Republic.

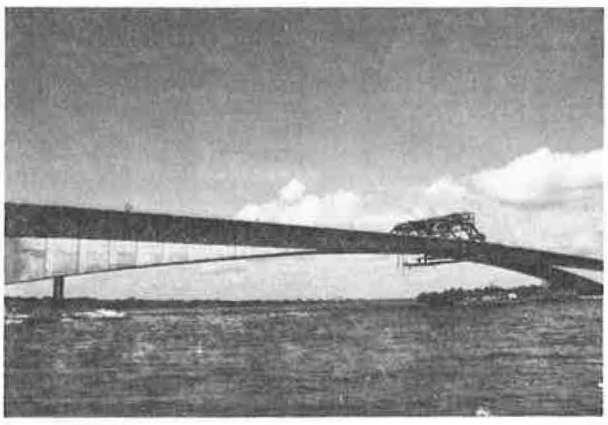

Figure 7. Pasco-Kennewick Bridge.

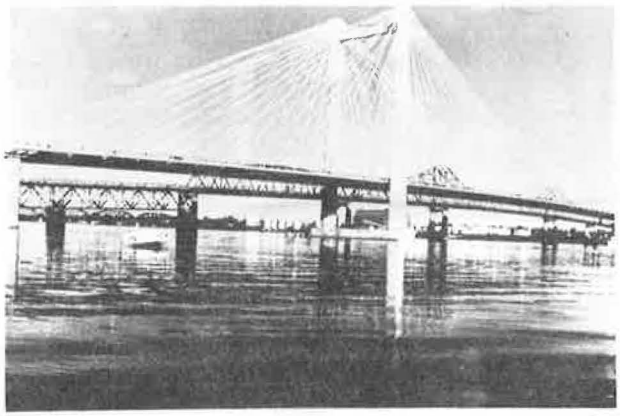

Figure 8. Kwong Fu Bridge.

Figure 9. Long Key Bridge.

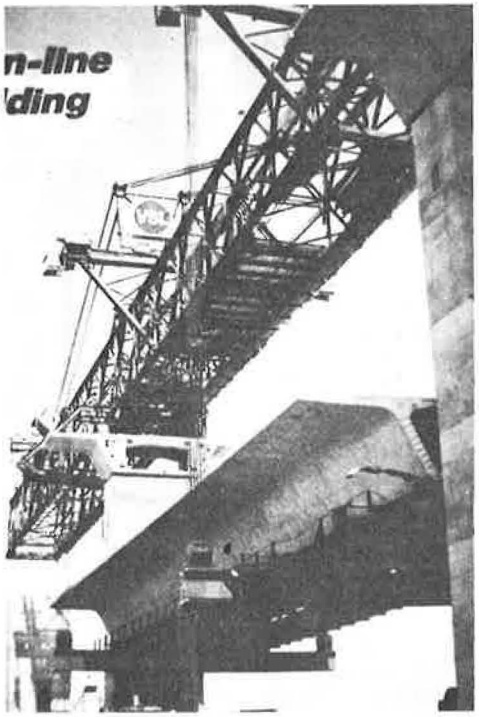

particularly when incorporating posttensioning techniques. Speaking in general terms for both steel and concrete bridges as described above, there are essentially four general methods of construction.

The traditional method of construction is the use of falsework supported from the ground. Such falsework may have temporary supports at suitable and close intervals that are spanned with steel girders or trusses to form over traffic openings. The falsework provides a broad work platform that serves as a soffit form. This conventional method, which generally uses pipe scaffolding, can be very economical, especially if the structures are over land and not very high. It can also lead to economical steel erection by providing temporary supports for steel modules until permanent joints can be built.

Cantilevering or double cantilevering, which results in free-span construction, is very appealing and is becoming a popular method of construction. This method is generally used for concrete bridges up to about a 600-ft span but has also been used in certain cases for longer spans. The steel box-girder San Diego-Coronado Bay Bridge was erected by the double-cantilevering method for its 660-ft main span. For cable-stayed construction, both concrete and steel spans can employ cantilever construction.

The incremental-launching method has been used for many bridges in Europe and for at least one bridge in the United States. Although mainly done in concrete, they can also be done in steel. In fact, steel, being a material that can take both tension and compression, would suit itself very well to this method because of the fluctuating static system during construction. As domestic examples, the railroad bridge over the Arkansas River was constructed this way by using steel and the Wabash River Bridge in Indiana was launched by using a prestressed concrete structural system.

A fourth type is the use of launching trusses. Such trusses can be launched forward to provide a support for erecting the superstructure in steel or concrete. After the span is erected, the truss is advanced for the next span. When building over water, the truss can be lowered onto a barge and moved forward to the other spans. Whenever there are many repeated spans, this type of construction can be economical for steel and concrete segments and for precast or cast-in-place segments.

DESIGN OF SEGMENTS

The design of a segmental bridge involves many facets, starting with the layout of the bridge. There is, of course, the classical criterion that the cost of the superstructure and substructure should be proportioned to result in a minimum total cost. Although a designer should economize the substructure and the superstructure each by itself, he or she needs also to think of the two together so that the choice of type of segment or segmental construction may depend of the considerations discussed above.

Whether to use a single or multiple box, I-shape or T-shape, wing or waffle sections, or steel or concrete can be a major decision in the design of a segmental bridge. The location of hinges to relieve shrinkage, creep, and temperature stresses and their effects on maintenance and riding quality are other important considerations.

The posttensioning or cable stressing of steel bridges is of recent interest in reducing the cost of steel bridges. These are being developed for various crossings that range from slightly more than 150 ft and up to 600 ft or more. Some of these cables can be prefabricated, attached to the structural element, and then prestressed in the shop or yard under controlled conditions so that systems construction is applied. The art and technique of posttensioning tendons have now advanced to a high state of perfection when applied to concrete. There is every indication that it can be applied to steel with resulting economy. This is exemplified by the Bonners Ferry Bridge, which is now under final design.

JOINERY AND DETAILS

One important item in segmental construction is the joinery between sections. For steel construction, field joints should be limited to bolting and welding should be limited to the shop. For concrete construction, the use of epoxy has not always been successful. Perhaps wet or poured-in-place joints and other methods could be developed to become more economical, thereby incorporating the advantage of precast construction with the homogeneous quality of cast-in-place construction.

Posttensioning detailing has developed to the extent that numerous types of joinery are available to the designer. The use of posttensioning detailing in concrete construction is well known and, recently, the use of tendons and anchorages in steel construction has proved to be equally applicable.

Joints in steel segmental construction are usually made to provide continuity between the segments, thus allowing the use of specially designed segments that can be fabricated, transported, and lifted economically. Joints made in the field are made predominately with A325 high-strength bolts, but A490 bolts, which are of higher strength than the A325 bolts, offer potential savings because fewer bolts are required. At times, field joints are welded but are usually more expensive than bolted field joints because edge fit-up requires tight dimensional tolerances, the welding process demands close controls, and inspection is more difficult to perform outside of a shop environment.

The trend in steel segmental construction is to design continuous multiple spans that have few expansion joints in the deck. Continuous spans of more than 1000 ft are possible with only one joint at each end. Thermal movements at piers can be accommodated by using laminated neoprene pads for relatively short distances and confined neoprene in a "pot" bearing with teflon sliding surfaces for longer distances. The pot bearing offers an economical and compact way of transmitting medium to large loads to the substructure and also can be fixed to the piers to resist lateral forces. Thus, joints can be located to optimize the performance of the structure.

AESTHETICS

From an aesthetic point of view, segmental structures should be designed to possess a certain simplicity and elegance to fit well into the environment. In his or her quest for economy, the designer should not neglect the aesthetic appearance of the bridge. Segmental construction lends itself to repetitive modules placed in uniform configuration. This can produce a beauty of its own, such as the wing-type segment of the San Francisco Airport. But if care and concern for aesthetics are not exercised, it can produce a stiff rectangular post-and-lintel appearance. It behooves designers to be aware of the aesthetic limitations of segmental construction and consider carefully the details as well as the overall appearance of the structure. Some of the details of design that should be considered for their appearance are joints between segments, junction of piers and superstructure, mating of railing to deck, junction of superstructure to the abutments, and the sitting of the abutments into its surroundings.

The overall appearance should be checked for a smooth rising and falling grade line from abutment to abutment. A sagging or inch-worn effect may cost less but detracts so much from the appearance of the finished structure that it should never be used. Likewise, in the plan, the bridge should be straight or curved in one direction only. A double curve S-shape can be used if well proportioned. But a bridge that irregularly deviates from one point to another is very displeasing and should be avoided. Occasionally, the inside curve of superelevation transition will dip, thereby producing the appearance of a sag in the bridge that has irregular layouts.

ECONOMICS

Economics is often the central issue in segmental bridge design and construction. To reach an optimum solution, design must be tied in with construction. Items to be considered in segmental construction are source of material, method of fabrication, and location of the fabrication yard; mode of production; transportation; storage areas; and erection systems. Contractors who wish to bid competetively must have a design that considers all items. Competitive bidding often can be enhanced by preparing two comparative designs of different materials, type of segments, or, in some cases, structural systems.

Some segment systems are of such recent development that there is no measure for long-term performance. It would be difficult to arrive at a life-cycle cost comparison between alternative designs, and therefore it is not presented here. With our current knowledge of material durability, corrosion processes, fatigue and fracture mechanics, and the performance of bridge systems already built, it is possible to make an engineering projection of how these segmental designs will hold up. Of course, we are continuing to learn in these areas, and every case of distress adds to our knowledge. However, the long-term performance promises to be as good as or better than previous conventional construction. It is somewhat reassuring that economic comparison based on competitive bidding is currently our best approach.

Deck sections are usually integrated into the fabrication of some types of segments, such as the box and wing sections. Precast and prestressed deck sections placed on longitudinal systems (such as steel and concrete I-girders) have recently been used to advantage. Perhaps more attention will be devoted in the future to segmental deck construction. New innovations are being devised to lower costs of construction for other types of segmental construction.

Good management techniques by the owner are as important as good design and are a major factor to help achieve total economy. The management function involves decisions on the best approach for items such as method of bidding, controlling specifications, design alternatives, value engineering, construction management, time for construction, fast tracking, and other items that may affect the biddings.

A design and construction turnkey package, which is prevalent in Europe, has not been used to any extent in the United States. It may offer an economic advantage to segmental bridge construction. A construction management team that monitors and schedules construction is now being used for the construction of buildings. However, it has not been used to any extent on bridges. This could become an advantage as inflationary trends demand shorter construction time to avoid extra cost, particularly on large jobs constructed over a long period of time. Also, designs held on the shelf until money becomes available will have a greater cost than when first proposed.

CONCLUSION

It can be observed that segmental construction is fairly well developed, but improvements can always be made. Recent studies carried out on the standardization of box segmental construction indicate that standardization of segmental units can lead to economy just as standardization of I-girders has in the past. Most important is the recent development of steel segmental construction. Because steel is lighter and easier to lift, it can fit into much longer segments that require fewer joints, which opens up interesting possibilities. Further use of posttensioning has, in effect, reduced the required steel quantity, thereby allowing for an optimum and economical structure. Thus, the use of segmental construction in both concrete and steel bridges has developed in many different directions and will progress to newer developments as the future unfolds.

Publication of this paper sponsored by Committee on Construction of Bridges and Structures.

Full-Span Form Panels for Highway Bridges

CLIFFORD O. HAYS, JR., AND JOHN M. LYBAS

Full-span form-panel bridges are bridges constructed of prestressed, precast panels spanning from pier to pier and covered with a composite topping concrete. This paper describes such full-span bridges. Research consists of field investigations, including corings, analytical modeling, laboratory testing, and field testing. Results demonstrate the safety of bridges designed by using the American Association of State Highway and Transportation Officials effective-width formula and describe details thought capable of reducing cracking observed in existing full-span form-panel bridges.

Bridge construction techniques that reduce the amount of on-site concrete forming generally reduce the cost of the structure. Prefabricated prestressed girders have been in common use for approximately 30 years. However, during much of that time it was general practice to cast the deck in the field by using wooden forms between the girders. Precast stay-in-place forms of concrete and steel replaced the wooden forms in recent years and eventually led to the development of precast composite deck panels, which are prestressed slabs that span between bridge girders and support the cast-in-place topping, thereby eliminating most of the field formwork. Past research (1-5) has led to their widespread acceptance and incorporation into American Association of State Highway and Transportation Officials (AASHTO) specifications (6).

For spans of less than 12 m (39.4 ft), however, the most economical bridge would often be a flat slab without girders. The high cost of formwork for such bridges has led to the development of full-span form panels, which are precast panels that are placed side by side, spanning between adjacent piers or abutments and providing stay-in-place forms for a cast-in-place topping. The scheme is shown in Figures 1 and 2. The Florida Department of Transportation (FDOT) has been a pioneer in the use of such panels and based design procedures on the results of research on deck panels that indicated that full composite action could be developed between the panels and assumed that the distribution of live load on the composite section could be safely given by provisions for flat slabs [6, Section 1.3.2 (C)]. Unfortunately, very regular crack patterns have been observed in full-span bridges. This cracking and associated questions about the design assumptions provided the impetus for the work described in this paper.

The study of full-span form panels included several phases:

1. A general field investigation, including corings;
2. Laboratory testing of one-half scale models;
3. Load testing of an actual bridge in the field;
4. Calculation of model and bridge response by using a linearly elastic finite-element model;
5. Calculation of model response to overload by using a nonlinear discrete-element model; and
6. Calculation of shrinkage stresses by using a finite-element model.

The most important aspects of the study are discussed in this paper. The details of the research are provided in the paper by Hays and others (7).

ON-SITE OBSERVATIONS

A total of nine bridges, which were constructed by the full-span slab method, were inspected. All but one were open to traffic. In addition, bridges constructed by competitive construction techniques (cast-in-place deck and girders with either cast-in-place deck or composite deck panels) were inspected.

Of the bridges constructed with full-span form panels, all exhibited essentially the same patterns of cracking. Longitudinal cracks in the deck were observed over almost every longitudinal panel joint and extended for virtually the full length of the bridge. The only significant exceptions were a few of the longitudinal joints closest to the outside of several bridges. These either did not have the crack or the crack ran intermittently over such joints. These outside joints are, of course, not as likely to have traffic loading. However, the one bridge visited prior to being opened to traffic already had several major longitudinal cracks. Thus, it appears that both shrinkage and traffic influence longitudinal cracking.

In addition to the longitudinal cracks, the decks of most, but not all, bridges were cracked transversely over the piers. However, this cracking was often less pronounced than the longitudinal cracking.

It should be noted that longitudinal cracking was also observed in the decks of bridges constructed by other techniques. For bridges that have panels spanning girder to girder, negative-moment cracking over the girders was observed more often than transverse cracking over the panel joints. For other competitive construction techniques, deck cracking was random and did not exhibit distinctive patterns.

BRIDGE DECK CORINGS

Vertical cores 15.2 cm (6 in) in diameter were taken from the decks of several bridges. Figure 3 shows a core taken over a pier that was midway between two longitudinal joints. The negative-moment crack in the cast-in-place topping, which appears approximately vertical on the top of the figure, does not extend to the reinforcing bar. The interface between the end of the form panel and the cast-in-place concrete over the pier is seen as a straight vertical line in the figure, which indicates a lack of bond on that surface.

Figure 1. Typical elevation of one span of bridge.

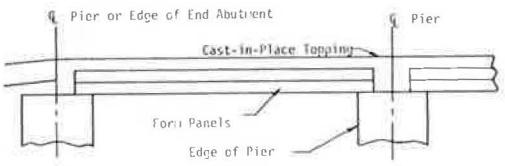

Figure 2. Typical cross section of form-panel bridge.

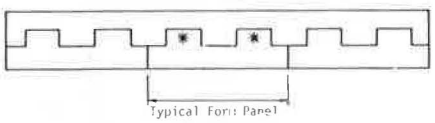

The extensive cracking in the cast-in-place concrete on the right portion of the bottom of Figure 3 occurs where a prestressing strand extends from the precast panel about 5.1 cm (2 in) into the core. During drilling, when one side of the drill was cutting through the prestressing strand, there was no strand on the opposite surface of the core. The resulting stresses caused the cracking around the end of the strand and may have exaggerated the loss of bond along the end of the panel.

Figure 4 shows a core taken above a longitudinal joint at quarter span. The longitudinal crack in the topping is approximately vertical on the top of the figure. A separation between the two form panels is seen in the bottom of the figure. A small amount of concrete and a rope are seen at the joint between the two panels, which indicates that the contractor was using rope to fill a small void between the panels. Both pieces of the panels were separated from the cast-in-place topping during the coring operation. The pieces were reassembled for this figure. However, the interfaces between the form panels and the cast-in-place topping exhibited a clean break that was obviously new and slightly irregular in texture, which indicates reasonable bond.

A number of other corings were obtained in the research, which generally indicated similar patterns of cracking. However, the results are only qualitative due to the high stresses created in drilling the cores.

Figure 3. Core taken at center of panel over pier.

Figure 4. Core taken at quarter span over longitudinal joint.

LABORATORY TESTING

A series of three, one-half scale, two-span continuous bridge deck models were tested in the structural laboratory at the University of Florida. The structures were loaded to failure by concentrated loads that simulated wheel loads. The design load for the slabs was one-half the AASHTO design wheel load of 71 kN (16 kips) and had an impact factor of 1.3.

Test Structures

The configuration of the laboratory tests is shown in Figure 5, and additional information is given in Table 1. The span and thickness of the laboratory models were scaled to one-half the corresponding values for a prototype bridge, while the width of the model was considered to be fully effective in resisting the wheel load. Of course, torsional stresses are much more severe in the model than in a much wider actual bridge deck. Thus, conditions with regard to shear transfer between a loaded and an unloaded panel are more severe in the model than in an actual bridge deck.

The minimum cast-in-place cover allowed by FDOT is 11.4 cm (4.5 in). Thus, the model had a cover of

Figure 5. Laboratory test specimens.

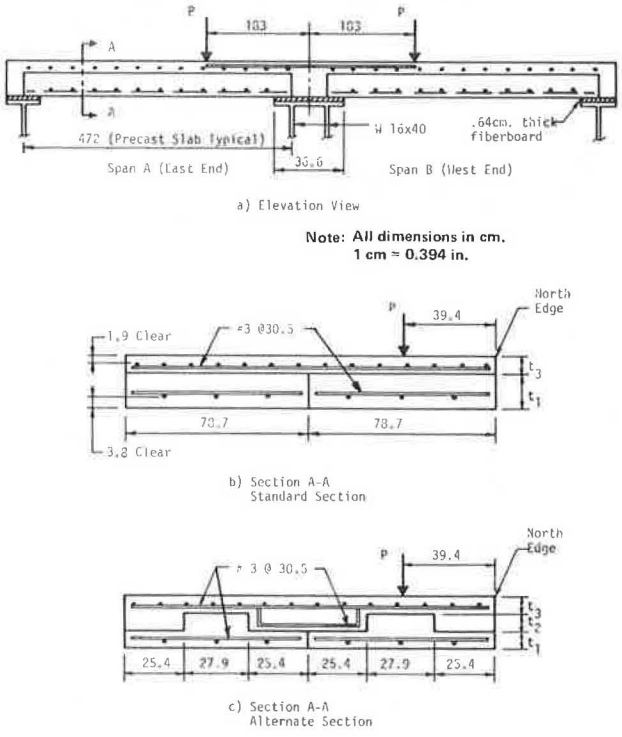

Table 1. Form slab laboratory specimens.

Specimen	Test	Section[a]	Span[a]	t_1[a] (cm)	t_2[a] (cm)	t_3[a] (cm)	No. of Strands in Two Panels[b]	Longitudinal Reinforcement[c] (number of No. 4 bars)
1	1	Standard	A, B	10.2	-	5.7	8	15
2	2	Standard	B	13.3	-	5.7	6	12
		Alternate	A	8.9	4.5	5.7	6	12
3	3, 4	Standard	B	19.1	-	5.7	4	8
		Alternate	A	8.9	10.2	5.7	4	8

Note: 1 cm = 0.394 in.

[a] See Figure 5 for description of section type and span and definitions of t_1, t_2, and t_3.
[b] All were 1.1-cm (0.4375-in) ϕ 1725-MPa (250-ksi) 7-wire strands.
[c] All mild steel reinforcement was grade 60 with a measured average yield stress of 935 MPa (63 ksi).

5.7 cm (2.25 in). Spans in the prototypes are probably most economical in the range of 6-12 m (19.7-39.4 ft). Thus, a laboratory span of 4.6 m (15 ft) was selected.

When the thickness of the slabs is decreased by a factor of one-half, the resulting shear strength is reduced by approximately 50 percent. Thus, the design wheel load for the model was considered to be one-half of that for the prototype. With the load and span each decreased by a factor of one-half, the moments acting at a section of the model are reduced to one-quarter of those for the prototype. It is desirable that the ratio of flexural strength to applied moment for the model be similar to that for the prototype. With the effective depth for the model approximately one-half that of the prototype, the reinforcement areas for the model should be about one-half that of the prototype; they should have the same reinforcement ratios.

In the design of the test structures, analyses were performed for load cases normally considered in the design of the prototype structure. Calculation of stresses under service load were based on elastic theory and were found by adding direct compressive stress due to prestressing, flexural stress due to prestressing, and flexural stress due to applied loads. The precast section was checked for stresses at the time of transfer of the prestress force to the concrete and during construction of the composite section. The composite section was checked for stresses at service traffic loads, which consider live load plus impact. Finally, it was ensured that the flexural strength of the composite section exceeded the moments resulting from the design loads modified by appropriate load factors, as given in Sections 1.2.22, 1.6.9, and 1.6.10 of the AASHTO specifications (6).

The thickness at the edges of the precast slabs was reduced in alternate sections, as indicated in Figure 5 and Table 1, thereby forming an inverted T-shaped slab. Stirrups were placed in the "pocket" that formed between two adjacent slabs (alternate section in Figure 5). It was hoped that this pocket and the stirrups would increase the effective depth of the section across the longitudinal joint and help the bridge act more monolithically. The stirrups were selected to be equal in area to the transverse steel used in the cast-in-place topping. The pocket was dimensioned such that the stirrups would be fully anchored on both sides of the joint.

The transverse reinforcement for the precast panels was the same as that used in the present FDOT specifications and is the minimum requirement for deck panels [6, Section 1.6.26(C)].

The transverse reinforcement for the cast-in-place topping is meant to transfer shear across the longitudinal joint between the precast slabs. Based on the shear-friction concept (8), the shear force is a linear function of the area of steel. Thus, the model that had a load of one-half the load of the prototype had one-half the area of steel used in the prototype.

The major variables in the laboratory tests were the amounts of longitudinal reinforcement in the cast-in-place topping and precast panels, as given in Table 1.

The strengths of the steel reinforcing are given in Table 1. The panels had a design f_c' of 34.5 MPa (5 ksi). However, at the time of testing the specimens, they exhibited an average strength of 41 MPa (6.0 ksi). The cast-in-place topping had a design f_c' of 23.4 MPa (3.4 ksi) and a measured strength of 29 MPa (4.2 ksi).

The precast panels were supplied by a commercial prestressing company. The surface of the slabs was given a broom finish, which appeared quite adequate for bond. Wide flange sections were used as supports for the precast panels (Figure 5); a layer of 0.6-cm (0.25-in) fiberboard was used above and below the supports as a leveling course. The topping was then cast over the present panels and covered with plastic sheets for approximately 48 h after placement. Then the cover and forms were removed and the specimen exposed to the laboratory environment.

For specimens 1 and 2, the topping was cast to form a monolithic unit. However, for specimen 3, a cold joint in the topping was constructed over the longitudinal joint where the precast slabs meet, thus providing a potential cracking plane.

Loading and Instrumentation

The test structures were loaded vertically by one hydraulic jack in each span (see Figures 5 and 6). The distribution of the load was accomplished through 20.3x30.5-cm (8x12-in) bearing plates with rounded corners, which provided an average pressure of 570 kPa (83 psi) under the 35.6-kN (8-kip) design wheel load.

Vertical deflections were measured at the positions shown in Figure 6 by using linear variable differential transformers (LVDTs) and mechanical dial gages. Note that the dial gages were used to measure the settlement of the fiberboard layer in the supports. The correction of the LVDT readings for these base deflections is illustrated in Figure 7. Note that the LVDT readings were with respect to the very slightly cambered position of the specimens prior to the application of the test load. The distance b', which is the part of the deflection due to the translation and rotation of the chord, was subtracted for the total deflection b to obtain the relative (or chord) deflection.

Behavior of Test Structures

Tests 1-3 corresponded to test structures 1-3. The

Figure 6. Location of gages for laboratory tests.

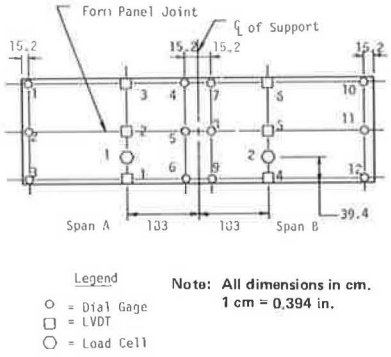

Figure 7. Corrections for chord deflections.

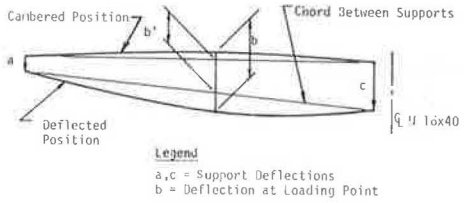

Figure 8. Variation of load with deflection of one span of each laboratory test.

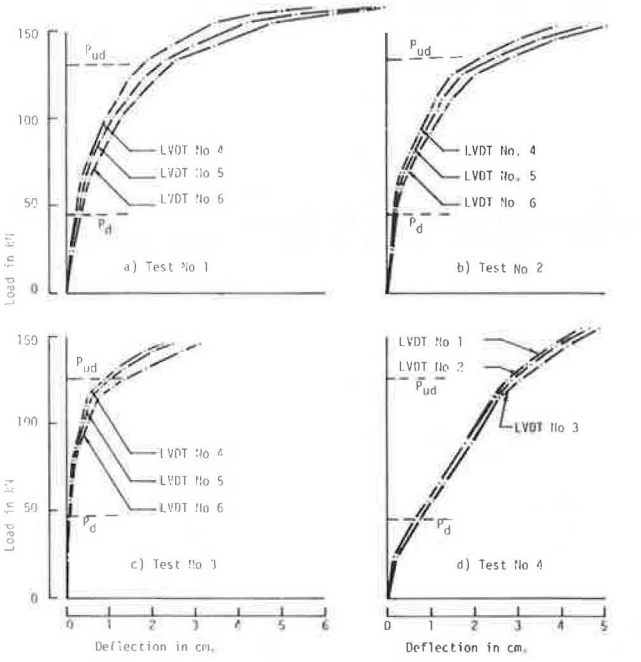

Note: LVDT numbers correspond to Figure 6.
1 cm = 0.394 in, 1 kN = 0.225 kip.

loads in the two spans were constrained to be approximately equal. However, one span failed first in all cases. Test 4 was a retest of the unfailed span of structure 3. For each test, Figure 8 shows the variation of load with deflection for the span that eventually failed. The AASHTO design load P_d and the ultimate flexural strength P_{ud} of the span, as obtained from Sections 1.6.9 and 1.6.10 of the AASHTO specifications (6), are indicated in the plots.

For the first two load increments, which were near the design load, the specimen responded linearly with either no observed cracking or some very minor hairline cracking over the supports that are associated with negative moment. At between 1.5 and 2 times the design load, positive-moment cracks opened in the bottom of the loaded (north) panel and in some cases the unloaded (south) panel. In all cases, positive-moment cracks extended across both the loaded and unloaded panels prior to failure. Before positive-moment cracking was observed, negative-moment cracks were very extensive and extended over the full width of the specimen.

After being extensively cracked, the specimens still increased in load capacity and exhibited good ductility until an inclined crack was observed between the load and the interior support on the edge of the loaded panel. Then, after exceeding the calculated structure strength, a final punching shear failure occurred. Except for the third test, which had a cold joint above the longitudinal joint between the form panels, no longitudinal cracking was observed except in conjunction with the final failure.

In contrast to the other test structures, structure 3 (test 3) had a cold joint in the topping concrete over the longitudinal joint between the precast form panels. For this structure, a longitudinal crack developed in the cold joint. The crack first appeared near the loading plate at a load of about twice the design loading. At failure, the longitudinal crack ran essentially the full length of span B but did not extend into span A (span A had the alternate cross section shown in Figure 5). Final punching failure occurred at a load about 5 percent less than that for test 2 but well above the predicted ultimate strength.

The punching failure for test 3 is shown in Figure 9. The failure mechanism for other test structures was quite similar. In Figure 9, the diagonal crack on the edge of the slab is inclined from the horizontal about 45°, as in a typical beam shear failure. However, where the crack becomes longitudinal in the neighborhood of the load, the surface of the crack forms a very shallow angle with the top surface of the slab and, even where it intersects the longitudinal cold joint in the topping, it does not generally extend below the topping concrete. The failure mechanism appears to be a combination of beam and punching shear and is perhaps aggravated by the loss of shear transfer across the longitudinal cold joint in the topping that is associated with the intersection of the punching crack with that joint.

The good bond between the cast-in-place topping and the form slabs is obvious in that no separation is visible at the 45° shear crack on the side of the slab.

The punching failure was quite sudden and would be cause for concern if not for several reasons. First, failure in all tests occurred after the predicted structure strength had been exceeded considerably and good ductibility was exhibited. Second, torsional response (which greatly increases the shear stresses around the longitudinal joint) is much more severe in the laboratory model than in prototype bridges.

FIELD TESTING

The prototype on which the field-testing phase of this project was performed was the Lloyd Creek Bridge, an eight-span bridge where all the spans are approximately 7 m (23 ft) in length. The precast panels are a constant 17.8 cm (7 in) thick and have a 14-cm (5.5-in) layer of concrete used as the topping.

Figure 9. Shear crack in laboratory specimen.

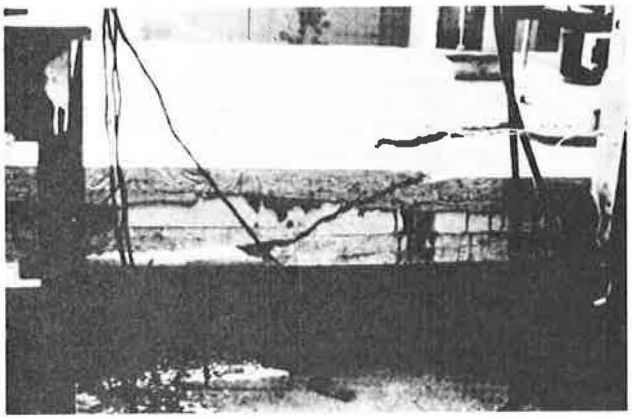

Figure 10. Hydraulic loading for field test.

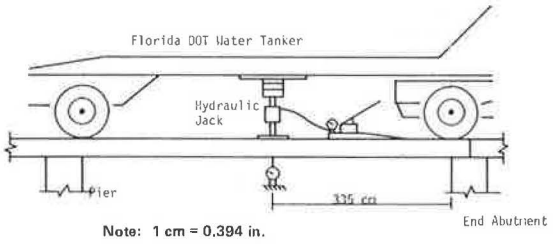

Note: 1 cm = 0.394 in.

Figure 11. Location of gages for field tests.

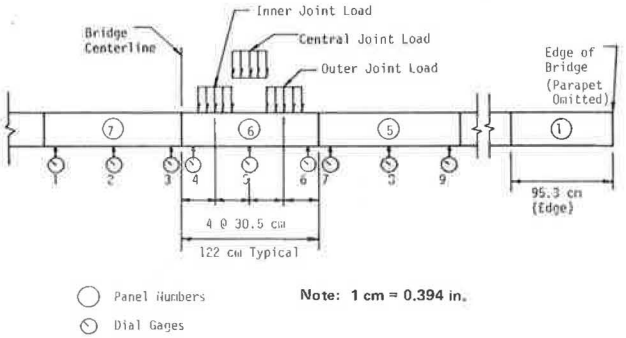

Note: 1 cm = 0.394 in.

Hydraulic Loading

In the first eight tests, load was applied by jacking against the underside of an FDOT tank trailer, as shown in Figure 10. The distance between the wheels of the tractor and trailer was such that two sets of the wheels rested almost completely on the supports. All other wheels were either off the bridge or raised above the slab. With the truck in this position, the load in the piers was virtually constant as the load in the jack varied; thus, support settlement was not a problem. The position of loading relative to the cross section of the bridge is shown in Figure 11. The bridge has 12 panels across a section; panels 1, 5, 6, and 7 are shown in Figure 11. The load was applied to panel 6, which is 3.35 m (11 ft) from the end abutment (Figure 10), at one of three positions in the cross section (the panel centerline) and at 30.5 cm (12 in) from either edge of the panel. These positions will be denoted central load, inner joint load, and outer joint load, as noted in Figure 11.

The loads were applied in increments of 35.6 kN (8 kips) to a maximum load of 142.4 kN (32 kips), roughly 1.5 times the design wheel load, including impact. Distribution of load was obtained by using one of two different bearing plates. The primary one was a 30.5-cm (12-in) diameter plate provided by FDOT. This gave a pressure under the 142.4-kN load of 1950 kPa (283 psi), which was thought to be high. To better simulate a wheel load, several tests were also run with a larger bearing plate. This wheel plate had an elongated central portion and semicircular ends, which followed recommendations by Yoder (9). This plate produced a pressure of 1000 kPa (145 psi) under the 142.4-kN load. Results from using the two different plates were very similar.

Deflection Measurements

By using mechanical dial gages, deflections relative to the ground were measured at the cross section of the application of load and at the positions in the section shown in Figure 11. The positions were either at a panel centerline or 3.8 cm (1.5 in) from a panel edge.

Test Procedure

At the start of each test, the truck was positioned as shown in Figure 10. Deflections were recorded with no load in the hydraulic jack and then after the application of each load increment. The load was then returned to zero and a final set of deflection readings were taken. In general, the initial and final deflection readings were not equal. Because the structure was known to behave elastically under the magnitude of loading applied, the difference was attributed to temperature variations. The deflections for each load increment were adjusted to account for this difference.

Tank-Trailer Loading

In addition to the load test under incremented hydraulic loading, the deflections of the bridge were also measured under the load of the truck itself. The truck was positioned with the rear axle of the trailer directly above the line of dial gages in the end span and the other axles off the bridge. The axle load applied to the span was 115.7 kN (26 kips).

Calculation of Deflections

The internal moments and deflections for the bridge were computed by using a finite-element model (10). The element used was a plate-bending rectangle with three degrees of freedom, vertical deflection, and two rotations at each node. The material was assumed to behave linearly elastically; the thickness of the elements was chosen such that the flexural section stiffness per unit length for the model and for the prototype was equal. In computing the stiffness of the prototype's composite section, the elastic moduli for the various concretes were assumed to be given by ACI 318-77 (8). Computations were performed by using one span that was seven form panels across. The assumption was that, in the actual bridge, form panels far from load would not contribute to the structure response. The continuity of the bridge deck over interior supports was modeled by using vertical and rotational springs. Details on the finite-element model are given in Hays and others (7).

Discussion of Measured and Computed Deflections

The variation of measured vertical displacement across a section of the bridge is shown in Figure 12 for three of the eight hydraulic loading tests for a load of 142.4 kN (32 kips). Computed displacements are shown on the same set of axes. Figure 12 represents results that were typical for the study; the balance of the results are presented in Hays and others (7).

The results shown in Figure 12 are for the three load tests with an outer joint load and a circular bearing plate. Of the two finite-element models considered, B1 was considered a reduced panel thickness for a distance h at the longitudinal joints, as shown in Figure 12, while B2 was considered a uniform thickness.

The measured deflections indicate various amounts of shearing deformations at the longitudinal joints. Considering all eight field tests, test 5 (included in Figure 12) produced the largest differential deflection across the longitudinal joint. This, however, was only 0.013 cm (0.005 in)--approximately 6 percent of the deflection at that point. Deflections measured due to the actual axle load indicated even less differential deflection at the longitudinal joints than those due to the loading through the single bearing plate.

Comparison of the computed and measured results in Figure 12 indicates that the model with a uniform deck thickness (B1) better simulates the overall magnitude of bridge deck deflection. However, the model with reduced thickness at the longitudinal joints (B2) is much better at simulating the shape of the variation of deflection across the section.

The fact that model B2 overpredicted the magnitudes of deflections indicated that it had a lower stiffness than the actual bridge. This may be attributed primarily to two factors. First, the elastic modulus of concrete for the model was computed by using the nominal or design value of f_c'. The actual value of E is probably larger than the value so computed. Second, the model considered only the loaded panel and three panels on either side, thereby neglecting a total of five outer panels of the bridge. Thus, using the reduced-thickness model along with a more accurate modulus of elasticity would be expected to give quite good deflection profiles.

Computed Moment Distributions

Longitudinal bending moments in the bridge deck were computed by using the finite-element model. Figure 13 shows the distribution of these moments over the cross section of the span where the loads were applied in the field tests, i.e., the same section considered for deflections in Figure 12. Results are shown [for a load of 142.4 kN (32 kips)] for two previously defined load positions and two variations of the model.

As shown in Figure 13, the model that considers reduced deck thickness at the longitudinal joints produced discontinuities in moment at the abrupt changes in deck thickness, the moments in the reduced-thickness region being approximately 2 percent of the adjacent moments. Furthermore, the maximum moments for the longitudinal joint model were 26-33 percent greater than those for the uniform-thickness model. The moments at edges of the finite-element model were less than 30 percent of those in the loaded panel, which indicated that the finite-element model (7 panels in width) was a reasonable representation of the actual bridge, which was 12 panels in width.

Finally, the computed longitudinal moments have implications for the AASHTO effective-width formula. Consider two wheel loads 6-ft center to center at a particular cross section of the span, as would be the case for the two tires on one axle of a trailer. Referring to Figure 14, if the outer joint load is one of the two wheel loads, the other load will be centered at point A. The maximum moment in the section will occur near the outer joint load and will be the sum of the moments caused by each of the two loads. By Maxwell's law, the moment at the outer joint load due to the load at A is equal to the moment at A due to the outer joint load, which

Figure 12. Deflections across transverse section.

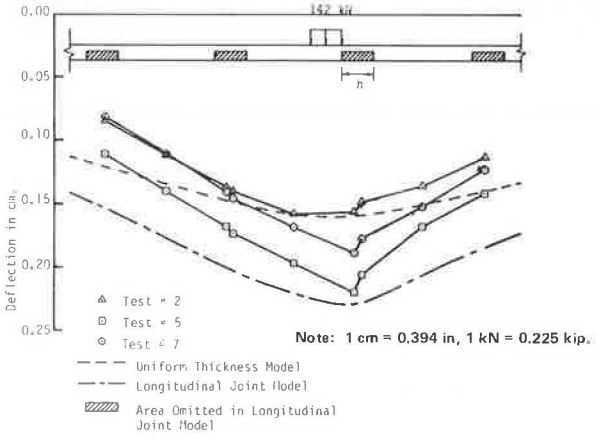

Figure 13. Longitudinal moments across transverse section at applied load.

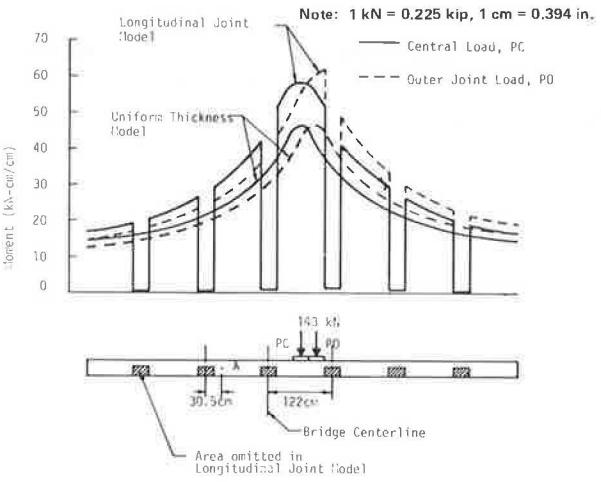

Figure 14. Proposed detail of full-span form panels.

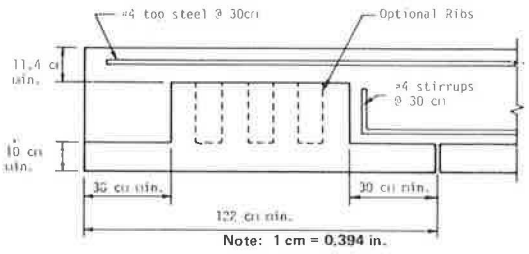

(from Figure 14) is approximately 26 kN-cm/cm (5.8 kip-in/in). The maximum moment due to the outer joint load is approximately 62 kN-cm/cm (13.9 kip-in/in). The sum is 88 kN-cm/cm (19.8 kip-in/in). Considering the AASHTO effective-width formula, along with a linearly elastic beam analysis for a single 142.4-kN (32-kip) load positioned along the span as for the finite-element analysis, the resulting maximum longitudinal moment at the cross section of the load is 125.9 kN-cm/cm (28.3 kip-in/in). Hence, the finite-element model implies that the AASHTO effective-width formula is conservative. A similar comparison for negative moments at a support (7) indicates even more conservatism in the AASHTO formula.

CONCLUSIONS AND DESIGN RECOMMENDATIONS

The following conclusions and practical recommendations were derived from the study described in this paper.

1. With reasonable surface treatment of the precast panels, loss of bond between the panels and the cast-in-place topping should not be a problem. A broom finish of the panels, along with wetting prior to placing the topping concrete, should result in excellent bond. A minimal amount of shear reinforcement would provide added assurance.
2. Shrinkage stresses induced in the topping concrete during curing are likely to be large enough to cause cracking, especially longitudinal cracking over the longitudinal joints between form panels (7).
3. It appears that the AASHTO effective-width formula is adequate for determining the design longitudinal moments due to live load. However, because there is some increase in peak elastic moment compared with a poured-in-place solid slab, it is recommended that a minimum panel width of 122 cm (48 in) be established. Panels with smaller widths that are designed by the effective-width formula would have adequate ultimate strength. However, such panels might be highly stressed under moderate overload.
4. It appears that the minimum transverse reinforcement in the topping of No. 4 bars at 30-cm (12-in) center-to-center, along with the minimum topping thickness of 11.4 cm (4.5 in), will provide adequate shear transfer over the longitudinal joint between adjacent panels. However, the joint detail shown in Figure 14 should provide improved performance in regard to longitudinal cracking and load transfer. The figure depicts the cross section of one form panel and part of the adjacent panel. The thickness of each form panel is reduced adjacent to the joint, thereby providing a larger thickness of cast-in-place topping over the longitudinal joint. Stirrups should then be placed in the topping over the joint to further improve load transfer. A reduced thickness of approximately 10 cm (4 in) should be sufficient to resist stresses in the precast panel yet provide improved joint behavior. The 30-cm width of the reduced-thickness portion is sufficient for anchorage of No. 4 stirrups at 30-cm center-to-center and allows tolerance on placing the stirrups in the pocket. The center portion of the panel could be either ribbed, as shown by dashed lines, or flat.
5. The present detail at the piers and end abutments is similar to that in Figure 5, except that the flexible bearing pads extend only under the precast panels. An improved detail that has more positive transfer of shear from panels to supports is needed to reduce deformation and cracking in the region of the support and to increase the overall stiffness of the bridge. This could be accomplished by placing horizontal shear keys in the ends of the precast panels or by providing for some direct bearing of the panels on cast-in-place concrete over the supports.
6. Reinforcement for positive transverse moment over the piers should be provided in accordance with Obranic (10). However, it is possible that with the increased shear transfer on the ends of the panel, some minor positive-moment cracking over the piers would not be too detrimental.

In summary, the full-span form-panel bridges visited during field investigations are quite safe and, based on the findings of this research, are in no danger of failure. However, one or two of the more highly traveled bridges might experience some maintenance problems in the future due to the cracking in the deck. Future bridges built with the recommended details should be equivalent to conventional, more expensive cast-in-place flat slabs not only in strength, but also in serviceability.

ACKNOWLEDGMENT

We would like to acknowledge FDOT for its financial support of the research on which this paper is based. Also, two graduate students--R.L. Cox, Jr., and G.O. Obranic, Jr.--worked long and diligently on the research and are owed a special thanks.

The opinions, findings, and conclusions are ours and not necessarily those of FDOT.

REFERENCES

1. R.M. Barnoff and D.E. Rainey. Laboratory Tests for Prestressed Concrete Deck Panels and Deck Plank Assemblies. Pennsylvania Transportation Institute, Pennsylvania State Univ., University Park, June 1974.
2. E. Buth, H.L. Furr, and H.L. Jones. Evaluation of a Prestressed Panel, Cast-in-Place Concrete Bridge. Texas Transportation Institute, Texas A&M Univ., College Station, Sept. 1972.
3. R.W. Kluge and H.A. Sawyer. Interacting Pretensioned Concrete Form Panels for Bridge Decks. Engineering and Industrial Experimentation Station, Department of Civil Engineering, Univ. of Florida, Gainesville, Final Rept. D610-635F, 1974.
4. R.W. Kluge and H.A. Sawyer. Interacting Pretensioned Concrete Form Panels for Bridge Decks. PCI Journal, Vol. 20, No. 3, May/June 1975, p. 34.
5. H.A. Sawyer and J.-B. Dansby. Transverse Reinforcement in Pretensioned Concrete Form Panels for Bridge Decks. Engineering and Industrial Experimentation Station, Department of Civil Engineering, Univ. of Florida, Gainesville, Progress Rept. D635P, 1974.
6. Standard Specifications for Highway Bridges, 12th ed. AASHTO, Washington, DC, 1977.
7. C.O. Hays, R.L. Cox, and G.O. Obranic. Full Span Form Panels for Short Span Highway Bridges. Engineering and Industrial Experimentation Station, Department of Civil Engineering, Univ. of Florida, Gainesville, Final Rept. U17F, Sept. 1980.
8. Building Code Requirements for Reinforced Concrete (ACI 318-77). American Concrete Institute, Detroit, 1977.
9. E.J. Yoder. Principles of Pavement Design. Wiley, New York, 1959.
10. G.O. Obranic. Analysis of Composite Bridge Decks with Pretensioned Concrete Form Panels. Univ. of Florida, Gainesville, Master of Engineering thesis, 1980.

Publication of this paper sponsored by Committee on Construction of Bridges and Structures.

Precast Concrete Deck Modules for Bridge Deck Reconstruction

CHARLES SLAVIS

Replacement of deteriorated and obsolete bridge decks is requiring increased attention from design and construction engineers. The need to shorten the time the bridge is closed to traffic has led to the use of precast concrete deck systems. Their value is demonstrated on bridges that must carry traffic for some portion of every 24-h period. Precast deck modules have been used on such diverse projects as expressway bridges in Pennsylvania and California and railroad bridges in British Columbia and Delaware. The Santa Fe Railroad has begun a multiyear program to replace timber decks with precast concrete on its 32 miles of bridges that have timber-deck and steel-girder designs. The precast deck modules used on these projects were produced at the site or produced at multipurpose plants and shipped to the bridge site. Placement was made with combinations of welded, epoxy, and cement-grouted connections. This paper reports on the state of the art of precast concrete deck replacements, their application in reconstruction, and their influence on deck design in new construction.

The deterioration of bridge decks, which is accelerated by the extensive use of salt for snow and ice control, has required the bridge engineer to address the question of repair versus replacement. Both options must consider the maintenance of traffic during construction and how this consideration affects cost. Where extensive repair is necessary and traffic maintenance is difficult as well as critical, the replacement option of using precast deck modules may prove very practical. This has been the case where a section of deck has been removed, a replacement section added, and traffic allowed to use the bridge during some portion of every 24-h period. In the case of highway bridges, the time allotment is controlled by peak traffic demand. In the case of railroad bridges, the time allotment is controlled by systemwide demand and scheduling.

Precast deck modules have also been used on long bridges to ensure that deck replacement was completed during a single construction season. This has even proved to be the most economical deck-construction method for some new bridges. The highway departments of Indiana and New York and the New York Thruway Authority were among the first agencies to use precast modules in field experiments with new bridges or deck replacement.

Precast deck modules share some common considerations, regardless of their application. The most important of these are design considerations: where the modules will be cast, how they will be transported, and what construction procedures will be used. These factors, along with structural requirements and any restrictions on time availability (either per 24-h period or per construction season), must be considered by the design engineer. A close look at several individual projects illustrates how these factors vary from project to project.

PENNSYLVANIA TURNPIKE

The Pennsylvania Turnpike had a 1627-ft-long bridge on its northeast extension in need of deck replacement. The distance between the bridge and the ground below reached a maximum of 140 ft (Figure 1). The existing bridge consisted of a concrete deck on steel girders. The design engineers concluded that precast deck modules were the best alternative. The modules allowed minimum personnel at the bridge site, where there was danger of construction at 140 ft aboveground. They also provided rapid erection to ensure completion of each parallel half of the bridge in a single construction season.

The modules were cast off site in a plant where production conditions allowed the use of a lower water-cement ratio concrete mix, more precise vibration, and a more controlled curing operation. The 7-ft 6.25-in by 28-ft 8-in by 6.75-in slabs, each weighing 18 000 lb, were trucked to the site as needed (Figure 2) and lifted directly into place (Figure 3). No on-site storage was necessary.

Because traffic was being maintained on one-half of the bridge for the length of the construction season, the removal of the old deck could proceed well in advance of the redecking operation. This made the task of preparing the girders to receive the precast modules much less complicated. The contractor placed slabs at the rate of 6 modules/day and completed slab placement in less than two months (Figure 4). Connection of the module was made by using epoxy mortar spread over the top flange of the

Figure 1. Pennsylvania Turnpike bridge.

Figure 2. Precast modules are trucked to placement site on operating half of bridge.

Figure 3. Modules are lifted from truck and placed directly on prepared girders.

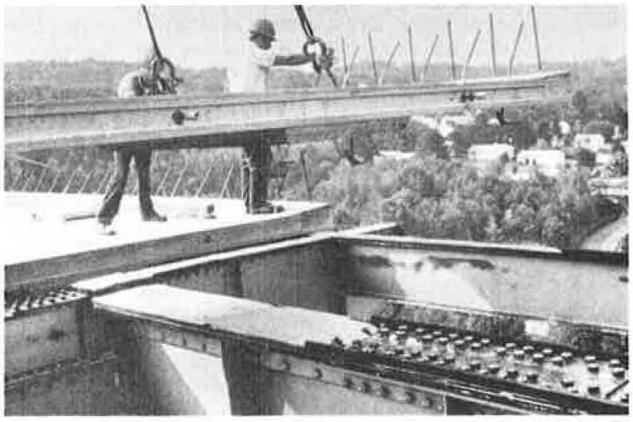

Figure 4. Placed modules were finished with cast-in-place parapet and latex-modified concrete wearing surface.

girder and supplemented by bolted spring clips located near the edge of each module. The final wearing surface on the bridge consisted of 1.25-in latex-modified concrete.

RAILROAD BRIDGES

The Santa Fe Railroad has undertaken a program of bridge deck replacement that has a different set of criteria but results in an operation very similar to the Pennsylvania Turnpike bridge. The deck to be replaced on the Santa Fe was not a single deck but a deck type that consisted of timber decking on steel-girder bridges. There is a total of 32 miles of this type of deck spread out over the more than 12 000 miles of the system. The basic deck module selected was 8 ft by 14 ft by 8 in and weighed about 6 tons. It was designed for a Cooper's E80 loading and was cast at a commercial prestressing plant in Albuquerque, New Mexico. The location of the plant on the Santa Fe line allowed transportation throughout the system, while maintaining the quality control that results from a plant-cast operation.

The Santa Fe redecking has some variations, depending on whether the deck to be replaced can be taken out of service for only several hours at a time (as in single-track territory) or for several days (as in double-track territory). The field operation is basically the same, but only a short section of the bridge is done at a time in single-track territory. The required steps consist of removing the rail, ballast, and timber deck; preparing the girders; placing the precast deck modules; and replacing the track (Figures 5-7). The use of an epoxy mortar spread on the girder was the only connection provided between the modules and the girder.

Although the total deck-replacement operation is easily defined with a single-track bridge, thorough planning must be combined with knowledgeable and efficient construction to ensure that the track is available for service within the 4- to 6-h time allotment.

The Santa Fe is not the only railroad to make use of precast concrete in replacing bridge decks. Ca-

Figure 5. After cleaning, girders were coated with epoxy grout to bond modules to girders.

Figure 6. Precast modules are cleaned prior to placement to ensure that epoxy grout will bond.

nadian Pacific replaced the deck on a 402-ft-long bridge near Revelstoke, British Columbia, while interrupting traffic for two separate, preassigned 12-h periods. The National Railroad Passenger Corporation (Amtrak) also used eight precast deck modules, complete with monolithic ballast curbs, to replace a deteriorated concrete deck on a single-track bridge near Newark, Delaware.

Figure 7. Final operation is addition of wood curbs and replacement of ties, ballast, and track.

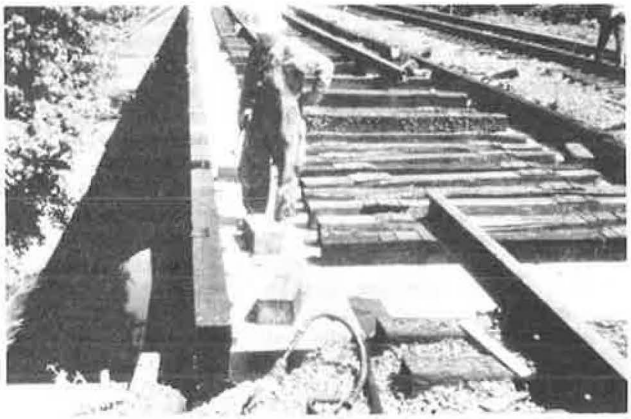

Figure 8. Casting bed was set up adjacent to bridge site.

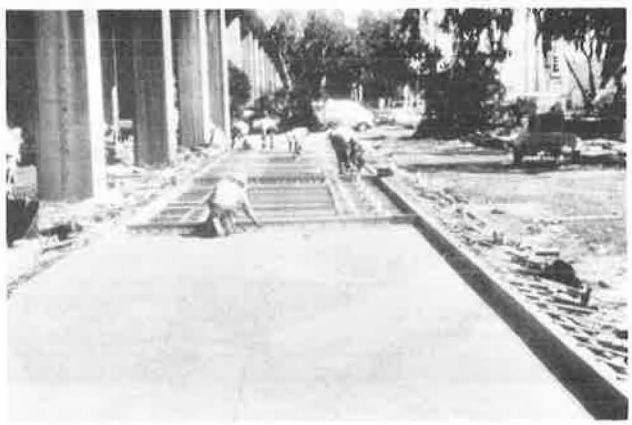

Figure 9. Existing deck is removed as part of each day's operation.

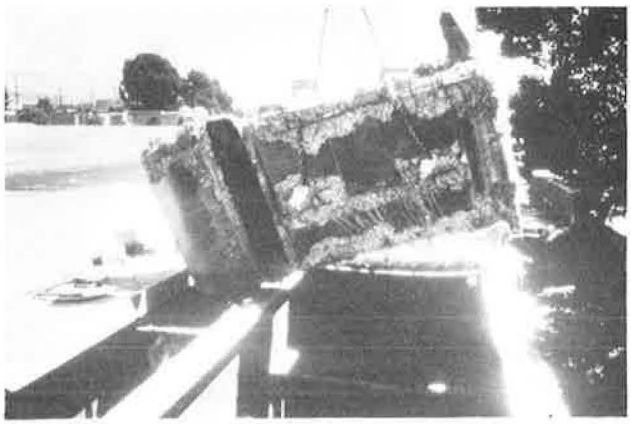

HIGH STREET OVERHEAD

The phasing of deck replacement within a prescribed time slot out of each 24-h period is not limited to the railroad industry. Repair work on modern urban freeways often takes place with all lanes operating at full capacity during peak hours. An excellent example of bridge deck replacement under such conditions was the High Street Overhead, which is a 1750-ft structure on CA-17 within the City of Oakland.

The High Street Overhead is a 32-span structure and has individual spans that range in length from 30 to 75 ft. The California Department of Transportation undertook a detailed study that resulted in the deck replacement of the outside southbound lane. Critical factors in the decision to use precast deck modules included average daily traffic in excess of 170 000 vehicles, heavy congestion during peak evening commute hours, and the lack of a practical means to provide a detour to accommodate the lost capacity resulting from the required lane closures.

The actual contract for the High Street bridge deck replacement required the contractor to have the outside southbound lane available for peak-hour traffic between 2:00 and 6:00 p.m. each weekday. There were also lane-closure restrictions on some weekends. The resulting schedule gave the contractor 20 h each weekday plus some weekends.

In addition to the severe time restrictions, there were several elements that distinguished the High Street deck replacement from other construction jobs. The contractor selected to set up a casting operation on the site, which was adjacent to the bridge (Figure 8). This eliminated any size restrictions on the modules necessitated by the need to transport them from a plant. The finished size of the modules was then dictated by the requirements of the structure and also by the ability and lifting capacity of the contractor's crew and equipment (Figures 9 and 10). Connection was provided with shear connectors welded to the girders and grouted into holes in the modules. Another element that required special attention was the deck surface. Unlike railroad bridges, which are covered with ballast, or total bridge projects, which conclude with paving the entire deck, the 20-h limitation required that tolerances on the deck modules ensure a finished surface capable of handling traffic at the commencement of each day's peak traffic period (Figure 11). The success of the High Street deck re-

Figure 10. Precast deck modules, complete with safety shape parapet, are lifted into place.

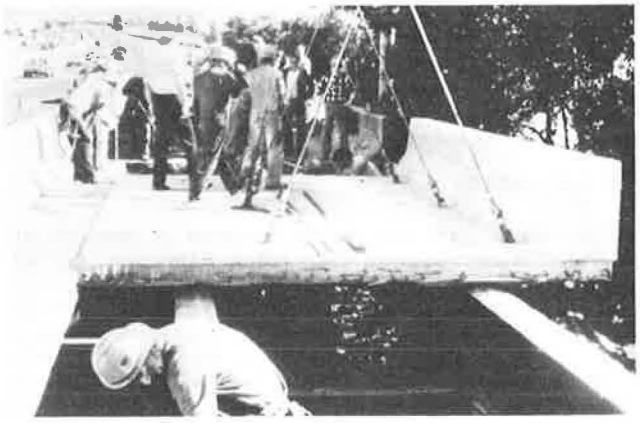

Figure 11. New deck is reopened to traffic during weekday peak period.

placement shows how advanced planning, engineering, project management, and quality control combine to result in a thoroughly successful project.

BENEFITS

Before discussing current research and anticipated future uses, a review of the established benefits of precast deck modules is in order. The most recognized benefit is erection time, which is more limited by economics than by any physical constraint of current technology. On-site casting and heavy lift equipment make projects even more impressive than High Street feasible when time restraints provide the necessary economic justification. If the engineer recognizes the prospective contractor's capabilities and designs the bridge accordingly, more economical designs will result. Further savings may be obtained if provision is made to allow contractor-proposed changes. This can be accomplished by including a value-engineering clause in the contract documents. The ability to cast modules to tolerances that can be used without need of further surfacing is another benefit that is available if economically justified. The benefits associated with quality control of precasting should also be considered.

FURTHER RESEARCH

The total number of bridges that have been redecked by using precast concrete deck modules is relatively small. The advantages of precast modules will not be fully realized until bridge engineers' concerns about the fatigue behavior and durability of the connections are answered. To this end, the Federal Highway Administration (FHWA) has sponsored research on connections, which supplements research and experiments associated with some early precast deck and modular deck installations. Although it is too early to report on the FHWA study, some of the earlier experimental decks were installed in 1973 and 1974, and the various deck-to-girder connectors are still performing as designed. Some problems have occurred in preventing moisture leakage between adjacent slabs where dry joints were used in early installations, but the use of a sand and cement grout or epoxy mortar in the joints seems to prevent this problem. The long-term durability of grout or mortar must still be determined.

The use of precast modules has been limited to steel-girder bridges in redecking applications, as bridges with prestressed concrete girders have not existed in large numbers until recent years. In anticipation of increased use of precast modules for deck replacement on this bridge design, the FHWA study includes connectors for modules to concrete girders.

CONCLUSION

The development of precast modules for deck replacement has both influenced and been influenced by the development of precast deck components for use in new construction. The use of prestressed concrete stay-in-place forms showed the advantages of both speed and safety in using precast components in bridge deck construction. The outcome of this is the development of the precast segmental box-girder bridge that has an integral wearing surface included in the precast segments. This cross-influence of precast bridge components can also be seen in the Florida Department of Transportation's current experiments with deck modules for short-span bridges. The Florida modules are full-span panels that are connected laterally to form a bridge deck. They are used without girders and, in effect, are a precast-slab-type bridge. These experimental modules have included integral decks or have had the deck cast in place once the modules are erected.

Precast, prestressed concrete is and will continue to be useful to the bridge engineer in designing for both new construction and reconstruction.

Publication of this paper sponsored by Committee on Construction of Bridges and Structures.

Eleven-Year Performance of Two Precast, Prestressed Concrete Bridge Decks

CHARLES F. SCHOLER

The widespread deterioration of bridge decks was recognized as a severe problem on Indiana highways in the 1960s. The concept that high-quality concrete would reduce the problem but is difficult to obtain in field-placement situations led to the development and evaluation of precast concrete bridge decks. Two decks that were precast and pretensioned were trucked to the construction sites. There they were erected, posttensioned, and connected to the supporting elements. One deck was a replacement on an existing structure. The other was on a new structure. Traffic ran on the surface of the concrete. No overlays were, or have been, placed on either structure. A careful survey of each structure after 11 years of service indicates that appearance and performance are little changed over this period of time. No spalling, cracking, or rust staining is apparent from the prestressing steel. Low maintenance, fast assembly or disassembly, and a good ride make the method worthy of consideration for many bridge deck applications.

This paper is a performance report on two precast, prestressed concrete bridge decks that have been carrying traffic for 11 years. The concrete surfaces are exposed to traffic and are giving good performance. One deck was a replacement for an old deck on an existing bridge and the other was placed on a new structure.

A completed deck consisted of precast concrete pieces. Each had a minimum thickness of 6 in, was as long as the transverse dimension of the bridge, and was at least 4 ft wide. The pretensioned slabs were placed transversely to the bridge girders and clamped to the top flanges of the girders by means of spring clips and bolts screwed into preset anchors in the concrete. A pretensioning stress was applied in the longitudinal direction of the slabs at a level intended to maintain compression stress in the concrete under full design load-bending stresses. The concrete slabs were posttensioned in the longitudinal direction of the bridge by using rubber-encased cables strung through preformed slab ducts. A thin neoprene sheet placed between the slabs minimized the stress concentrations due to surface irregularities. The neoprene sheet and the nominal posttensioning stress of approximately 80 psi were sometimes helpful in preventing water movement through the joints.

The concept of precast bridge decks was brought about because of the severe deterioration of concrete decks on many bridges in the State of Indiana. This was evident by the mid-1960s.

A major impetus for this work was the belief that the durability of bridge decks is greatly enhanced by high-quality concrete (i.e., concrete that has a low water-cement ratio), is well air entrained, well consolidated, well cured, and with steel accurately positioned. These requirements are frequently difficult to obtain under field-construction conditions; hence, precasting the deck would increase the probability of a high-quality product. The satisfactory performance of these two decks, which were exposed to traffic and routine winter maintenance, indicates that this belief is correct. The initial investigation toward the use of these decks commenced in 1967 as a Highway Planning and Research Program (HPR) study with a laboratory study of its feasibility (1).

In 1969, the HPR study was extended to include construction of an experimental bridge deck in the field and to test, observe, and evaluate its performance over the next few years. It evolved that two decks were included in the investigation. The first was a replacement deck for an existing bridge on IN-37 near Bloomington, Indiana, and the other was a deck for a new bridge on IN-140 near Knightstown, Indiana. Both were installed during the summer of 1970. Both were periodically monitored through the use of strain gages until 1973.

Details of the installation and performance, as measured by the strain gages installed on the decks and supporting elements, were reported by Kropp in 1973 (2).

Casting of the concrete decks was done in beds designed for box girders; thus, the widths were limited. The joints were a modified tongue and groove and were formed by casting against sheet-metal

Figure 1. Old deck is broken up and dropped onto underlying creek bed.

Figure 2. Existing beam and stringers were adjusted in elevation to accommodate flat-cast deck segment.

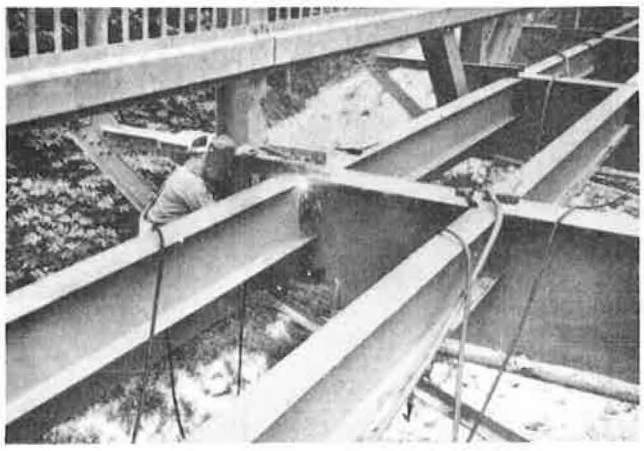

forms. The resulting irregularities resulted in imperfect fits; hence, water would later leak through some joint locations and, in extreme cases, spalling due to high stress concentrations occurred during posttensioning. Although it was a concern at the time, it has not progressed or caused further problems over the 11 years of service.

To better understand the concept of the precast, prestressed concrete bridge decks, Figures 1 through 15 detail their fabrication, erection, and performance over the past 11 years.

The Knightstown deck had an epoxy sealer applied to it by maintenance forces during the first summer. This material is now flaking away from the shoulder area and is no longer apparent within the wheel paths. Concrete quality is good, and the only deterioration in the decks is small spalls at the lips of the joints. Many of these were damaged at the time of construction, as has been mentioned earlier, but the repairs have not held up as well as those at Bloomington. Minor repair is needed at several locations. One spall due to steel corrosion occurred, but it is not connected to the prestressing steel. Rather, it appears to be a bar, which was possibly used to position the small tubes that were later to accommodate the posttensioning steel. This single location needs a repair in excess of the bituminous cold mix that had been placed to smooth out the spalls at the lips of the joints.

The performance of the concrete and the deck system has been successful for the past 11.5 years. No indications of severe distress in the near future have been found on these structures.

It is concluded that precast decks offer an excellent method of obtaining quality concrete and quality deck performance. The construction sequence is such that the method could be used for rapid replacements of decks, if that was desirable. Also, many operations could be done simultaneously.

Load tests conducted over the first 2.5 years of deck service indicated no significant changes in the performance of the decks. The decks do not have a rough or objectionable ride. Drivers do not realize they are passing over a unique deck system. Also, these decks could be overlaid and likely will be in future years.

Figure 3. Precast deck elements are placed as deck replacement. End elements had blockouts to accommodate posttensioning anchors, and were later filled with epoxy mortar.

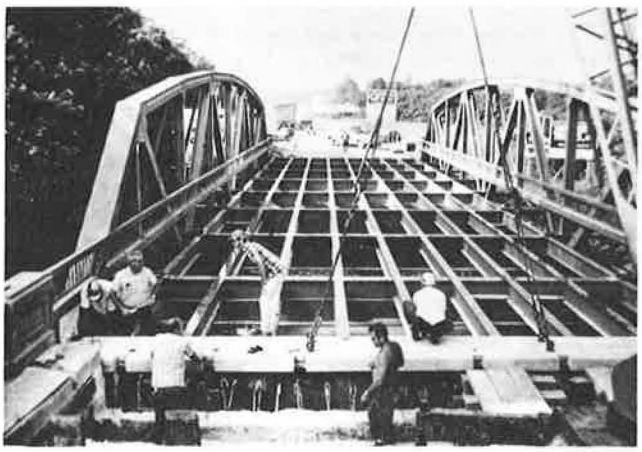

Figure 4. Precast, prestressed deck elements are positioned directly from delivery truck.

Figure 5. Completed deck near Bloomington prior to opening to traffic, 1970.

Figure 6. Precast deck near Bloomington after 11 years of service. No wearing surface or protective coating has been applied to deck. Rubber expansion joint shown here has performed well; however, southbound lane's joint has been damaged, probably by a snow plow.

Recommendations for further implementation of this concept are that flat butt joints be used to reduce spalling at joints and that, when replacement decks are urgently needed, the contractors be provided with incentives for rapid removal of old concrete, placement of new deck elements, and preparation of the approaches.

ACKNOWLEDGMENT

I acknowledge the Joint Highway Research Program, Engineering Experiment Station, Purdue University,

Figure 7. End element showing epoxy-mortar-filled blockouts as it appeared after 11 years of service.

Figure 8. Minor damage to lips of female joints occurred during construction when a steel-wheeled roller placing asphalt on the approach backed onto bridge. Epoxy repair is still performing well.

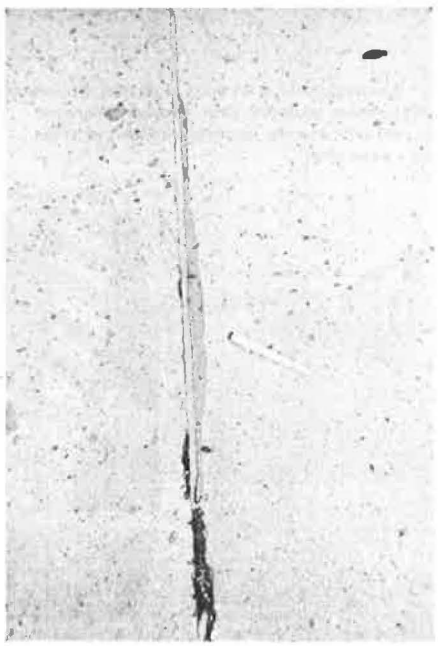

Figure 9. Only deck area that has required maintenance is a small spall. Filled lifting points are also visible.

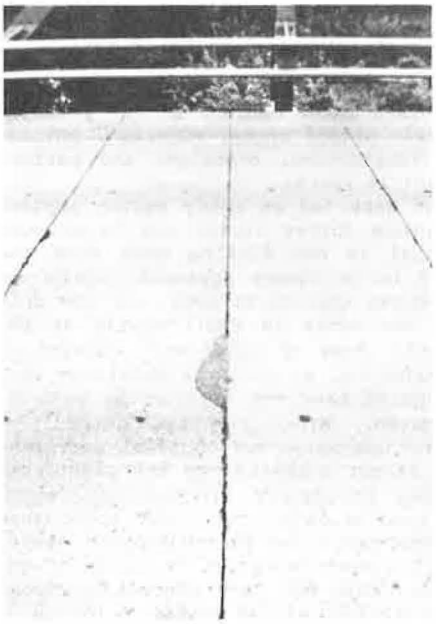

Figure 10. Knightstown deck was designed with built-in crown and with stirrups at ends of each slab to accommodate cast-in-place curb.

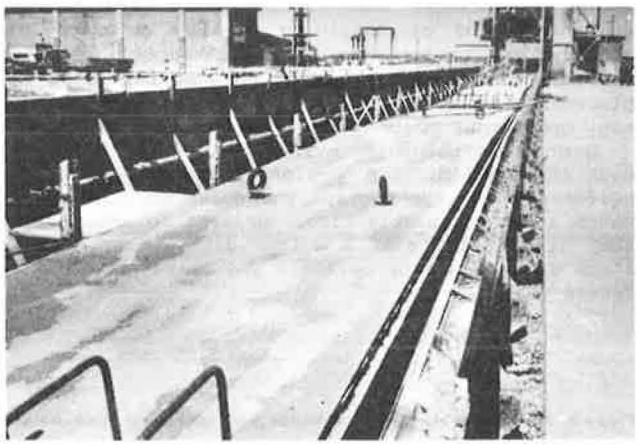

Figure 11. Erection of Knightstown deck was started at center of span; lifting was done with one crane, but two were used for positioning elements.

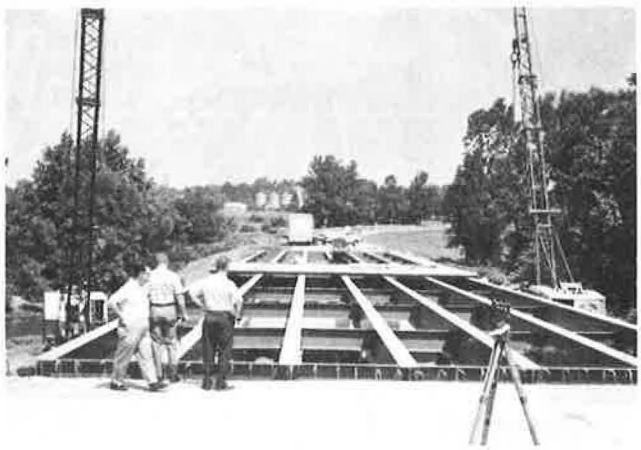

Figure 12. Slabs were fastened to underlying steel with rail clips. Clips were not entirely placed or tightened until posttensioning was completed.

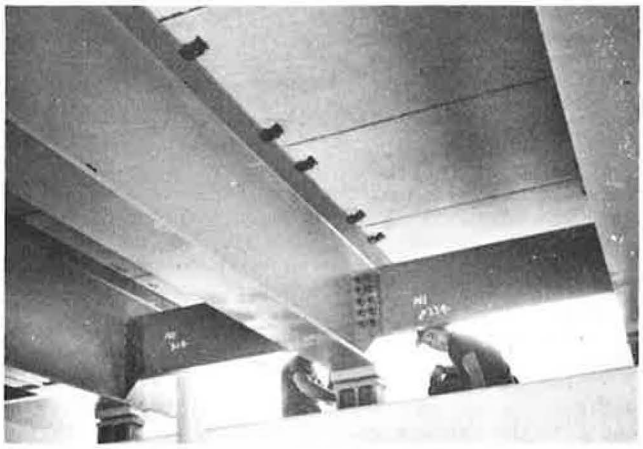

Figure 13. View of final posttensioning operation taking place in 1970.

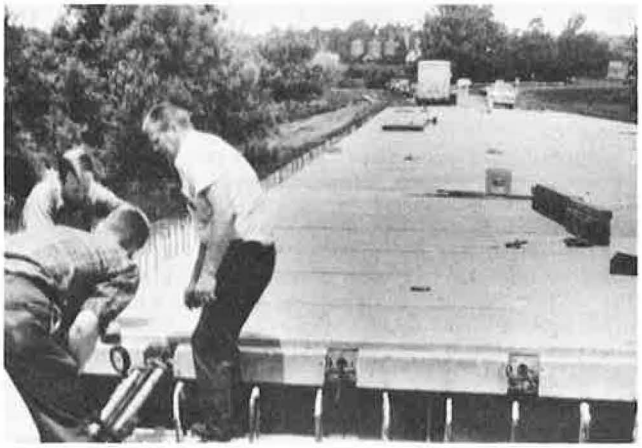

Figure 14. Northbound view of Knightstown bridge deck after 11 years of service.

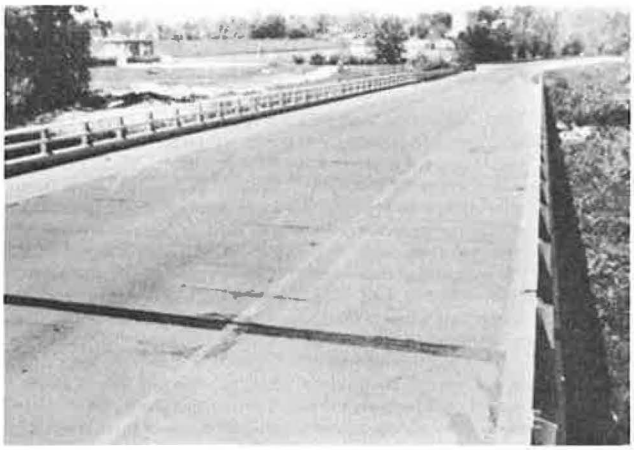

Figure 15. Underside of precast, prestressed, posttensioned deck elements at Knightstown shows clips and water stains on bottom of slabs. Neoprene strips and joint filler were not effective in preventing water from passing through joints.

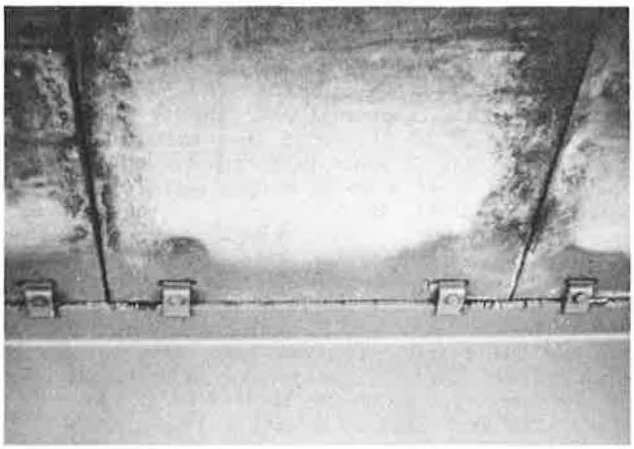

that, in cooperation with the Indiana Department of Highways and the Federal Highway Administration, U.S. Department of Transportation, sponsored the research and constructed the precast, prestressed bridge decks. I further express my appreciation to my colleague, M.J. Gutzwiller, for his counsel and for making the presentation of this paper at the January 1982 Transportation Research Board Annual Meeting.

REFERENCES

1. J.H. Ford. Use of Precast-Prestressed Concrete for Bridge Decks. Joint Highway Research Program, Purdue Univ., West Lafayette, IN, Rept. 20, July 1969.
2. P.K. Kropp. Use of Precast-Prestressed Concrete for Bridge Decks. Joint Highway Research Program, Purdue Univ., West Lafayette, IN, Rept. 7, March 1973.

Publication of this paper sponsored by Committee on Construction of Bridges and Structures.

BEBO Concrete Arch Structural System

NEAL FITZSIMONS

In December 1969, U.S. Patent 3,482,406 was issued to cover a new concept of using precast concrete. Normally considered a rigid material, the precast concrete is placed in a state of "flexible stability" to attain a safe and efficaceous earth-covered structure for spanning up to about 60 ft under fills of from less than 2 ft to more than 40 ft and service loads in excess of 300 tons. The key to the in-service success of the Beton Bogen (BEBO) concrete arch, which was originally tested in 1966, is the balancing of arch deformations against the counterdeformation action of passive earth pressures generated by the deformation of the uniform arch ring itself. The engineering problem was to design a standardized system that attained this balanced result over a range of practical spans. Further, the system had to be easily fabricated, transported, and placed; able to sustain lateral forces generated by asymmetrical backfilling and compaction operations; and, once in service, be virtually maintenance free. To date, 76 bridges have been built by using the BEBO system in Europe and the Near East under a wide variety of foundation conditions. Some of these projects included multispan designs, but only a very few required wingwalls. The system has been successfully adapted for nine underground garages by using reinforced concrete ties. The usual span for these structures is 60 ft, and they have overhead clearances of 10 ft. Since its original 1966 prototype structure, the BEBO system has been modified and improved, but its basic successful concept has been retained. Postconstruction performance has substantiated original expectations, and competitive bidding has demonstrated its economy of construction.

Of the 566 000 bridges in the inventory of the Federal Highway Administration (FHWA), more than 212 000 have been designated as deficient either structurally or functionally. Many of these have spans less than 55 ft. With this fact in mind, it was decided that it would be worthwhile to study the Americanization of a Swiss bridge system called the Beton Bogen (BEBO) concrete arch. The BEBO concept was developed by a Swiss civil engineer, Werner Heierli, who was familiar with the phenomenon of soil-structure interaction through his studies at the Massachusetts Institute of Technology in 1961 and 1962. In 1966, a full-scale test structure was erected and tested near his home city of Zurich (Figure 1). (In this figure, an asymmetrical load of 340 tons is shown on the 49-ft 2.5-in clear span. The arch ring is slightly less than 6.5 in thick and the span/rise ratio is 3.4:1.) The experiment was so successful that the Swiss federal government decided to apply it to a site on Federal Highway Number 1. Built in 1967, this bridge still serves with a maintenance-free record. Since that time, 80 other structures have been built by using the BEBO concept. They include bridges on a variety of sites, cut-and-cover tunnels, and underground parking garages. In addition, the West German government required a second test structure and a university-based research program to ascertain that all structural details were safe and durable. In August 1981, the first bridge outside of Europe and the Middle East was built in Edina, Minnesota.

HISTORICAL BACKGROUND

It was the Roman engineer that made the arch the standard structure for highway bridges and aqueduct stream crossings. The Roman arch was invariably a semicircle with massive piers (or abutments) and deep arch stones.

The two hazardous times in the life of a Roman arch were the dropping of the wood centering during construction and an extraordinary flood. During the Dark Ages, Roman arches became convenient local quarries for precut stone, and akin to this hazard was military destruction. Service load failures were virtually unknown.

It was Perronet (1708-1792) who perfected the circular arch segment as a means for substantially increasing bridge spans without a concomitant increase in rise. Other forms of the arch appeared in the 18th century even for shorter spans, and the ellipse became particularly popular. As the craft of architecture began to merge with mathematics and mechanics into the art of engineering, so the use of mathematical forms such as the parabola was introduced into bridge practice for both timber and stone.

Throughout the 19th century, most practical engineers used empirical rules developed from the geometry of successful bridges, although elastic analysis is found in American texts at the turn of the 20th century. When concrete was introduced as a structural material for arch bridges, the fixed-end assumption persisted for some time, even though the two-hinge theory was well developed. After World War I, reinforced concrete structures became increasingly popular and elaborate hinge configurations were designed for reinforced concrete arch-rib bridges for spans more than 55 ft. For shorter spans, the old masonry rules remained as common practice.

Before closing this historical survey, it is interesting to note Brunel's Maidenhead Bridge of 1837. This railroad bridge's three arches each spanned 128 ft but had a rise of only 24 ft. Such a daring flat design provoked much controversy and speculation that it was doomed to collapse. After its first century of service without the slightest problem, no one doubts its safety; but this same question arose during the Edina BEBO project.

AMERICANIZATION OF THE SWISS CONCEPT

Despite the obvious success of the BEBO arch system in Europe, there was some doubt as to whether it was a competitive form for the United States. Although the mathematical basis for structural analysis of the BEBO design was widely accepted in American universities, it was American practitioners who had to decide on the structural merits of the system.

Figure 1. Original BEBO test structure in Zurich, Switzerland (1966).

Many of these engineers were not familiar with the mathematical intricacies of finite-element analysis, and even those that were looked at a mass of computer printouts with less than enthusiasm. Therefore, one step in the Americanization process was to develop a simplified analytical technique by which local, county, state, and federal engineers along with consultants could review BEBO plans with a minimum of time and effort. Other programs that were developed included hydraulic analysis for stream crossings and foundation design.

The structural analysis program is calibrated to the more refined finite-element method (FEM). It is basically concerned with service loads and variations in overfill depths, whereas FEM not only considers these cases, but it also determines stresses in the precast elements generated during handling, transporting, erecting, and backfilling. As it turns out, the most critical stresses in the elements may not occur during service but rather during their preservice life. Thus, the steel in an arch element is the same whether the overfill is the minimum of about 1 ft or as much as 6 ft or more.

The original BEBO structures were built of precast reinforced concrete plates about 6 ft by 20 ft by 8 in. The units were set on a special steel erection frame and then doweled and grouted together at the joints. Each day after one set of plates was in place, the frame was jacked into position for the next set of plates. In general, spandrel walls were not used; instead, the fill was sloped down over a special set of end plates.

Talks with American engineers, precasters, and contractors quickly revealed that the plate system would have limited success in the United States. It was decided to concentrate on a single-leaf or twin-leaf modification, the latter having had some application in Europe for smaller spans. Further, because of the nature of the American precast market, it appeared advisable to consider precasting the spandrel walls, the wingwalls, and the arch base.

The final geometry of the American version of BEBO was based on structural considerations (preservice and service), hydraulic characteristics, and regulations that govern the transportation of heavy loads in each of the 50 states.

The project sequence for the Americanized system is as follows:

1. A catalog model is selected based on site geometry, hydraulic requirements, and clearances.
2. The foundation slab size is determined by local site conditions.
3. The site is excavated to foundation grade and the foundation slab is cast in place.
4. The erection of the precast elements begins with the precast arch bases and ends with the wingwalls.
5. Backfilling is accomplished in prescribed lifts. Grossly unsymmetrical fills are not permitted.
6. Paving, landscaping, riprapping, guardrails, and other nonstructural items are completed and the bridge put in service. Elapsed time is about two to six weeks, depending on the overall size of the project, seasonal factors, etc.

EDINA EXPERIENCE

The American engineer responsible for Americanizing BEBO was fortunate to have an experienced precaster who had a penchant for innovation on his first project of this type to be built in the United States. Through a cooperative effort with the Swiss firm, all the details of producing a bridge meeting all American Association of State Highway and Transportation Officials (AASHTO) standards as well as local standards and requirements were completed in a matter of months. The City of Edina followed standard competitive procedures, and the final low bid for using the BEBO structure was approximately the same as the estimate, the lowest being $113 000. An alternate system was offered at $22 500 more than this low bid. Figure 2 shows the completed bridge. It has a span of 40 ft 4 in and a rise of 9 ft 8 in. The total width is 74 ft and there is 2 ft of fill over the crown. The service load is HS-20. There are 12 arch elements, each 48 ft 5 in long, 6 ft wide, 10 in thick, and weighing 18 tons. There are two spandrel elements, each 44.5 ft long, 12 ft high, 12 in thick, and weighing 18 tons. There are eight wingwall elements, four high units (sloping from 13 down to 9 ft), and four low units (sloping from 9 to 5 ft). The high units weigh 9.5 tons and the low units 7 tons. All wingwall units have a stem thickness of 10 in.

Figure 2. First BEBO arch built in the United States in Edina.

The cast-in-place foundation required about a week, but the erection of the precast elements was accomplished in less than two days. With more experience, it is believed that only one day would be enough. Because there are no special hinges between the arch elements and the foundation, about 2 h for grouting was all that was needed. Backfilling took another day or so. Because of the newness of the system, the Edina engineering department made a series of on-site measurements.

SUMMARY

From experience gained since studies of applying the Swiss short-span arch-bridge system to the United States began in 1979, it appears that it has certain advantages within the span range of from about 15 to 55 ft and within span:rise ratios of about 4:1 to 2:1.

From an engineering standpoint, the system has the following characteristics:

1. Low installation cost;
2. Low maintenance cost (virtually none);
3. Short construction time;
4. Meets AASHTO design standards for Interstate use;
5. Live load impact effects muffled;
6. Live load stress reversals;
7. Temperature stress reversals minimal, thus increasing durability;
8. Structurally durable and reliable;
9. Useful hydraulic properties;
10. Readily site adaptable;
11. Desirable conservation characteristics (natural stream bed);
12. Aesthetically pleasing;

13. Resistant to extreme flooding;
14. Maximum use of local materials;
15. No bridge deck to deteriorate and no joints in road;
16. Low hazard from ice glazing;
17. Minimal inspection required by owner; and
18. Not sensitive to unequal settlement.

From the precasters and contractors viewpoints, the system has the following characteristics:

1. Meets load limitation and clearance standards for transporting in all states;
2. Requires no special processes (prestressing, steam curing, etc.);
3. Requires no special materials;
4. No special erection equipment needed;
5. Low initial capital investment;
6. Requires no new skills, but present skills must be augmented;
7. Precise pricing possible once operation established;
8. Increases construction season;
9. Not sensitive to backfilling when prescribed backfilling operations are used; and
10. Small on-site work force.

For the above reasons, it is believed that the Americanized version of the Swiss BEBO system will find many applications in the United States.

Publication of this paper sponsored by Committee on Construction of Bridges and Structures.

Bridge Structure Construction System That Uses Treated Lumber

G. DUANE BELL AND KENNETH A. OLSON

For generations, timber has been considered an economical material for bridge construction. Although for years railroads made good use of treated timber in their bridges, little thought was given to design or permanence of timber for highway bridges, which resulted in timber being viewed as a second-class material. Even though preservative-treated wood was eventually used, it is only in recent years that serious consideration has been given to the design of treated timber for use in short-span highway bridges. Treated timber offers economical advantages, but it provides other advantages as well. Treated-timber material will not crack, crumble, or rot. It cannot be damaged by continuous freezing and thawing, and it is not affected by temperature, alkali soil, or acids. When properly designed, a timber bridge provides flexibility and lower costs in design, simplicity in construction, short construction duration, little or no maintenance, minimal weather considerations during construction, and compatability with the surrounding environment. One type of economical timber bridge is the longitudinal laminated-floor design, which is especially easy to construct. To form the superstructure, 3- or 4-in planks are set on edge in the direction of the span; they are offered in spans up to 38 ft in length. Deck planks are laminated together into panels approximately 6 ft wide by using ring shank dowels. Panels are attached to each other at the site by using dome head drive spikes through a shiplap joint. The structure, which is usually completed in a few days, minimizes cost and inconvenience to the taxpayer.

If the term "wood bridge" is mentioned, most of us immediately picture an old-fashioned covered bridge (Figure 1) or perhaps an old, broken down, poorly constructed wood crossing (Figure 2). Actually, the first wood bridge probably was a log laid across a chasm. For years thereafter wood was an important material used in the construction of bridges.

Railroads and their company engineers long ago recognized the value of wood as a basic bridge material. Wood was readily available. It was durable; easy to use; easily maintained, repaired, or modified; and the use of wood preservatives made it permanent. By applying engineering practices, treated wood became a predominate material. Virtually thousands of timber railroad bridges were built, and many still provide excellent service.

Wood bridges for roads or highways, however, were often built with little thought given to design or concern for permanence. Wood was usually a material put together quickly and cheaply to meet society's basic need of getting from one stream bank to another. Thus, for highway bridges, wood evolved as a second-class material. Gradually, data on timber construction offered by most engineering schools decreased. Many practicing engineers have had almost no background in timber construction. It is ironic that wood as a construction material has been around almost as long as man and yet is probably the least understood common building material. Wood is a highly desirable raw material because it is a renewable resource that is provided by significant amounts of forests in the United States. It is a long way from that small stream crossing for the horse and buggy compared with the demands that present-day traffic puts on major highway bridges. (You might say it is like comparing a Model T with a Cadillac. In between there are a lot of bridge needs, and a good many of them are on rural and township roads. The Model T is inadequate, but the Cadillac is more than is needed. The key is to match the solution to the need; i.e., adequate design, permanence and integrity, and economical cost. That is where treated timber can help.)

There is nothing second-class about timber bridges (Figure 3). Treated timber offers economical advantages over other materials. It will not crack, crumble, or rot. It cannot be damaged by continuous freezing and thawing. Salt will not pit it, water will not rust it, and it is not affected by temperature, alkalai soil, or acids. As a matter of fact, chemical companies such as DuPont have been using preservative-treated wood box culverts in effluent discharge systems for years. They found treated wood to be the best material available to withstand the chemical action of toxic wastes.

When properly designed, treated timber provides flexibility; it can be easily modified, expanded, dismantled, or moved from one location to another should needs change. Treated timber provides econ-

Figure 1. Typical old-fashioned wooden bridge.

Figure 2. Example of old wood crossing.

Figure 3. Example of timber bridge.

omy, simplicity in construction, longevity, dependable material availability, short construction duration, little or no maintenance, minimal weather considerations during construction, and compatability with the surrounding environment.

The departments of transportation in some North Central and Midwestern states now recognize the advantages of using treated timber for bridges on secondary roads. Many specifying engineers are requesting treated timber.

There are several variations in timber bridge design. Most of them have advantages, but the type that offers the greatest combination of desirable characteristics is the longitudinal laminated-deck design. Figures 4 and 5 show an abbreviated two-sheet drawing of a typical longitudinal laminated-deck timber bridge. This design accommodates spans up to 38 ft, is simple, and is easily constructed. It also conforms to American Association of State Highway and Transportation Officials (AASHTO) (1) standard specifications for highway bridges [Section 1.2.5 (for highway loadings)] and bridges designed for HS 20-44 loadings. Section 1.3.4 covers distribution of wheel loads on timber flooring. Paragraph B pertains to longitudinal flooring, normal to direction of span. We mention this because frequent questions from engineers are about that specification and about laminated floor versus splined or doweled floor. After several years of confusion about the definition of a doweled floor, an amendment came about as a result of extensive testing done on an actual timber bridge. Test results showed the design more than met the strength and deflection requirement as prescribed by AASHTO for a splined or doweled deck.

The longitudinal laminated-deck timber bridge consists of shop-assembled deck panels (Figure 6). Panels are about 6 ft wide, made up of 3- or 4-in-wide planks set on edge; the depth of the plank varies with the length of span. Span lengths are from 18 ft (where 10-in planks are used) to 38 ft (where 16-in planks are used). Planks are predrilled with holes at 12-in centers and are usually treated with creosote or penta in heavy oil, then attached to each other by means of 11- or 15-in ring shank dowels. Creosote or penta in heavy oil are preferred preservatives because they provide a higher and more uniform moisture content over a longer period. Adjacent deck panels are fastened to each other with drive spikes nailed vertically through a shiplap joint, which consists of one-half of a plank connected at the bottom of one panel and one-half of a plank connected at the top of an adjacent panel (Figure 7). Deck panels are supported on timber caps, which in turn are supported on piles (Figure 8). During deck installation, a 6x12-in wood-spreader beam is installed under the deck at midspan (Figure 9).

Two basic types of curbs and rails are used. Where 10-kip rail is required, a 6x12-in treated-timber curb is bolted through scupper blocks to the deck by using split ring connectors. The railing is a treated glu-lam timber connected to 8x12-in treated-timber rail posts. Posts are anchored with drive spikes to the deck and bolted to the curb (Figure 10). Where 10-kip rail is not a requirement, there is a simplified rail design that uses smaller timber curbs and posts with standard steel beam guardrail.

For the abutments and wings, timber piling is driven to a minimum of 15-ton bearing, then aligned for placement of the timber cap and timber backing. Then 3-in treated-timber backing planks are installed on the timber piling. A vertical timber functions as a pile stay, which helps keep the cap in place and prevents the abutment from moving forward after back-filling (Figure 11). The wing plank and abutment plank join at the corner pile to form an interlocking fingerlike connection (Figure 12). When abutments are placed farther back in the bank and 14x14-in caps are used, piles can be spaced farther apart, which results in savings in abutment construction (Figure 13). Piers can consist of either timber piling or cast-in-place concrete or steel piles, depending on site and ice conditions (Figure 14).

Testing of the bridge was done under the direction of an independent inspection agency. In the bridge used for testing, the deck consisted of four

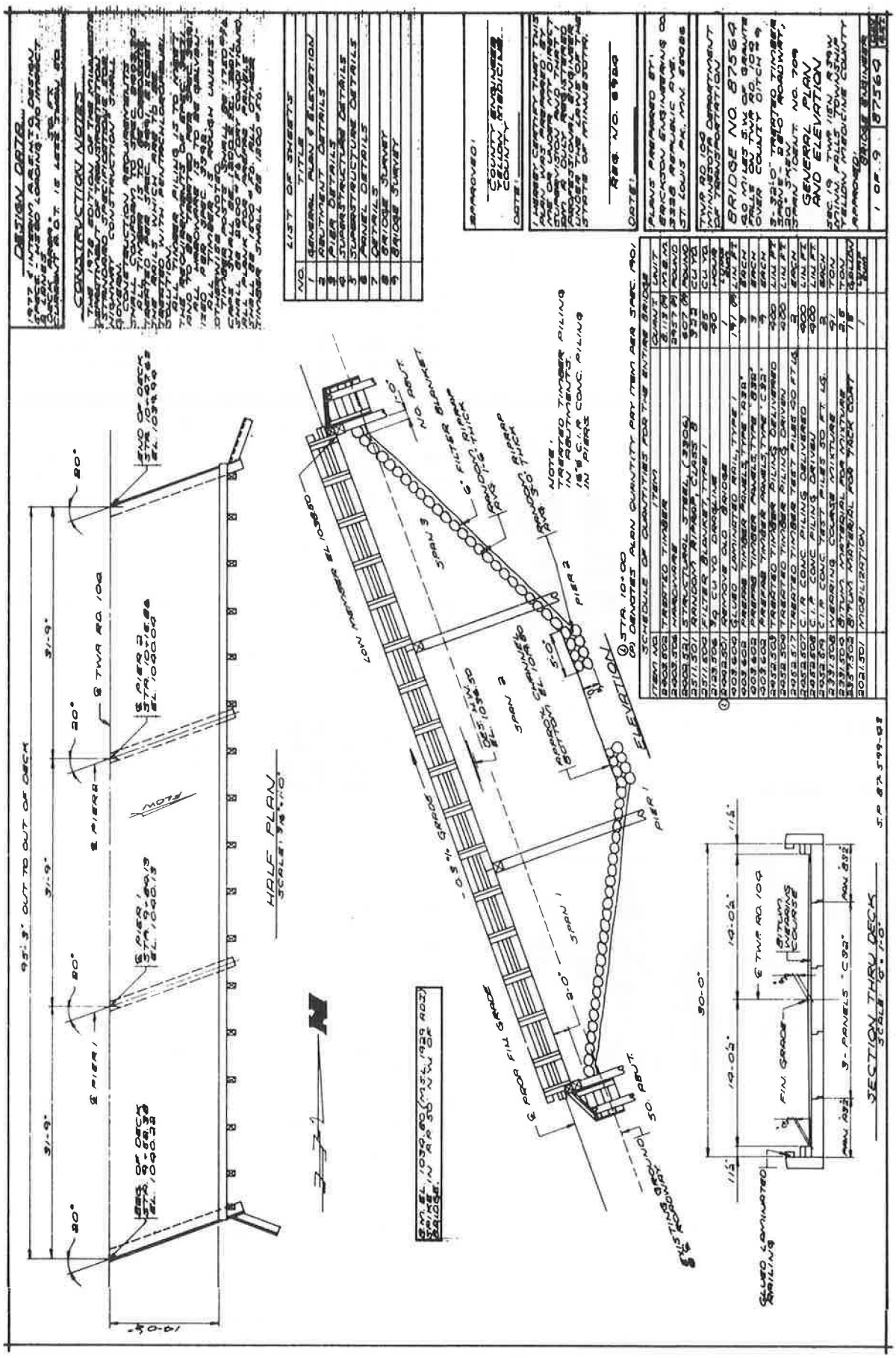

Figure 4. Plans for typical longitudinal deck timber bridge.

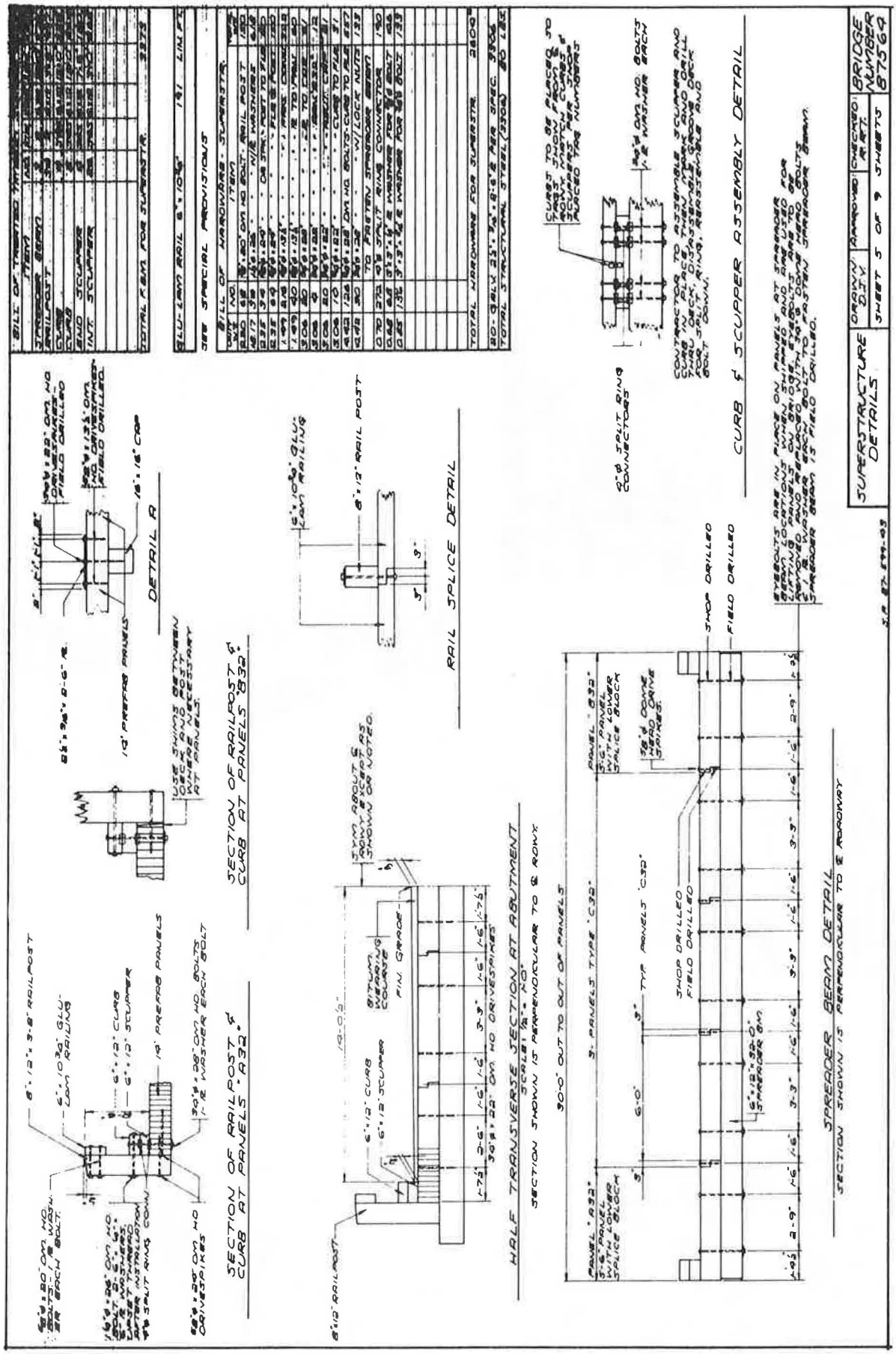

Figure 5. Superstructure details of longitudinal deck timber bridge.

deck panels that were 12 in deep, 6 ft wide, and 26 ft long. A timber-spreader beam was installed under the deck at midspan. A 10-kip railing was also installed. The testing of the deck was done by applying a load with bundles of steel to simulate wheels 20x10-in in dimension (Figure 15). The test series consisted of several sets of conditions, including tests for simulated single-axle loading (two wheels) and the single-wheel loadings (one wheel). A total superimposed load of more than 70 000 lb was applied in the single-axle test. That is more than twice the required loading. Yet the deflection was only one-half what the calculated deflection formula would indicate. The single-wheel test had even better results. For testing the 10-kip railing, a

Figure 6. Shop-assembled deck panels.

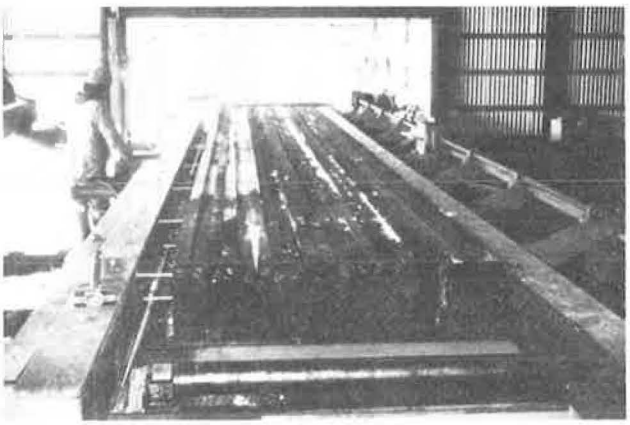

Figure 7. Fastening of deck panels.

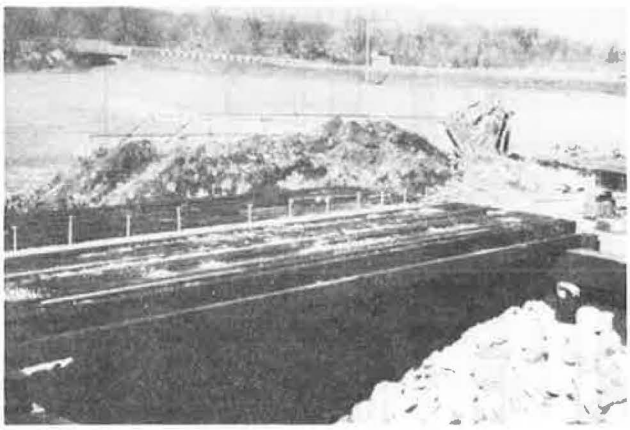

Figure 8. Support for deck panels.

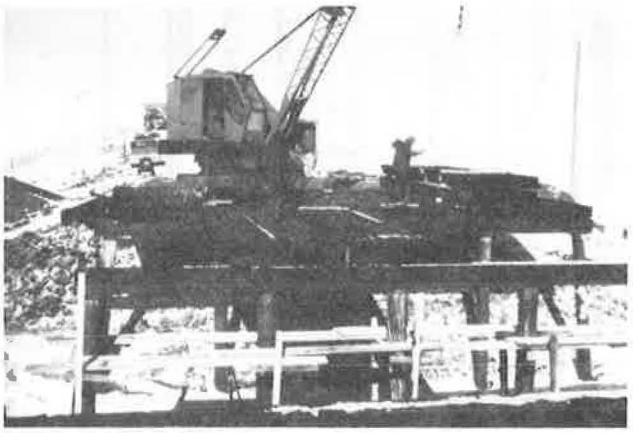

Figure 9. Installation of wood-spreader beam.

Figure 10. Bridge rail and curb.

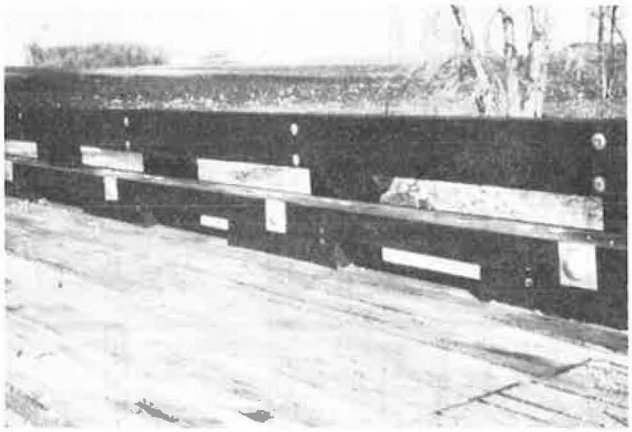

Figure 11. Vertical timber functioning as pile stay.

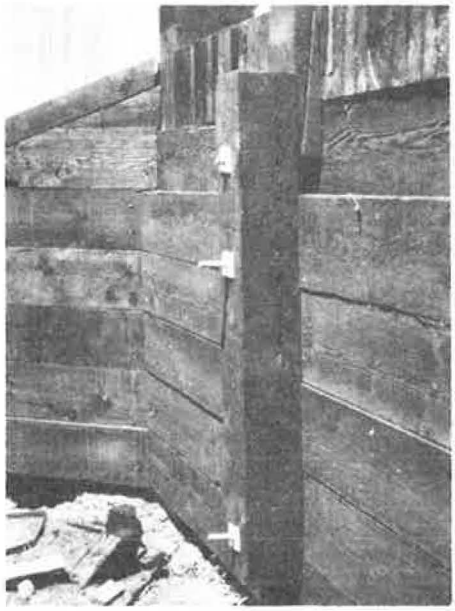

horizontal load of 10 000 lb was applied to the railing and to a rail post by using a calibrated hydraulic ram system and held for 1 min; it showed excellent results.

Figure 12. Wing and abutment planks.

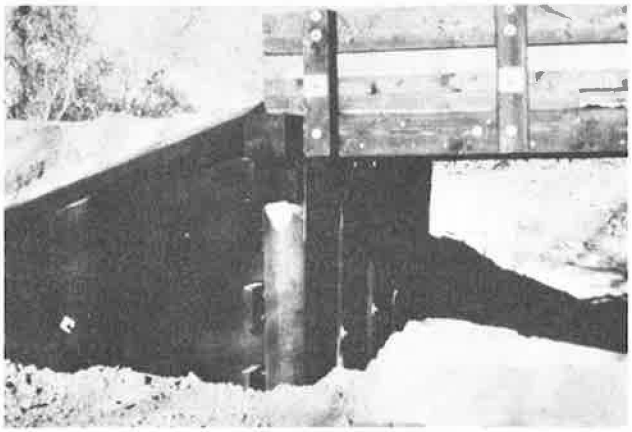

Figure 13. Alternate abutment configuration.

Figure 14. Steel piles used in piers.

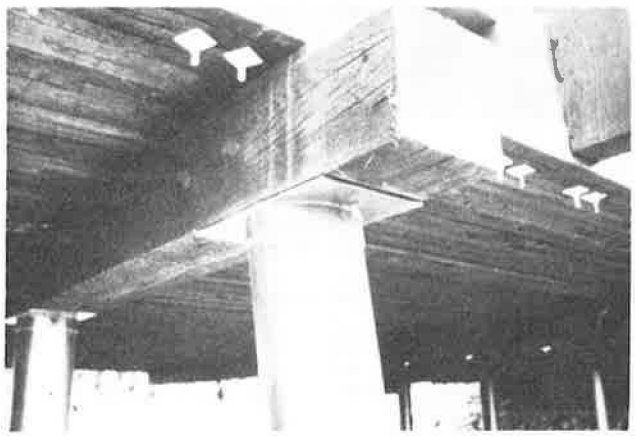

We have mentioned the advantages of the longitudinal laminated-deck timber bridge. Its simplicity in construction is a big one. It is not uncommon for a small contractor or a county crew to install a timber bridge by using one carpenter foreman, a machine operator, and one or two laborers. It does not take a lot of sophisticated equipment or many highly skilled workers to do the job (Figure 16). Minimal weather consideration is another ad-

Figure 15. Testing the deck.

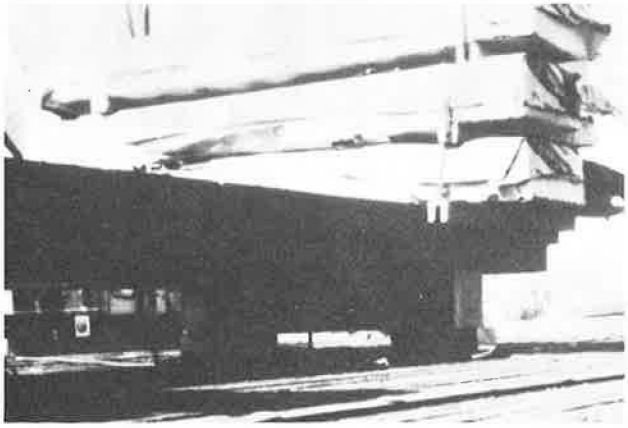

Figure 16. Construction of timber bridge.

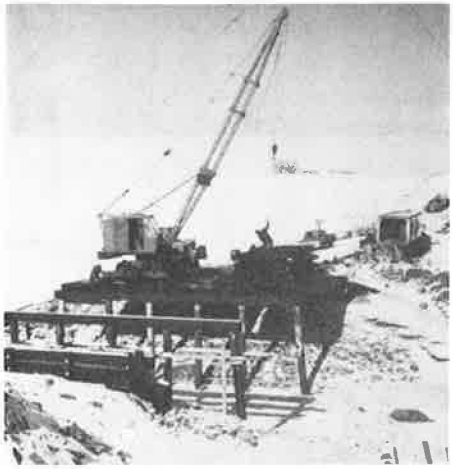

Figure 17. Work is easily done during winter months.

Figure 18. Panels are stockpiled at the job site.

Figure 19. Panels are quickly installed.

Figure 20. Completed timber bridge.

Figure 21. Timber bridge for vehicles.

Figure 22. Timber bridge for pedestrians.

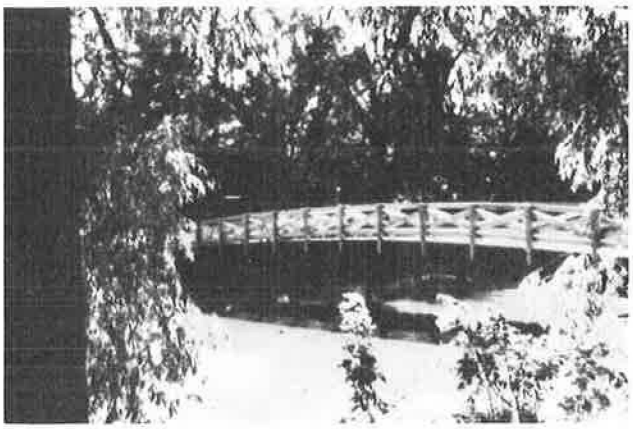

Figure 23. Treated-timber bridge.

vantage. It is not uncommon to build timber bridges during the month of January in Minnesota. We will not say that efficiency is at its best, but it sure beats trying to pour concrete (Figure 17). The need for only a short construction duration is another advantage. Very often complete timber bridges are installed in a matter of a few days, and a good part of that is spent in driving piles and building abutments and piers. In fact, complete decks are usually installed in less than a day. Panels are lifted directly from trucks or from a stock pile at the job site and set into place in a matter of minutes (Figures 18 and 19); before long the bridge is complete (Figure 20).

We do not believe that there is any bridge material that can provide the aesthetic qualities of a timber bridge (Figure 21). That is true, not only of vehicular bridges, but it is especially true at sites where timber pedestrian bridges have been installed (Figure 22).

Figure 24. Example of treated-timber bridge.

Like any new type of construction or material, contractors new to timber bridges may bid unrealistically high when bidding the first few times. With a little experience, however, the cost of treated timber becomes consistently equal to, or usually less than, other bridge materials.

Recently, a consulting engineering firm offered data on total in-place cost comparisons on approximately 200 county and/or township bridges built over a period of three years. Treated-timber bridges averaged about $30/ft². Their closest competitor--concrete Quad-T--was about 10 percent more. Other types of bridges were even higher. And, incidentally, most of those timber bridges were of the longitudinal deck design.

We do not have to remind you of the tremendous need for bridge replacement or that the need for new bridges will cost the taxpayer millions of dollars. Never has there been a time when economy was more important. Many of those bridges are in rural areas on county, township, or municipal roads and at sites where simple, multiple short-span, and economical bridges are ideal. With treated-timber bridges, there is an opportunity to have some of the best of all worlds (Figures 23 and 24).

REFERENCE

1. Standard Specifications for Highway Bridges, 12th ed. AASHTO, Washington, DC, 1977.

Publication of this paper sponsored by Committee on Construction of Bridges and Structures.

Live Load Distribution in Concrete Box-Girder Bridges

RAYMOND E. DAVIS, VU DINH BON, AND FRANK M. SEMANS

Traditional methods for designing bridges that reduce the significant parameters affecting distribution of live loads to a single entity (e.g., stringer spacing or deck width) represent archaic oversimplifications. They are held over from the precomputer era and result in a spectrum of designs that range from ultraconservative to those that would be unsafe but for generous safety factors. Development of such distribution factors has usually been based on the assumption that all lanes on a structure are loaded with design vehicles, and such design methods become particularly meaningless when used in conjunction with hybrid loadings such as California's Permit-series, which comprises a single, heavy rating vehicle in combination with a single H-series design vehicle. Sophisticated analytical tools developed in the postcomputer era can provide very exact designs (perhaps more exact than warranted by live load specifications), but these tools are too cumbersome for use in a production environment. Presented here is an alternate, intermediate design method that combines relative exactness with a shortcut design approach that employs nomographic analysis for traditional designs and influence-line analysis for hybrid loadings.

For many years, the concrete box-girder bridge has enjoyed special popularity on California's freeway network. Prior to 1959, design of such structures for live load was based on a distribution-factor approach in which individual I-sections were assumed loaded with S/5 wheel lines of a standard H-series vehicle, where S is the spacing (in feet) between centerlines of webs.

In 1959, California design engineers, who appreciated the large torsional rigidity of the closed box section, suggested to the American Association of State Highway Officials (AASHO) a change in this distribution factor to S/7. Sophisticated techniques for analyzing such structures were unavailable at the time, and the recommendation had little scientific basis; nonetheless, the new specification was tentatively adopted, contingent on California's agreeing to embark on a research project to study box-girder load-distribution phenomena.

The research program began in 1960 with field testing of the Harrison Street Undercrossing (1,2), a 34-ft-wide structure that had a single span of 80 ft. The cross section comprised four cells spaced at 7 ft 3 in and provided a live load distribution of S/5 = 1.450 wheel lines according to the earlier specification and S/7 = 1.036 wheel lines according to the revised specification.

Field testing entailed heavily instrumenting the structure with strain- and deflection-measuring devices and running a Euclid truck across the span in 13 transverse positions while internal strains and deflections were recorded. The two-axle test vehicle was heavily ballasted with reinforcing bar ingots to 57 kips. Tests were run in three phases: with and without intermediate diaphragms and after addition of 3-ft-wide barrier curbs and rails.

Analytic techniques for data reduction involved plotting of individual strains as functions of transverse position of the test vehicle and, subsequently, hypothetical placement of more than one vehicle on these strain plots for superposition of strains and conversion to stresses and stress integration in individual I-sections for determination of stringer moments. These stringer moments were compared with computed moments on the span due to a single wheel line of the test vehicle to permit assessment of an S/D factor for hypothetical combinations of test vehicles critical for each stringer.

The 28-ft roadway between the 3-ft-wide barrier curbs permitted two lanes under the specifications

current at that time, and application of two hypothetical test vehicles to strain plots produced a distribution factor of about S/8. A 1-ft-wide standard barrier curb on the same basic superstructure, which had a 32-ft-wide roadway, 3 traffic lanes, and 3 hypothetical vehicles on the strain plots, indicated a value of about S/5.5 with no change in the value of S. A distribution factor based only on stringer spacing was inadequate and would require, at least, inclusion of the number of traffic lanes as an additional parameter.

Tests of a 1:3.78 scale, reinforced concrete model were conducted at the University of California, Berkeley, by Scheffey concurrently with tests of the full-scale prototype. The model was loaded with a single, concentrated force, but it was demonstrated in the analysis of the data by Davis and others (3,4) that its behavior closely paralleled that of the prototype.

Subsequent to completion of initial field tests and analyses, a long-term study was initiated jointly by the California Division of Highways and the University of California, Berkeley, to develop analytical techniques for assessment of box girder structural behavior. This phase of the work resulted from a request for methods of assessing shears in skewed concrete box girders. It soon became evident that behavior of the skew box was complex and that analysis of such structures would follow a lengthy progression of development of analyses of geometrical configurations characterized by simpler behavior.

Concurrent development of the electronic computer and its adoption by the engineering discipline permitted application of established analytical techniques of numerical complexity that had previously precluded such use. In 1966, Scordelis (5) published the first program (MULTPL) to be developed as part of this research contract, which was for analysis of simply supported box-girder bridges employing a direct stiffness application of folded-plate techniques to closed box sections. Initial application of the folded-plate analysis to the Harrison Street Undercrossing field-test data had demonstrated that the method could predict moment distributions with precision.

In 1967, Scordelis (6) described three additional programs for box-girder analysis: (a) MUPDI, a folded-plate analysis; (b) SIMPLA, a finite-segment approach; and (c) FINPLA, a finite-element analysis. A second-generation MUPDI (MUPDI2) permitted application of folded-plate analysis to continuous structures that contained rigid, intermediate diaphragms and provided automatic moment integration for individual stringers. The MULTPL and MUPDI programs require simple support conditions at abutments, while SIMPLA can analyze structures with fixed (built-in) conditions at end supports.

The S/7 distribution factor adopted in 1959 continued to be used in California except for a slight modification in the late 1960s, which was to a "whole width"/7 factor.

In 1969, Scordelis, Davis, and Lo (7) noted that an S/7 distribution factor for the Harrison Street Undercrossing would produce 7.25/7 = 1.036 wheel lines per interior girder and W_e x 1.036/S = 6.125 x 1.036/7.25 = 0.875 wheel lines on each exterior girder for a total of 4.86 wheel lines on the structure. Such a design would be conservative for 3-ft barrier curbs and two lanes of traffic, and it would be unconservative for 1-ft barrier curbs and three lanes of traffic.

In 1970, Sanders (8), who used data from a study by Scordelis of 200 California bridges and the Scordelis programs, estimated a range of live load distribution factors of S/5.7 to S/8.3.

In 1969, Scordelis and Meyer (9) published an exhaustive study of wheel-load distribution in concrete box-girder bridges and developed a formula that included parameters thought to influence load distributions; i.e., span between supports, span between inflection points, number of lanes, cell width, and number of cells. The formula provides a ratio (α) of the number of wheel lines taken by a girder to the number of wheel lines taken by the girder in a rigid structure; the latter factor may be calculated as the ratio of the stiffness of a given girder to the stiffness of the cross section. (The formula will not be repeated here, since the original publication may be consulted by interested readers.)

In 1974, California adopted a load factor design and introduced a special Permit-series live loading to reconcile discrepancies between design and rating criteria (10). The special loading stipulated a series of P-series vehicles of greater weight and size than the H-series trucks with one such vehicle in a given lane of a bridge and a single H-series vehicle in an adjacent lane.

Prior to 1974, American Association of State Highway and Transportation Officials (AASHTO) specifications stipulated traffic lanes of variable widths that divided the roadway between curbs equally. In that year, the specifications were changed to provide 12-ft-wide lanes with no partial traffic lanes.

The Scordelis-Meyer formula soon became obsolete for the following reasons:

1. The derivation was based on lane widths of 10-16 ft. The 1974 change in specifications significantly altered the basic assumptions.
2. The formula recognizes a difference between wheel-line distributions to exterior and interior girders but assumes vertical exterior webs. Most California box girders designed in the past decade have used sloping or curved exterior webs, where stiffnesses of exterior and first interior girders will be affected, and a correct formula must include separate α-factors for exterior, interior, and first interior girders.
3. The formula recognizes a difference in wheel-line distributions at midspan and interior supports. Based on proof of small error, distributions throughout the positive-moment region were derived by assuming that all wheel reactions were concentrated at midspan. It appears that this same assumption was made for support moments, and this condition may not be critical.
4. Since Permit-series vehicles are much longer than HS-20 trucks, some reassessment of validity of the first assumption mentioned in 3 above is necessary.
5. The Scordelis formula was based on the assumption that all lanes were loaded with H-series trucks. The same assumption used in conjunction with heavier Permit-series loadings would result in ultraconservative designs. It is difficult to visualize the application of any formula to hybrid loadings, which are comprised of mixed-vehicle modes. The Office of Bridge Maintenance, California Department of Transportation (Caltrans), frequently rates bridges for vehicle configurations that differ from P- or H-trucks; i.e., any proposed design tool should be capable of treating any loading.
6. A very significant deficiency in the formula is its unwieldiness for a production environment. Significant effort was expended by the Caltrans Research Unit that investigated methods of application, such as nomographs, parametric curves, etc.; the number of significant parameters precludes use of such devices.

OBJECTIVES OF RESEARCH

The current project was initiated to overcome the above-mentioned problems and incorporate into the design the results of box-girder studies in California. A need has been identified for the production of design methods sufficiently flexible to permit treatment of any reasonably specified loading.

RESEARCH PROCEDURES

Development of a load-distribution formula proved to be infeasible. The Scordelis formula was too unwieldy for production design because of the number of parameters. An even worse situation could now be expected, since (a) a new parameter--the web slope--would be added, (b) a third equation (for first interior girders) would be added to two equations now required for separate distributions to exterior and interior girders, and (c) three additional equations would be required for distribution at supports. A distribution formula for hybrid (e.g., P-series) loadings would be difficult to develop.

It was decided to present the distribution concept in the format of parametric influence lines, which have ranges of parameters typical of the majority of designs for any arbitrary loading, and simplified nomographs for application to H-series loadings.

A particular advantage of the influence-line approach is its applicability to unusual loadings. A vehicle of one variety can be placed at a critical location on an influence line and percentages of total moment due to that vehicle distributed to each stringer can be read from the plot. The process may be repeated for vehicles of other types and stringer moments due to various vehicles accumulated.

Some disadvantages are also evident, such as the following:

1. Precedent almost demands inclusion of a distribution formula for every basic structure type in the AASHTO specifications. It is difficult to predict how engineers will react to substitution of a booklet of parametric influence lines for such a formula.
2. The multiplicity of parameters required limitations on parametric ranges and use of mean values within these ranges. Some error will occur in designs where parametric values depart from mean values.
3. Interpolation will be required when parametric values fall between plotted ones. Extrapolation may not be safe for unusual parametric values that are outside plotted ranges. A sophisticated analysis by means of such programs as MUPDI and SIMPLA may be required in such cases.
4. The major disadvantage lies in limitations of applicability. Subsequent to development of Scordelis' formula, work on box-girder analysis has proceeded at the University of California and at Caltrans. Models have been constructed and analytical techniques developed to assess behavior of curved and skewed box girders.

The finite-element program CELL was developed by Willam and Scordelis (11,12). Tests by Aslam and Godden (13) of small aluminum models that had varying skews demonstrated that the program could assess skew box behavior with precision. Nix (14) used the program to study behavior of a heavily skewed box-girder railroad structure and noted significant diminutions of longitudinal stringer moments. Wallace (15,16) made 51 parameter studies and demonstrated analytically that total stringer moments could be reduced as much as 44 percent for a 45° skew and 70 percent for a 60° skew.

Davis (17) designed a 1:2.82 scale, reinforced concrete model with 45° skewed supports to be tested at the University of California, Berkeley (18-21), for further verification of CELL as applied to skewed concrete box girders. With redistribution of shears and diminution of moments, influence coefficients developed for structures on orthogonal supports will not apply to structures with heavy skews.

Influence surfaces might solve problems introduced by skew supports, but they are tedious to use and of questionable applicability to structures of configurations that differ from those for which they were developed. Each surface provides a value of a parameter at only one location. The volume of plots required to cover the range of parameters precludes their use. No simplistic tool can be developed that will cover the entire range of parameters that may be anticipated.

DEVELOPMENT OF INFLUENCE LINES

SIMPLA2 was used to establish data for input to the influence-line plotter program. Seven studies were made to determine realistic, transverse distributions of longitudinal girder moments for 60-, 100-, and 120-ft spans that have 3, 4, and 6 cells of widths at 7 and 7.5 ft.

Figure 1 depicts transverse distributions of percentages of total girder moments for one wheel line of an H20-S16 truck on a 60-ft span box girder, which has three 7-ft-wide cells, a 27-ft-wide deck, and fixed simple-support conditions for left exterior and first interior girders. Percentages of total longitudinal moment taken by these two girders are calculated just below the cross section. With two vehicles on the span, the exterior girder must resist 100.6 percent and the interior girder 129.2 percent of the total live load moment due to one wheel line.

Distributions for the right girders would be the same. The four girders must be designed to resist a total of 4.60 wheel lines of moment. The "whole width"/7 concept would result in a design for 3.86 wheel lines (16.1 percent less). Similar studies of other cross sections and boundary conditions indicated errors ranging from +5.6 to -18.5 percent (the negative sign is indicative of unconservative designs). The large negative errors are prohibitive.

Three computational approaches are listed in order of increasing difficulty to produce (a) one wheel line of an H20-S16 design vehicle at the point in a span where it produces maximum moment, (b) the center wheel located at midspan, and (c) all three wheel reactions lumped at midspan. The permissible error of computation must be considered. Five structures were considered in these calculations.

A typical calculation by the first method may be described as follows. An influence line was drawn for midspan moment in the left exterior girder due to a load of 1 kip on this girder with the SIMPLA2

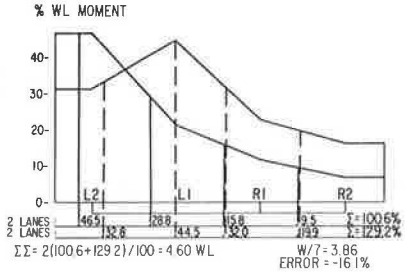

Figure 1. Calculation of error in use of S/7 formula.

program. Influence lines were drawn for moment in this girder due to loads on the other girders and for total moment in the cross section due to a 1-kip load in any transverse location.

A plastic overlay, which shows reactions for one wheel line of the design vehicle, was moved along the influence lines, and ordinates were multiplied by wheel reactions and summed until a maximum total moment was obtained. Use of just one wheel line ensured maximum possible moment due to a vehicle (since the longitudinal position for maximum moment in, say, girder A with girder A loaded is not necessarily that for maximum moment in girder A with girder B loaded).

Percentages of total moment taken by each girder were computed for successive transverse positions of the wheel line. (These percentages need not sum to 100; they are maximum percentages of total moment taken by a girder as functions of transverse position of the wheel line).

In the second set of calculations, midspan influence ordinates and those 14 ft on either side of midspan were multiplied by corresponding wheel reactions. These calculations required no bracketing and less effort than the former ones.

Third, the moment percentages were calculated as the ratios of influence ordinates at midspan for individual girder moments to those for the total section based on all wheel reactions being lumped at midspan. The differences between percentages resulting from the first and second computational methods were inappreciable and those between the first and third were prohibitively large (results of the third calculation were always conservative).

The first method of computation would produce the most accurate distribution factors but would require drawing all longitudinal influence lines and tedious bracketing. Because the second method did not introduce substantial error, moment percentages for each girder were obtained directly from the SIMPLA2 output with wheel reactions input in known positions.

Transverse distributions of moment at supports were investigated independently. It would seem most reasonable to assess such distributions for vehicle positions that produce maximum negative moments at supports. Two methods of computation were considered: (a) longitudinal influence lines were established for each girder with SIMPLA2 and an H20-S16 wheel-line overlay placed on these lines by trial and error until a maximum moment was obtained, and (b) the influence coefficient was calculated only for a single hypothetical maximum moment location and multiplied by the lumped value of three wheel reactions of one wheel line of the H20-S16 vehicle. The second mode of calculation entails much less effort; however, error due to the approximation must be within permissible limits.

Errors in moment percentages calculated by the second, less-exact method were as large as 8.9 percent and always unconservative. An assumed, permissible unconservative error of 4 percent suggested a uniform increase of 12 percent in the exterior girder support moment percentages for the idealized vehicle and an 8 percent increase in interior girder percentages in loaded girders only.

Additional calculations were made of positive moments at locations 7 and 14 ft from midspan. Moment percentages for positive-moment regions were compared with those previously calculated; there were no significant differences in moment percentages.

These studies were based on the H20-S16 design vehicle. The P-series vehicles are much longer, and some reduction in moment distribution coefficients may be expected.

Separate runs were made by using the SIMPLA2 program for P-loads, and moment percentages were compared by means of a reduction factor. These factors were plotted for short spans, and an approximate lower bound was established as a conservative estimate of maximum allowable reduction factors for short spans. Equations for this lower bound are as follows. For short spans (60 to 120 ft), the equations are given below:

Girder	Midspan	Support
Exterior	$R = (L - 48)/[600(1 + K)]$	$R = 0$
Interior	$R' = R/2$	$R' = 0$

In these equations, R and R' are the reduction factors, K is the exterior girder slope factor, and L is the span length (in feet).

The reduction factor for P-loads for short spans peaks at a span length of 120 ft at 12 percent for exterior girders and 6 percent for interior girders. For spans that exceed 120 ft, the reduction factor decreases with increasing span because the controlling alternative lane loading covers the whole span and is longer than the P-13 truck. Reduction factors are listed below for long spans (120 to 270 ft), where R, R', L, and K have the same significance as above:

Girder	Midspan	Support
Exterior	$R = (L - 240)/[1000(1 + K)]$	$R = 0$
Interior	$R' = R/2$	$R' = 0$

An evaluation made by the Caltrans Structures Loads Committee suggested that the new, relatively precise method be used as the design for more realistic trucks for which bridges are rated than for the "artificial" P-13 truck. Investigation indicated that the 13-axle truck would always be more critical than the vehicles for which such ratings are usually made.

RECOMMENDATIONS FOR IMPLEMENTATION

The four different approaches developed for the design of box-girder bridges are given below:

1. There is nomographic analysis for structures that have 3 to 8 cells, spans of 60 to 270 ft, cell widths of 7 to 15 ft, exterior web slopes of 0 (vertical) to 1 (1:1), depth-to-span ratios commensurate with ordinary reinforcement (60- to 150-ft spans) and prestressed (80- and 270-ft spans), and with the critical number of lanes loaded with H20-S16 design trucks. Specified reduction factors (0.90 for three lanes, 0.75 for four or more lanes) are included. The method will not apply to partial loadings for mixed-vehicle modes.
2. There is influence-line analysis for the same parameters as above but that includes provisions for partial and hybrid (mixed-vehicle) modes and rating for special vehicles.
3. There is programmed analysis, which permits automated application with interpolation of the influence-line analysis.
4. There is also the application of sophisticated computer codes developed by Scordelis for special uses (e.g., unicellular or bicellular spine beams, boxes with more than eight cells, heavily skewed structures, structures with arbitrary plan geometry, composite steel and concrete boxes, etc.).

Figure 2 depicts a typical structure cross section to which these methods might be applied. The report by Davis and others (22) provides a detailed study of such an application. The following dimensions are pertinent: span (L) = 80 ft, number of cells (N) = 4, cell width (CW) = 8.5 ft, (W_e) =

CELL: Vol. 1. California Department of Transportation, Sacramento, Rept. CA-DOT-DS-1129-1-76-3, Oct. 1976.
16. R.E. Davis and M.R. Wallace. Skew Parameter Studies--An Implementation of the Finite Element Program CELL: Vol. 2. California Department of Transportation, Sacramento, Rept. CA-DOT-DS-1129-2-76-4, Oct. 1976.
17. R.E. Davis. Structural Behavior of a Skew, Reinforced Concrete Box Girder Bridge Model: Vol. 1, Design. Division of Structures, California Department of Transportation, Sacramento, Rept. FHWA-CA-ST-4187-78-01, Jan. 1978.
18. A.C. Scordelis, J.G. Bouwkamp, S.T. Wasti, and D. Anicic. Structural Behavior of a Skew, Two-Span, Reinforced Concrete Box Girder Bridge Model: Vol. 1, Design, Construction, Instrumentation, and Loading. Univ. of California, Berkeley, Rept. UC SESM 80-1, June 1980.
19. A.C. Scordelis, J.G. Bouwkamp, S.T. Wasti, and D. Anicic. Structural Behavior of a Skew, Two-Span, Reinforced Concrete Box Girder Bridge Model: Vol. 2, Reduction, Analysis, and Interpretation of Results. Univ. of California, Berkeley, Rept. UC SESM 80-2, June 1980.
20. A.C. Scordelis, J.G. Bouwkamp, S.T. Wasti, and D. Anicic. Structural Behavior of a Skew, Two-Span, Reinforced Concrete Box Girder Bridge Model: Vol. 3, Response During Ultimate Loading to Failure. Univ. of California, Berkeley, Rept. UC SESM 80-3, June 1980.
21. A.C. Scordelis, J.G. Bouwkamp, S.T. Wasti, and D. Anicic. Structural Behavior of a Skew, Two-Span, Reinforced Concrete Box Girder Bridge Model: Vol. 4, Detailed Tables of Experimental and Analytical Results. Univ. of California, Berkeley, Rept. UC SESM 80-4, June 1980.
22. R.E. Davis, V. Dinh Bon, and F.M. Semans. Transverse Distribution of Loads in Box Girder Bridges: Vols. 1-6. Office of Structures Design, California Department of Transportation, Sacramento, Rept. FHWA/CA/SD-80/2, 80/3, 80/4, 80/5, 80/6, and 80/7, Sept. 1980.

Publication of this paper sponsored by Committee on Concrete Bridges.

Design of a Skew, Reinforced Concrete Box-Girder Bridge Model

RAYMOND E. DAVIS

A 1:2.82 scale model of a two-span, continuous, reinforced concrete box-girder bridge, which has supports skewed at 45°, was constructed and tested at the University of California, Berkeley. The cross section and significant dimensions were similar to those of two previously tested models, one straight on orthogonal supports and one curved on radial supports. The objective of the research was to compare behavior of the three models and to verify an analytically predicted diminution of longitudinal stringer moments that result from skewing supports. All three models were designed by the California Department of Transportation. Because traditional design criteria make no provision for skewed supports, the skew model was designed by means of a sophisticated finite-element computer code called CELL. Girder moments proved to be significantly less than those in the orthogonally supported model and had a 19 percent reduction in the main longitudinal reinforcing steel. Distribution of girder shears was changed significantly from that of the model on normal bearings. As a basis for implementation, this paper discusses some features of the skew model design process.

For many years, the California Department of Transportation (Caltrans) has been interested in anomalies that characterize the structural behavior of reinforced concrete box-girder bridges with skewed supports. Initially, interest was centered on effects of skew on girder shears. Excessive cracking of webs observed at obtuse corners suggested enhancement of girder reactions that had commensurate increases in diagonal tension.

Complexities in the analysis of skew boxes restricted early efforts toward mitigation of observed excessive web cracking to establishment of curves for augmentation of exterior and first interior girder shears at obtuse corners of such boxes. (Traditionally, skewed boxes in California have been designed as structures of the same spans on orthogonal supports and detailed with skewed supports.) Curves for shear augmentation were established with little scientific basis and furnished, at best, only estimates.

A request in 1959 by design management for a more definitive study of this problem initiated a protracted study of reinforced concrete cellular structures performed jointly by Caltrans' Structural Research Unit and the University of California, Berkeley. The research effort included tests of full-scale prototypes and small and large-scale models. Structures of increasing complexity were studied on a progressive basis, as follows: (a) simple span boxes without diaphragms on normal supports; (b) simple span boxes with rigid intermediate diaphragms, or continuous boxes without intermediate diaphragms on normal supports; (c) continuous boxes with intermediate diaphragms, which consider effects of bent and diaphragm flexibility; (d) curved boxes with radial supports; (e) nonprismatic boxes; (f) skewed boxes; (g) prestressed boxes; and (h) composite concrete and steel boxes. Analytic methods employed in the development of computer codes by the University of California relied heavily on the folded-plate theory and finite-strip, finite-segment, and finite-element methods.

A valuable computer code developed as part of the research effort employs a finite-element analysis to assess behavior of cellular structures of arbitrary plan geometry. This program, called CELL, was first used within Caltrans to analyze a heavily skewed, and curved, box-girder bridge to carry rail traffic and to assess the influence of intermediate diaphragms on that behavior. The program has been used in studies of boxes of varying skews and aspect ratios to establish functional relations between skew angle and shear augmentation factors. Estimated curves of such factors previously used by Caltrans were proved to be unconservative.

A serendipitous result of these studies was the

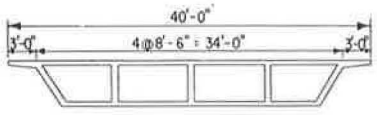

Figure 2. Cross section of structure for sample analysis.

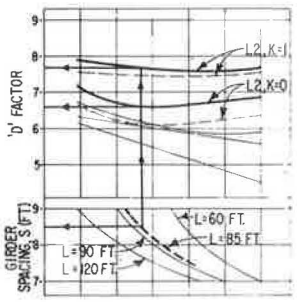

Figure 3. Sample nomographic analysis.

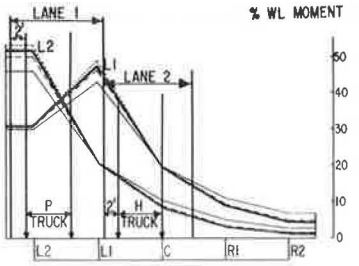

Figure 4. Sample influence-line analysis.

7.25 ft, and slope factor (K) = (2.81/4.69) = 0.60.

By using the (typical) nomograph shown in Figure 3, and noting carefully the correction factors indicated by asterisks, a designer can obtain D-factors, where values of S/D (or, for exterior girders, W_e/D) represent distribution factors.

The typical influence-line analysis is illustrated (in part) in Figure 4. Interpolations are required for span and slope factors and eight separate diagrams must be considered (for three girders each). Resulting moment percentages are obtained for P-series and H-series trucks separately.

Influence-line analysis (which, incidentally, is a misnomer) may be easily applied without a computer, and it is compatible with arbitrary loading conditions. It is probably the only simple approach to distribution of such loads. The method becomes cumbersome in a production environment, so the computer code has been written in FORTRAN IV language. Caltrans' program (LANELL) is immediately accessible in the time-share option system via a cathode-ray tube (CRT) remote terminal. The designer enters seven parameters from the keyboard and obtains as readout suitably interpolated values for the number of wheel lines of P-series and H-series trucks to be distributed to each girder and to the whole structure. Factors have also been established for curvature correction.

For the rare design that cannot be treated by the first three methods, the Berkeley programs may be used, e.g., for spine beams, MUPDI3 and SIMPLA2; for heavily skewed structures or boxes with arbitrary plan geometry, CELL; for short radius structures, CURDI; and for composite steel boxes, FINPLA.

ACKNOWLEDGMENT

Work described herein was performed as part of a research project entitled, Development of a Box Girder Load Distribution Formula, which was jointly sponsored by Caltrans and the Federal Highway Administration (FHWA).

Opinions, findings, and conclusions expressed in this paper are ours and do not necessarily reflect official views or policies of Caltrans or FHWA. This report does not constitute a standard, specification, or regulation.

REFERENCES

1. R.E. Davis, J.J. Kozak, and C.F. Scheffey. Structural Behavior of a Box Girder Bridge. HRB, Highway Research Record 76, 1965, pp. 32-82.
2. R.E. Davis, J.J. Kozak, and C.F. Scheffey. Structural Behavior of a Box Girder Bridge, and Appendices. Bridge Department, California Division of Highways, Sacramento, Rept. SSR 2-65, 1965.
3. R.E. Davis, C.F. Scheffey, G.A. Castleton, and E.E. Evans. Box Girder Model Studies. Bridge Department, California Division of Highways, Sacramento, Rept. R&D 4-70, 1970.
4. R.E. Davis, C.F. Scheffey, G.A. Castleton, and E.E. Evans. Model and Prototype Studies of a Box Girder Bridge. Journal of the Structural Division, ASCE, Vol. 98, No. ST1, Jan. 1972.
5. A.C. Scordelis. Analysis of Simply Supported Box Girder Bridges. Univ. of California, Berkeley, Structural Engineering and Structural Mechanics Rept. SESM 66-17, Oct. 1966. NTIS: PB 175646.
6. A.C. Scordelis. Analysis of Continuous Box Girder Bridges. Univ. of California, Berkeley, Structural Engineering and Structural Mechanics Rept. SESM 67-25, Nov. 1967. NTIS: PB 178355.
7. A.C. Scordelis, R.E. Davis, and K.S. Lo. Load Distribution in Concrete Box Girder Bridges. Proc., American Concrete Institute First International Symposium on Concrete Bridge Design, Toronto, Ontario, Canada, April 1967, ACI Publ. SP-23, 1969.
8. W.W. Sanders, Jr., and H.A. Elleby. Distribution of Wheel Loads on Highway Bridges. NCHRP, Rept. 83, 1970.
9. A.C. Scordelis and C. Meyer. Wheel Load Distribution in Concrete Box Girder Bridges. Univ. of California, Berkeley, Structural Engineering and Structural Mechanics Rept. SESM 69-1, Jan. 1969. NTIS: PB 183923.
10. R.C. Cassano and R.J. LeBeau. Correlating Bridge Design Practice with Overload Permit Policy. TRB, Transportation Research Record 664, 1978, pp. 230-238.
11. K.J. Willam and A.C. Scordelis. Computer Program for Cellular Structures of Arbitrary Plan Geometry. Univ. of California, Berkeley, Structural Engineering and Structural Mechanics Rept. UC SESM 70-10, Sept. 1970. NTIS: PB 196143.
12. K.J. Willam and A.C. Scordelis. Cellular Structures of Arbitrary Plan Geometry. Journal of the Structural Division, ASCE, Vol. 98, No. ST7, July 1972.
13. M. Aslam and W.G. Godden. Model Studies of Multicell Curved Box Girder Bridges. Journal of the Engineering Mechanics Division, ASCE, Vol. 101, No. EM3, June 1975.
14. H.D. Nix. Analysis of a Skewed Concrete Box Girder Bridge (Floral Park Underpass)--An Implementation of the Finite Element Program CELL. Bridge Department, California Division of Highways, Sacramento, Rept. BD 73-8, June 1973.
15. M.R. Wallace. Skew Parameter Studies--An Implementation of the Finite Element Program

demonstration that significant diminutions of longitudinal bending moments might be realized in skewed structures. A potential for significant economies was manifested by curves drawn for simple span structures, which suggested the possibility of reducing dead load resisting moments by nearly one-half in structures skewed 45° and by nearly 70 percent for skews of 60°.

The reduction of resisting moments is usually explained as the result of a tendency to span the normal distance between supports. This explanation is overly simplistic. Diminution of longitudinal resisting moments in the girders is realized at the expense of increasing torsional moments that act on the structure. As orthogonal supports are changed to skewed, formerly symmetrical reactions become asymmetrical as those at obtuse corners are increased and those at acute corners are decreased in magnitude. Resultants of support reactions move away from the centroidal axis of the structure, and torsional forces are introduced. Closed cellular sections possess high torsional rigidity, and increases in torsional moments are less significant than diminutions of longitudinal moments. It was desirable to evaluate qualitatively the influence of torsional forces in skewed structures.

Tests conducted by the University of California of small-scale aluminum models that had varying skews and aspect ratios verified the accuracy of CELL. However, Caltrans' Structures Design management was understandably reluctant to adopt the indicated large reductions in reinforcement quantities because they lacked verification with a larger-scale reinforced concrete model, the behavior of which might also be directly compared with that of the (orthogonal) straight and curved boxes tested previously.

SCOPE OF PAPER

Responsibility for construction, testing, and analysis of behavior of the skew model was assumed by the University of California, Berkeley. Responsibility for design of the model and implementation of results was assumed by Caltrans' Structural Research Unit. This paper describes the techniques used in the model design. [This paper is a condensation of the work by Davis (1), in which the design of the model has been described in detail.]

MODEL DESCRIPTION

The model comprised reinforced concrete elements that had a linear scale reduction of 1:2.82. A No. 4 reinforcing bar in the model, which was built to this scale exactly, simulates main No. 11 reinforcing bars in the prototype. A 6-mm (0.236-in) bar in the model (smallest available with deformations) approximately simulates a No. 5 or a No. 6 bar in the prototype with minor variations in spacing.

Constructed on the test floor of Raymond E. Davis Hall at the University of California, the model was 3.66 m (12 ft) wide (from edge to edge of deck), 25.6 m (84 ft) long (measured between acute corners), and approximately simulated a 10.4-m (34-ft) wide continuous bridge with two 31-m (101.5-ft) spans. The structure was identical in cross section to the curved and straight models tested previously. Transverse reinforcement in the top and bottom slabs was the same as in previous models in order to maintain similitude.

The cross section and transverse reinforcement patterns were originally established in the design of the Harrison Street Undercrossing, a full-sized prototype tested by the California Division of Highways in 1960 (2,3) and a 1:3.78 scale model tested contemporaneously by the University of California (4,5) in the initial phases of the box-girder research program.

MODEL DESIGN

The methods used to design the skew model appear tedious but were characterized by much more thoroughness than would be expected for a full-sized structure. Caltrans' Structural Research Unit employs its own modified version of CELL, which permits storage of the decomposed stiffness matrix for future use in analyses of various loading conditions. An optional mesh-plotting routine is included, since errors in the geometry of large meshes are easily made.

The mesh employed is depicted in plan to a small scale in Figure 1 and, in part, to a larger scale in Figure 2. The same geometrical mesh is used for the top and bottom slabs (this mesh-generating scheme in the current version of CELL mandates vertical webs); however, material properties of elements in the two slabs may differ. A current research project will remove some of the deficiencies in CELL, thereby permitting sloping webs and adding a prestressing facility and automated girder moment integration. This last feature will eliminate much of the effort expended in the design of this model.

The mesh was made rectangular to satisfy a requirement of the CELL postprocessor (CELLPOP) (6) that all cross sections have the same number of girders (e.g., if girder moments within longitudinal limits of end supports are desired). All elements beyond supports are made null elements (i.e., with zero thickness) in the materials properties section of the input data. A second study made with a skewed mesh without null end elements yielded similar results.

Careful choice of numerical designations of nodes and elements allows maximum use of program mesh-generation features. Although punched-card input is conceivable, the repetitive nature of the data greatly decreases key data entry if this work is done on a cathode-ray tube (CRT) terminal with standard utility routines that allow rapid proliferation of data blocks (e.g., in Caltrans' IBM System, the INCLUDE routine). In all, 688 slab elements were described on 50 card images, and 362 vertical elements, including all transverse diaphragm elements followed by longitudinal web elements, were described on 22 card images. Materials properties for upper and lower slabs were specified separately.

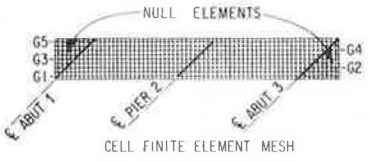

Figure 1. Finite-element mesh for design of model with CELL program.

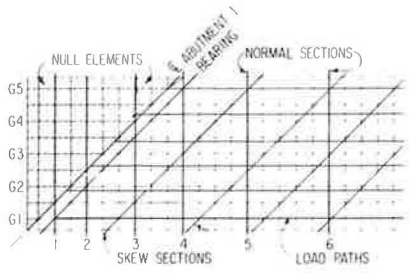

Figure 2. Partial finite-element mesh showing skew reference lines for vehicle location, orthogonal reference lines for moment, and shear calculations and wheel paths.

Specifications of nodal coordinates required separate card images for each of 737 nodes; however, because of the rectangular nature of the mesh, ordinate values are repetitive in blocks of 11, and the proliferating routine was used to advantage. A single block with 11 different ordinates was established. The block successively proliferated to 10, 100, and 800, followed by deletion of 63 card images. Numerical nodal designations (different for each card image) and the abscissae (all the same for each card image in an 11-card group) may be readily entered.

Materials properties were described on eight card images and included separate elastic moduli in the x- and y-directions, shear moduli, mean values of Poisson's ratio in two directions, and element thicknesses. One null element with zero thickness was included to represent nonexistent elements in the bottom slab that correspond geometrically to cantilever upper slab elements and nonexistent elements outside abutment bearings.

Eleven boundary-condition cards specified zero displacements in the z-direction at supports, in the x- and y-directions (also) at the center pier to prohibit rigid body translation, and in the y-direction (also) at the two central abutment supports (to prevent rotation of the whole structure about the z-axis). An additional entry on all of these cards located reactions at bottom slab nodes.

A designer who has developed skill in using a CRT and utility routines can establish data-input files without key data personnel. A partial listing of input for geometric and physical properties is shown in Figure 3.

CELL INPUT FOR MODEL DESIGN: LOADS

General

Current American Association of State Highway and Transportation Officials (AASHTO) specifications for bridge design call for 3.66-m (12-ft) traffic lanes and no fractional lanes. Tread of the AASHTO design vehicle is 1.83 m (6 ft), and minimum distance from a wheel line to edge of a lane is 0.6 m (2 ft). Six vehicle paths were chosen as the most probable critical paths for the five girders. Four paths would suffice but for asymmetry produced by having intermediate diaphragm elements in only one span. Six vehicle paths produce 12 separate wheel paths; because those in proximity to one another are separated by only 0.3 m (1 ft), six compromised wheel paths shown in Figures 2 and 4 were established by moving truck paths a maximum distance of 0.15 m (0.5 ft) transversely. Thirteen lines paralleling the skew were chosen to establish live load positions at intersections with parallel wheel paths, and 19 orthogonal cross sections were established for moment calculations (see Figure 2).

Exterior load paths are coincident with exterior girder webs, and intersections with skew lines fall on nodal points. Intersections of skew lines and inner wheel paths lie within elements, and concentrated loads may be distributed to element nodes by the tributary-area method.

Typical input for a single live load condition is shown in Figure 5. The requirement of a list of 219 nodes at which stresses are to be calculated for 78 live, and 1 dead, load cases studied again suggests tedium in the input; however, the repetitive nature of input again permits rapid proliferation of a single file, which is followed by a separate entry of nodal points and magnitudes of applied loads.

Determination of Longitudinal Girder Moments

Finite-element output from CELL was translated into

Figure 3. Partial list of input to CELL program.

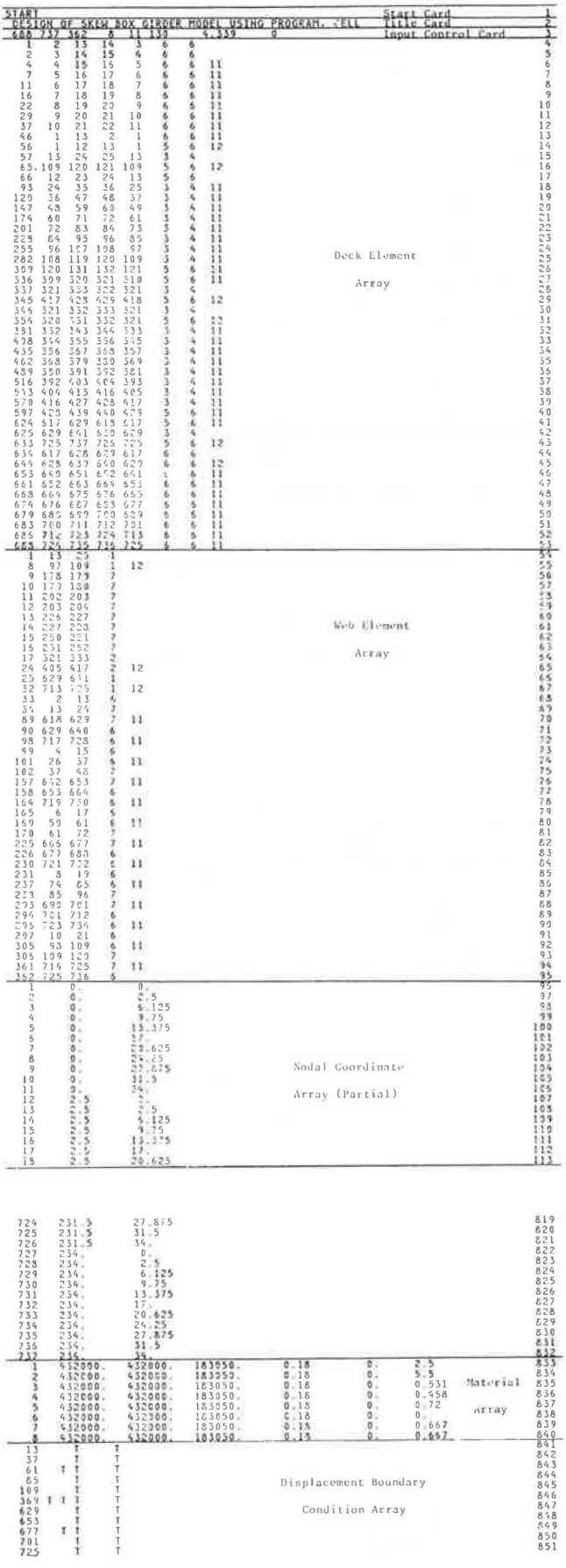

Figure 4. Critical and compromised wheel paths.

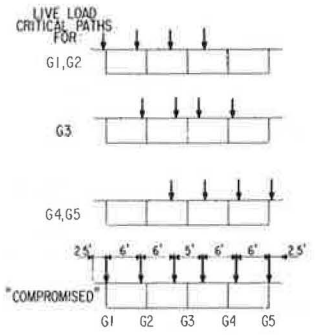

Figure 5. Typical input for one live load case for CELL program.

```
LOAD    2                                                    Loading Start Card                    1
   4    0                                                    Loading Control Card                  2
  36                                  -0.119                                                        3
  47                                  -0.226   Concentrated                                         4
  48                                  -0.429   Nodal Loads                                          5
  37                                  -0.226                                                        6
   1    1    1  219   32          0.          Output Control Card                                   7
$# 52  53                                                                                          8
  23  24  25  26  27  28  29  30  31  32  33  45  46  47  49  49  50  51                           9
$# 116 117                                                                                         10
  54  55  78  79  80  81  82  83  84  85  86  87  88 111 112 113 114 115                           11
$# 213 214                                                                                         12
 118 119 120 121 155 156 157 158 159 160 161 162 163 164 165 210 211 212                           13
$# 310 311                                                                                         14
 215 216 217 218 219 220 265 266 267 268 269 270 271 272 273 274 275 309                           15
$# 352 364                                                                                         16
 312 313 314 315 316 317 318 319 342 343 344 345 346 347 348 349 350 351                           17
$# 396 395                                                                                         18
 365 366 367 368 369 370 371 372 373 374 386 387 388 389 390 391 392 393                           19
$# 469 470                                                                                         20
 396 419 420 421 422 423 424 425 426 427 428 429 463 464 465 466 467 468                           21
$# 577 578                                                                                         22
 471 472 473 518 519 520 521 522 523 524 525 526 527 528 573 574 575 576                           23
$# 652 653                                                                                         24
 579 580 581 582 583 617 618 619 620 621 622 623 624 625 626 627 650 651                           25
$# 705 706                                                                                         26
 654 655 656 657 658 659 660 683 684 685 686 687 688 689 690 691 692 693                           27
$# 725                                                                                             28
 707 708 709 710 711 712 713 714 715  13  37  61 109 321 417 629 677 701                           29
                                                  List of Nodes for
                                                  Internal Forces
```

Note: Data in Columns 3 to 10 of card images with $# in Columns 1 and 2 belong in Colums 73 to 80 of following card.

longitudinal bending moments by the CELLPOP program (6). The program chooses significant values from the matrices of deck and web stresses in two CELL data-output files, takes mean values of longitudinal membrane stresses (N_{xx}) at webs and midbays, converts them into element forces, and integrates incremental moments about computed neutral axes of webs to determine total longitudinal moments. Output from CELLPOP was plotted as influence lines for two adjacent load paths per girder.

Statics Checks

Any finite-element analysis requires statics checks to prove that equilibrium is achieved. A poorly chosen mesh or elements of poor configuration may produce incorrect results. Membrane stresses (N_{xx}) are given in units of FL^{-1}. Total force in an element is the product of the mean value of N_{xx} and the element length. Zero stress points are found by proportion from membrane stresses at the tops and bottoms of webs. Unit stresses at joints in adjoining elements may be compared by dividing N_{xx} by the element thickness. Membrane stresses at the lower, outer edges of the cross section are double those listed in the CELL output, since the program averages values at this joint between real and zero thickness slabs; doubling was performed in the postprocessor.

Forces and moments in slabs and webs are found in the usual manner and are summed. Longitudinal forces should sum to zero. Moment sums at cross sections were used in statics checks.

Reactions at supports may be taken from the generalized force vector in the CELL output for dead load. This vector will list values for all loads in the node listing at the bottoms and tops of webs. Output values at structure supports comprise combinations of upward reactions, and downward reactions due to the dead load of elements that frame into support nodes. Output values from the generalized force vector will not, by themselves, provide correct statics checks.

A minimum number of statics checks were made for the model design, but agreement was excellent. Sums of these corrected reactions agreed within 0.03 percent with the calculated dead load of the superstructure, while the total internal resisting moment at cross section 6 (see Figure 2) agreed with the calculated dead load moments within 0.23 percent.

Live Load Moments

Positive Moments

Output influence coefficients for live load were plotted with a programmable desk calculator and attached plotter for two load paths (on each of two graphs) for a total of 19 cross sections for five girders. Comparisons of mirror images of influence lines plotted for load paths 1 and 2 and for paths 5 and 6 demonstrated that influence of the intermediate diaphragm in span 1 was small, that mirrored influence lines differed inappreciably from one another, and that a portion of the plotting could be eliminated by considerations of symmetry.

Two influence lines were plotted on each sheet, since any vehicle axle would be expected to be orthogonal to the structure centerline and the wheels of this axle at the same abscissa. Influence lines were digitized to obtain total moments; the two adjoining load paths are read simultaneously. Influence coefficients for pairs of load paths in adjacent lanes were plotted on separate cross sections. The vehicles on these two load paths need not be at the same abscissae.

Calculations of live load moments were performed with more precision at many more cross sections than would be required in designs of full-sized structures. Conversion of influence coefficient plots into longitudinal resisting moments was performed by digitization on a transparent overlay drawn to the same horizontal scale as that used in the influence-line plots. This overlay comprised a single horizontal line for reference and three vertical lines spaced at 4.3 m (14 ft) on this scale to facilitate reading influence ordinates at the axle abscissae on adjacent load paths. Values of these ordinates were input to a desk calculator program to compute total live load moments for a standard AASHTO design vehicle moving in either direction; the output provides the maximum of these two values. The plastic overlay was placed in successive horizontal positions until a maximum moment had been calculated. Maxima were tabulated for load paths 1 and 2, summed with those of load paths 3 and 4, and augmented by the impact factor.

Negative Moments

Maximum negative moments over the center bent result from the alternative lane loading and imposition of two concentrated loads. The lane loading requires measurements of areas under influence lines and maximum negative ordinates. A program that integrates areas on a digitizer by circumnavigating their boundaries with the digitizer's crosshair probe was used.

Certain positions of the live load produced small negative moments in girders over abutment supports near obtuse corners of the structure due to the fact

Figure 6. Dead load shears from CELL program.

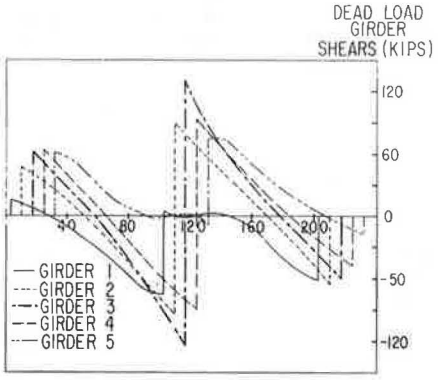

Figure 7. Comparison of CELL and calculated shears.

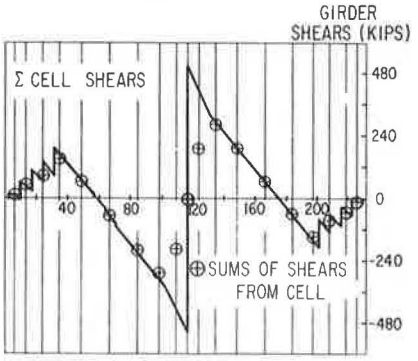

that end diaphragms provide components of longitudinal extension to these girders.

Total Moments

Digitized values of live load moments were tabulated at each cross section, modified by an impact factor, and added to dead load moments to create envelopes of total moments. The design for resisting moment subsequently differs little from standard design procedures.

Determination of Girder Shears

Dead Load Shears

Girder shears are obtainable directly from the program via a second postprocessing program called CELLSHR, which chooses proper values of N_{xy} at the tops and bottoms of girder webs from CELL output matrices and multiplies the averages of these two values by web depths. Signs must be reversed to agree with beam convention.

The dead load shears plotted in Figure 6 are very different from those that might be expected for a structure with orthogonal bearings. The shear at girder G1, which is at the acute corner at abutment 1, exhibits a very low value. Shears for center, first interior, and exterior girders at the obtuse corner exhibit nearly the same magnitudes. Shears for girders that frame into the bent on the acute angle side are very small. Maximum shears at the bent occur in the center girder.

Statics checks were made for dead load shears determined theoretically and by the program (see Figure 7). Agreement was not as good as in the case of bending moment. Calculated total shears from CELL fall very close to the curve of theoretical total shear out in the span. At the pier, deviations of CELL shears are evident and result from the fact that orthogonal sections intersect the bent cap where there is no convenient way to determine shears. Lesser deviations are evident at the abutments, but shear predictions break down at supported nodes.

Statics checks were greatly improved when cross sections were taken parallel to supports. The total load of the superstructure in span 1 was calculated with precision, and the total reaction at abutment 1 was deducted to provide a total bent shear of 200 t (440 kips); the sum of CELL reactions at the bent was 180 t (397 kips).

Live Load Shears

Calculation of live load shears required an influence-line approach, since the CELL program was run for 78 separate locations of the unit load on the deck. The plotting of influence lines was automated, again with curves for two adjacent wheel paths on each plot, and the maximum shear values were obtained by trial-and-error digitization with the transparent overlay. Envelopes of live load shears for each girder were added to dead load shears, and stirrup spacings were determined in the usual manner.

Bent Cap Design

Considerable effort was expended in writing additional postprocessing programs to determine bending moments in the bent cap. CELL does not directly output membrane stresses in the direction of skew, and such data must be formulated from deck and bottom slab stresses by rotations of axes. The bent cap designed on the basis of these stresses proved to be very lightly reinforced because forces in outlying slabs were not taken into account; indeed, the effective width of deck slabs is moot. CELL does not output bent cap shears. For these reasons, the bent cap was finally designed for bending moment and shear in the usual manner by using bent cap reactions obtained from the program.

Girder Deflections and Camber

Vertical girder displacements under dead load are given directly in the program output. Engineers who have been involved in the construction of heavily skewed structures are aware of the difficulties involved in establishing camber diagrams that resemble actual deflection patterns in finished structures because of the propensity for warping. Direct output of reasonable configurations of dead load displacements is a great aid in the design of skewed structures.

Postprocessor Program Modifications

After completion of the skew model design, the two postprocessing programs--CELLPOP (for calculation of individual girder moments) and CELLSHR (for calculation of girder shears)--were combined into one program, called CELL moments and shears (CELLMOSH), which had automatic tabulated output and plot tapes for automated plotting of moment and shear influence lines.

CONCLUSIONS

Volume of longitudinal No. 4 reinforcement in the skew model proved to be about 81 percent of that in the model on orthogonal supports. Previous calculations suggest even greater savings for simple spans,

and it is believed that they would also be greater for wider continuous structures of equal length. Savings are realized at the expense of significant increases in design effort. The alternative to expenditure of this effort for heavily skewed boxes may be very unrepresentative designs. Automation of program input, output interpretation, and development of expertise on the part of designers would be essential to realization of appreciable savings.

ACKNOWLEDGMENT

Design, construction, and testing of the skew box-girder model were performed in conjunction with a research project entitled, Structural Behavior of a Skew, Reinforced Concrete Box-Girder Bridge Model, which was sponsored jointly by the Federal Highway Administration (FHWA) and Caltrans.

The opinions, findings, and conclusions expressed in this paper are mine and do not necessarily reflect the official views or policies of Caltrans or FHWA. This paper does not constitute a standard, specification, or regulation.

REFERENCES

1. R.E. Davis. Structural Behavior of a Skew, Reinforced Concrete Box Girder Bridge Model: Volume 1, Design. Office of Structures Design, California Department of Transportation, Sacramento, Rept. FHWA-CA-50-4187-78-01, Jan. 1978.
2. R.E. Davis, J.J. Kozak, and C.F. Scheffey. Structural Behavior of a Box Girder Bridge. HRB, Highway Research Record 76, 1965, pp. 32-82.
3. R.E. Davis, J.J. Kozak, and C.F. Scheffey. Structural Behavior of a Box Girder Bridge, and Appendices. Bridge Department, California Division of Highways, Sacramento, Rept. SSR 2-65, 1965.
4. R.E. Davis, C.F. Scheffey, G.A. Castleton, and E.E. Evans. Box Girder Model Studies. Bridge Department, California Division of Highways, Sacramento, Rept. R&D 4-70, 1970.
5. R.E. Davis, C.F. Scheffey, G.A. Castleton, and E.E. Evans. Model and Prototype Studies of a Box Girder Bridge. Journal of the Structural Division, ASCE, Jan. 1972.
6. K.J. Willam and A.C. Scordelis. Computer Program for Cellular Structures of Arbitrary Plan Geometry. Univ. of California, Berkeley, Structural Engineering and Structural Mechanics Rept. UC SESM 70-10, Sept. 1970.

Publication of this paper sponsored by Committee on Concrete Bridges.

Response of 45° Skew, Reinforced Concrete Box-Girder Bridge Model to AASHTO Trucks and Overload Construction Vehicles

ALEX C. SCORDELIS, JACK G. BOUWKAMP, S. TANVIR WASTI, AND FRIEDER SEIBLE

A detailed study of the structural response of a 45° skew, two-span, four-cell, reinforced concrete box-girder bridge model under different types of vehicle loading is presented. The model, which was a 1:2.82 scale replica of a typical California highway prototype bridge, was 72 ft (21 m) long by 12 ft (3.7 m) wide and was supported by 45° skew end abutments and a 45° skew center bent supported by a single column. The vehicle loadings used consisted of scale models of standard American Association of State Highway and Transportation Officials HS 20-44 trucks and overload construction vehicles (class 2). In addition, influence lines for reactions and deflections were obtained by positioning a forklift truck at selected points on the bridge deck. The experimental response of the bridge model in the form of reactions, deflections, moments, and steel and concrete strains is compared with the theoretical response values obtained from a finite-element computer program CELL. The influence of skewness on the major design quantities is also assessed.

Multicell reinforced concrete box-girder bridges are widely used in the California highway system. The growing number of complex intersections, the lack of space in crowded urban areas, and the demand for road layouts without abrupt changes in direction frequently necessitate the use of bridges with skew, curved, or arbitrary plan geometry. Most design calculations for live load distribution in straight, skew, and curved box-girder bridges are based on the same empirical formula in which the effects of skewness or curvature are generally ignored.

The 1977 American Association of State Highway and Transportation Officials (AASHTO) specifications (1) specify a design method wherein a box-girder bridge is divided up into a number of interior girders plus two exterior girders. Each of these girders is designed as a separate member by applying to it a certain fraction of a single longitudinal line of wheel loads from a standard AASHTO HS 20-44 truck. The fraction is $N_{WL} = S/7$, in which S is the web spacing.

California uses a design procedure in which the whole bridge width is considered as a single unit and the distribution factor for the whole width unit is given by N_{WL} (total) = deck width in feet/7. The total moment at any section is assumed to be uniformly distributed across the width of the bridge.

In current practice for a skew bridge, design live load moments are determined for either of the above empirical wheel loadings by analyzing a straight bridge that has the same span but without any skew. Empirical rules, approximations, and engineering judgment are then used to account for skewness in determining longitudinal reinforcement cutoff points and some increase in web reinforcement for shear in the obtuse corners of the bridge.

In fact, the presence of skew generally reduces the total midspan moments in box-girder bridges because of the distribution of the reactions along the end abutments. The reduced moment for a simple span, 45° skew, four-cell box-girder bridge is shown in Figure 1 for a uniformly distributed surface load calculated with the finite-element computer program CELL (2) and compared with the generally used solu-

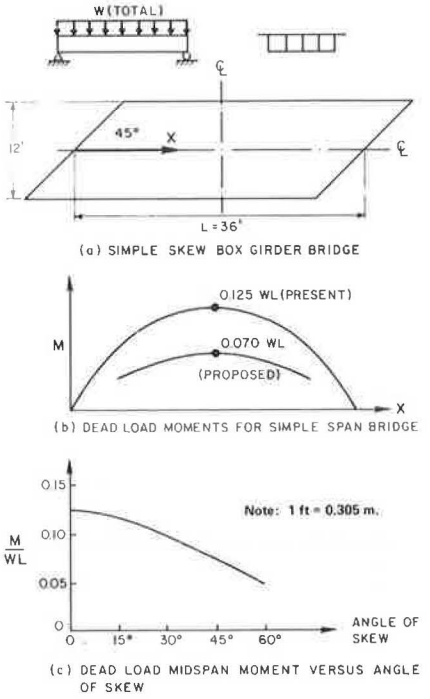

Figure 1. Reduction of total dead load moment at section due to skewness.

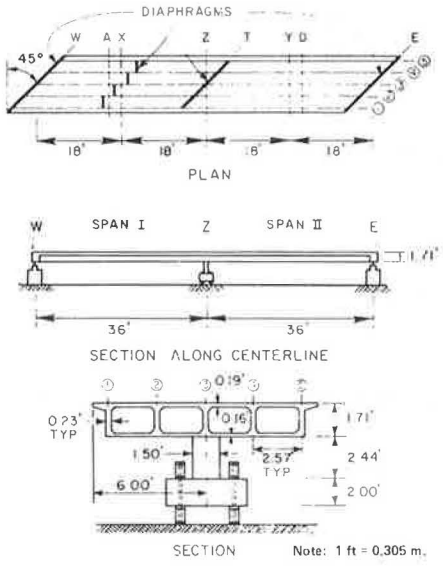

Figure 2. Overall dimensions of bridge model.

tion for a similar straight bridge model with the same span. The variation of the total midspan moment with the change in the angle of skew is also shown in Figure 1. Comartin and Scordelis (3) put forward a simplified design method for the design of simply supported skew box girders and have recommended the use of the computer program CELL for the design of continuous skew box-girder bridges. Godden and Aslam (4) verified the theoretical results from CELL by testing small-scale 1:29 elastic aluminum models of skew box-girder bridges. Also, a detailed study of 51 mathematical models of skew reinforced concrete box-girder bridges by using CELL has been reported by Wallace (5).

A continuous research program on box-girder bridges, which is directed toward improved design methods, has been conducted at the University of California, Berkeley, in which analytical and experimental studies have been successively conducted on the structural behavior of box-girder bridges that are straight, curved, skew, or of arbitrary plan geometry (6-19, and paper by Davis in this Record). As part of this investigation, a large number of computer programs have been developed for the analysis of these bridges by using folded-plate, finite-strip, finite-element, or finite-segment methods. A summary of these programs (with examples) can be found elsewhere (6). In addition, a number of the analytical and experimental investigations are summarized by Scordelis (7).

The most recent extensive investigation was made on the behavior of a 45° skew, two-span, four-cell, reinforced concrete box-girder bridge model (16). In this paper, the bridge behavior under standard AASHTO truck loads, construction-vehicle overloads, and moving forklift loads is studied in detail, and the influence of skewness on the major design quantities is assessed. Other aspects of the investigation, such as the structural response of the bridge model to point loads at working stress and overload stress levels (17), the behavior under conditioning overloads and ultimate failure loads (18), and the time-dependent behavior under sustained dead load (19), have been reported on elsewhere.

CONSTRUCTION OF BRIDGE MODEL AND EXPERIMENTAL PROGRAM

The overall dimensions of the 45° skew, two-span, four-cell, reinforced concrete bridge model as well as the designation of longitudinal girder lines and transverse sections are shown in Figure 2. The bridge was supported by 45° skew end abutments and a 45° skew center bent supported by a single circular column. The model was a 1:2.82 scale replica of a typical California two-lane box-girder bridge. The chosen scale guaranteed true representation of material behavior and was determined from the size of the standard reinforcing bars [60 ksi (414 MPa) yield] used in the prototype and model. A No. 11 main longitudinal bar in the prototype was exactly simulated by a No. 4 bar in the model.

The bridge model was designed by the Structural Research Unit, Office of Structures, California Department of Transportation (Caltrans), and was constructed by an outside contractor in the Structural Engineering Laboratory, Davis Hall, University of California, Berkeley. The design of the skew model, which is described in detail in Davis (see paper in this Record), was made with the aid of the CELL program (2) and resulted in the use of No. 4 reinforcement that was, by total volume, only about 81 percent of that that would be used in a similar straight bridge on orthogonal supports that had the same spans.

A brief summary of the construction of the bridge model and the test setup is given in Figure 3. Figures 3a, b, c, d, and g depict various stages in the construction of the bridge model, which was done in the same manner as the contruction of a prototype in the field. Figure 3e shows the additional dead load in the form of concrete blocks, which was necessary to simulate the proper prototype dead load behavior. Figure 3f illustrates the two midspan loading frames used for the application of point loads, AASHTO truck loads, and failure loads, respectively. Figure 3h shows the bridge model during the final load test to failure.

The instrumentation of the model was designed to measure loads, reactions, deflections, and strains. Load cells were used to measure individual end reactions under each girder, column reactions at the center bent, and loads applied by means of hydraulic jacks at midspan sections X and Y. Deflections were

measured at 32 points by linear potentiometers as well as by mirror scales along the exterior girders of the bridge model. Steel strains were monitored by 128 waterproofed, weldable strain gages and concrete strains by 86 concrete strain meters. A low-speed scanner unit with 8K storage, magnetic tape recorder, digital voltmeter, teletype, and terminal boxes controlled and recorded the measurements.

The experimental program consisted of the following parts: (a) dead load, (b) working stress loads, (c) overloads, and (d) failure loading. The application of AASHTO truck loads, construction-vehicle overloads, and moving forklift truck loads was conducted as part of the working stress load stage after the bridge model had been subjected to conditioning loads that produced nominal tensile stresses of 30 ksi (207 MPa) in the reinforcing steel. In order to allow the positioning of the truck models on the bridge deck, the concrete blocks that represented part of the prototype dead load shown in Figure 3e had to be removed.

The AASHTO truck models, one of the construction vehicles, and the forklift truck used for the loading of the skew bridge model are shown in Figures 4a, b, and c, respectively.

Figure 3. Sequence of construction, overall test setup, and loading to failure of skew bridge model.

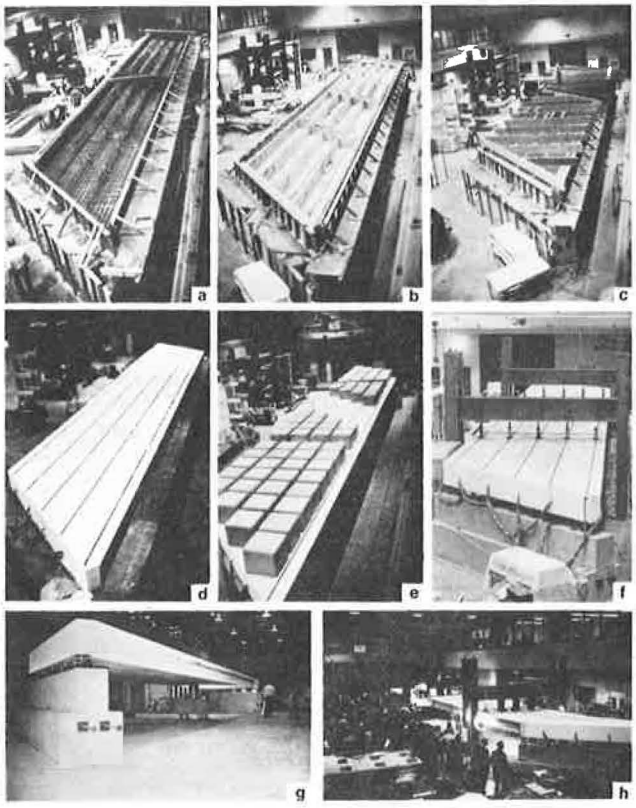

Figure 4. AASHTO trucks, construction vehicles, and moving forklift truck on bridge deck.

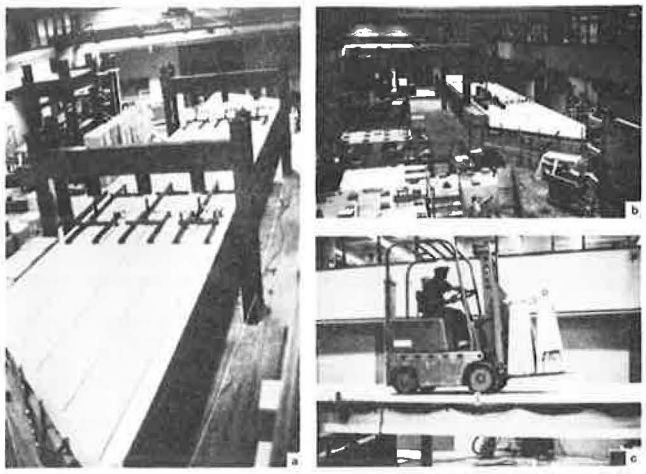

THEORETICAL ANALYSIS

For comparison with experimental data, a theoretical analysis was conducted by using the computer program CELL (2), which is a general finite-element program for the linear elastic analysis of cellular bridge structures in which the structure is assumed to be an uncracked homogeneous concrete assemblage of plane plate elements that represent the top and bottom flanges and the vertical webs. Both membrane and plate-bending action are accounted for in the elements comprising the structure. Convergences and accuracy of solutions were assured by comparing different mesh sizes and by statics checks of external and internal forces at various sections in the bridge model.

As in the AASHTO specifications, each truck was modeled by six vertical concentrated loads that were appropriately scaled down to simulate the prototype loads on the model (Figures 4a and b). The moving forklift truck was modeled in the theoretical analysis by four vertical point loads (Figure 4c).

The results from the theoretical analysis by using CELL were in the form of reactions, deflections, and internal forces. The internal forces were directly converted by a postprocessor program to individual girder and total sections moments at various transverse sections of the bridge model for direct comparison with similarly reduced experimental data.

AASHTO TRUCK AND CONSTRUCTION-VEHICLE LOADING

The model was loaded by scaled-down versions of the standard AASHTO HS 20-44 (MS 18) truck [truck load = 72 kips (320 kN)] and a proposed overload class 2 construction vehicle [total load = 320 kips (1470 kN)]. All linear dimensions were reduced by the scale factor 1:2.82, and similitude required that the loads be reduced by a factor of 1:8 to produce the same stress in the model as in the prototype. Thus, for the model the total load for each truck was 9.0 kips (40.0 kN) and for each construction vehicle 41.25 kips (183.5 kN).

The positions and directions of the truck and construction-vehicle loads on the bridge are shown in Figure 5 (also Figure 4). A total of 11 combinations of two-lane truck loadings, 3 combinations of three-lane truck loadings, and 8 combinations of construction-vehicle loadings were used.

Reactions

A summary of experimental and theoretical reactions is given in Table 1 for selected cases of vehicle loadings. The total west end and east end reactions shown are the statically equivalent bridge centerline reactions obtained from individual reactions under each girder for both experiment and theory.

Excellent agreement exists for the vertical end reactions R_W and R_E, while the vertical center footing reaction R_F is slightly higher in the experimental than in the theoretical analysis. The

moment and torque reactions (M and T) show generally good agreement between experiment and theory except for a few load cases.

The influence of skewness of the end abutments can readily be seen from the direction and magnitude of the total end moments M_W and M_E, which for most load cases act in a sense so as to reduce the midspan moments produced by the vehicle loads.

Figure 5. Positions and directions of truck and construction-vehicle loadings on bridge deck.

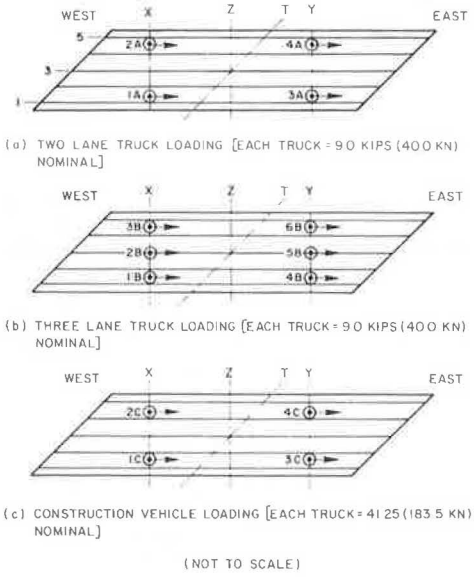

(a) TWO LANE TRUCK LOADING [EACH TRUCK = 9.0 KIPS (40.0 KN) NOMINAL]

(b) THREE LANE TRUCK LOADING [EACH TRUCK = 9.0 KIPS (40.0 KN) NOMINAL]

(c) CONSTRUCTION VEHICLE LOADING [EACH TRUCK = 41.25 (183.5 KN) NOMINAL]

(NOT TO SCALE)

Deflections

Experimental deflections are shown in Figure 6a for vehicle loadings producing maximum deflection at transverse sections X and Y in the diaphragmed and undiaphragmed span, respectively. Theoretical values are not shown, since the analysis, which is based on an uncracked structure, does not give displacement values that can be directly compared with the experimental results obtained from the cracked reinforced concrete model. However, it should be noted that with a magnification factor of about 1.5-2.0 applied to the theoretical deflections from CELL (3), the overall shape of the deflected experimental model can be very closely approximated for all load cases in the working stress range.

For the two- and three-lane truck loads shown in Figure 5, the loading is relatively uniform across the width of the bridge, which results in an almost uniform distribution of deflections that have slightly higher deflections toward the acute side of the span. For the construction vehicle, only one lane is loaded on the acute side of the span, which results in substantially larger deflections at the loaded position. By comparing results at sections X and Y, these loadings also demonstrate the effect of the transverse midspan diaphragm. For construction-vehicle loads at position 2C and 4C (Figure 5) in the diaphragmed and undiaphragmed spans 1 and 2, respectively (Figure 1), it can be seen in Figure 6a that the transverse distribution of deflections is slightly more uniform in the diaphragmed span.

The maximum deflections for the two-lane truck, three-lane truck, and construction-vehicle loadings

Table 1. Comparison of theoretical and experimental reactions under truck and construction-vehicle loads.

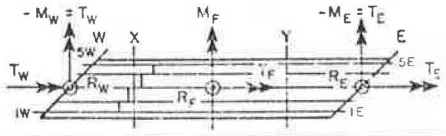

Load Case	Solution	Reactions: West End R_W (kips)	West End M_W (kip-ft)	West End T_W (kip-ft)	Center Footing R_F (kips)	Center Footing M_F (kip-ft)	Center Footing T_F (kip-ft)	East End R_E (kips)	East End M_E (kip-ft)	East End T_E (kip-ft)	Total R (kips)	Load (kips): Section X (P_X)	Section Y (P_Y)	Total (P)
Two-Lane Truck Loading														
4A	T	-0.5	-9	9	6.5	-10	15	3.1	-11	11	9.0	-9.0	0.0	-9.0
	E	-0.6	-7	7	7.0	-9	15	3.1	-14	14	9.6	-9.0	0.0	-9.0
3A+4A	T	-1.2	-4	4	11.8	-16	12	7.5	17	-17	18.0	-18.0	0.0	-18.0
	E	-1.4	-1	1	12.0	-17	11	7.3	12	-12	17.8	-18.0	0.0	-18.0
2A+4A	T	4.2	-37	37	11.5	-4	17	2.4	-15	15	18.0	-9.0	-9.0	-18.0
	E	4.0	-34	34	12.7	-2	20	2.5	-20	20	19.2	-9.0	-9.0	-18.0
1A+2A	T	6.7	-22	22	23.0	0	0	6.3	21	-21	36.0	-18.0	-18.0	-36.0
+3A+4A	E	6.5	-15	15	23.9	4	-1	6.2	16	-16	36.6	-17.8	-18.2	-36.0
Three-Lane Truck Loading														
4B+5B+6B	T	-1.8	-26	26	17.6	-24	18	11.2	7	-7	27.0	0.0	-27.0	-27.0
	E	-2.0	-1	1	18.1	-27	17	11.0	21	-21	27.1	0.0	-27.0	-27.0
1B+2B+3B	T	10.1	-32	32	34.5	0	0	9.4	31	-31	54.0	-27.0	-27.0	-54.0
+4B+5B+6B	E	9.4	-22	22	35.1	5	-1	9.1	22	-22	53.6	-27.1	-26.9	-54.0
Construction-Vehicle Loading														
4C	T	-2.1	-35	35	28.5	-40	58	14.9	-39	39	41.2	0.0	-41.3	-41.3
	E	-2.5	-27	27	30.5	-52	70	15.2	-52	52	43.2	0.0	-41.3	-41.3
2C+4C	T	18.9	-147	147	51.6	-14	64	12.0	-55	55	82.5	-41.3	-41.2	-82.5
	E	18.4	-138	138	56.5	-20	86	12.3	-69	69	87.1	-41.3	-41.2	-82.5

Notes: T = theoretical and E = experimental.
1 kip = 4.448 kN, 1 kip-ft = 1.356 kN-m.

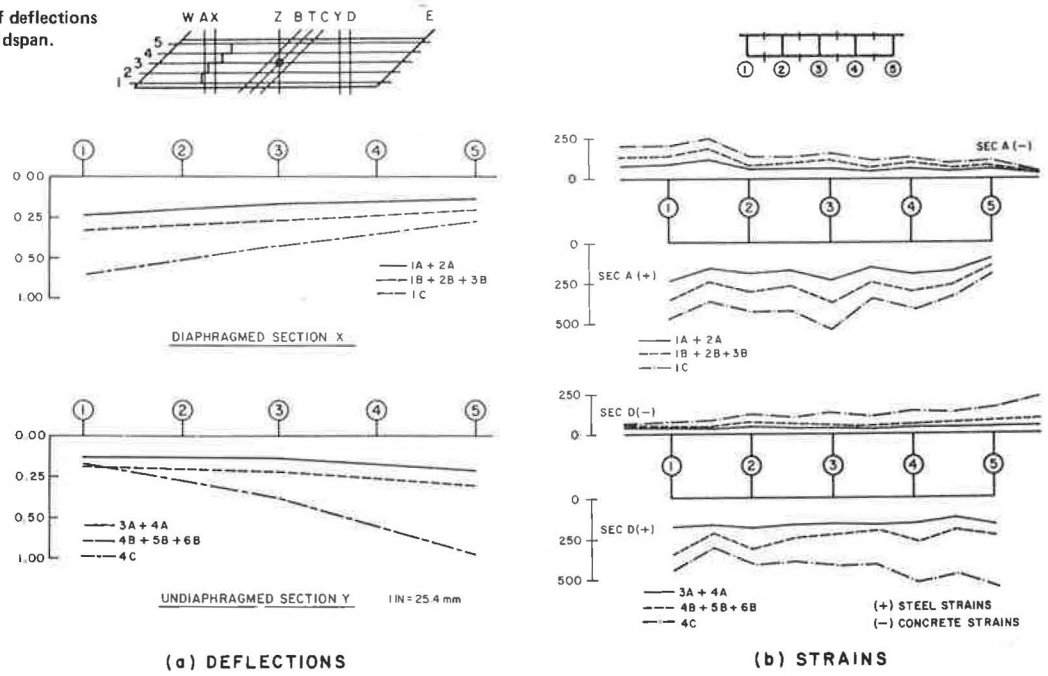

Figure 6. Transverse distribution of deflections (inches) and strains (μ-strains) at midspan.

were 0.22, 0.33, and 0.74 in (5.6, 8.4, and 18.8 mm), respectively. The corresponding deflection to span ratios were 1/1960, 1/1300, and 1/580, and these would be the same in a full-scale prototype structure because of similitude.

Strains and Maximum Stresses

The transverse distribution of experimental longitudinal strains at midspan sections A and D for truck and construction-vehicle loadings producing maximum effects are shown in Figure 6b. Similar to the transverse distribution of displacements in Figure 6a, the two- and three-lane truck loadings, which are uniform across the width of the bridge, show strain distributions that are also quite uniform. For the heavy concentrated load of a construction vehicle on the acute side of the diaphragmed span 1C, only small changes in the general shape of the transverse strain distribution are noticeable at section A, while at section D for a load in the undiaphragmed span 4C, a shift of the longitudinal strains toward the loaded (acute side) of the span can be noticed.

Multiplying the maximum strain values from Figure 6b by the modulus of elasticity of the reinforcing steel and adding the nominal average dead load steel stress for sections A and D of 12 000 psi (83 MPa), it can be seen that the total maximum steel stress for the two- and three-lane truck loadings of 18 450 and 22 100 psi (127 and 152 MPa), respectively, is below the allowable value of 24 000 psi (165 MPa). For the construction-vehicle loading, a maximum calculated total steel stress of about 27 000 psi (186 MPa) occurs.

Live load concrete stresses calculated from compressive strains are quite small and would be well within the allowable stresses when added to the nominal dead load stresses.

Total Moments and Individual Girder Moments

Tables 2, 3, and 4 summarize the girder moments and their transverse distribution for a variety of vehicle load combinations. (For truck locations, see Figure 5.)

The maximum moments in the bridge model get progressively larger as one proceeds from the single truck load to two-lane truck, three-lane truck, and finally the construction-vehicle loading. By comparing the total experimental and theoretical section moments, fairly good agreement can be found in the diaphragmed span (section A), while in the undiaphragmed span (section D) the experimental moment was found to be consistently higher than the theoretical moment. Looking at individual girder moments, it can be seen that, at section A, consistently a much larger moment is carried in girder 1 experimentally than that predicted by theory. Here the close proximity of the staggered midspan diaphragm (Figure 1) to the instrumented section A may have caused this discrepancy. The percentage distribution of total midspan moments to individual girders for critical vehicle loads in Table 4 shows that the experimental distribution is virtually the same for two-lane truck, three-lane truck, and construction-vehicle loading in the diaphragmed span, while in the undiaphragmed span at section D the construction-vehicle loading clearly shows a shift in the transverse distribution of the midspan moment to the acute side of the span. By comparing these percentage values with optimum ones obtained for a uniform stress distribution across the bridge, the two- and three-lane truck loadings in section D show good agreement, while the construction-vehicle loading deviates significantly. At section A, again, the high experimental contribution of girder 1 can be noted causing a stronger deviation from the uniform stress distribution.

Effect of Skewness: Comparison with Straight and Curved Box-Girder Bridge Models

To show the effect of skewness on reactions, deflections, strains, and moments in a continuous multicell box-girder bridge under vehicle loading, the following three cases are considered:

1. A fairly uniform vehicle loading across one span (4B+5B+6B),
2. A concentrated vehicle load on the obtuse side of a span (3C), and

Table 2. Section A experimental and theoretical girder moments under critical truck and construction-vehicle loads (moments about gross section neutral axis).

	Single Truck Loading (kip-ft)				Two-Lane Truck Loading (kip-ft)						Three-Lane Truck Loading (kip-ft)				Construction-Vehicle Loading (kip-ft)							
	1A		2A		1A+2A		1A+3A		1A+2A+ 3A+4A		1B+2B+3B		1B+2B+3B+ 4B+5B+6B		1C		2C		1C+3C		1C+4C	
Girder	E	T	E	T	E	T	E	T	E	T	E	T	E	T	E	T	E	T	E	T	E	T
1	16	10	7	5	23	15	14	9	18	12	37	24	27	18	53	31	32	21	44	26	35	20
2	15	16	6	7	21	21	13	12	17	16	33	32	26	24	48	46	29	29	41	40	33	31
3	12	14	7	7	20	21	11	12	16	16	33	32	26	24	48	47	29	26	41	41	34	32
4	10	11	9	10	19	22	8	10	15	16	29	32	22	24	41	44	29	30	33	37	27	29
5	5	8	7	9	12	16	5	7	9	13	18	23	13	17	24	31	20	23	19	26	15	20
Σ	58	59	36	38	95	95	51	50	75	73	150	143	114	107	214	199	139	129	178	170	144	132

Notes: E = experimental and T = theoretical.
1 kip-ft = 1.356 kN-m.

Table 3. Section D experimental and theoretical girder moments under critical truck and construction-vehicle loads (moments about gross section neutral axis).

	Single Truck Loading (kip-ft)				Two-Lane Truck Loading (kip-ft)						Three-Lane Truck Loading (kip-ft)				Construction-Vehicle Loading (kip-ft)							
	4A		3A		4A+3A		4A+2A		1A+2A+ 3A+4A		4B+5B+6B		1B+2B+3B+ 4B+5B+6B		4C		3C		2C+4C		2C+3C	
Girder	E	T	E	T	E	T	E	T	E	T	E	T	E	T	E	T	E	T	E	T	E	T
1	8	7	10	8	18	15	6	6	14	11	26	22	20	16	34	29	43	33	28	24	37	27
2	11	10	11	9	21	20	10	9	16	15	33	30	25	23	48	42	48	38	41	35	42	31
3	11	12	7	8	18	20	10	10	14	14	29	30	22	23	49	49	32	33	43	42	26	27
4	13	14	7	6	19	20	12	13	13	15	28	31	20	23	56	54	27	27	50	48	22	21
5	13	11	5	4	19	16	12	10	14	12	27	23	21	17	57	44	25	18	53	39	19	14
Σ	56	54	40	35	95	91	50	48	71	67	143	136	108	102	244	218	175	149	215	188	146	120

Notes: E = experimental and T = theoretical.
1 kip-ft = 1.356 kN-m.

Table 4. Experimental percentage distribution of total moment at sections A and D for critical truck and construction-vehicle loadings.

	Section A Girders					Section D Girders				
Item	1	2	3	4	5	1	2	3	4	5
Uniform stress distribution	17	22	22	22	17	17	22	22	22	17
Two-lane truck										
1A+2A	24	22	21	20	13					
3A+4A						19	22	19	20	20
Three-lane truck										
1B+2B+3B	25	22	22	19	12					
4B+5B+6B						19	23	20	20	19
Construction vehicle										
1C	25	22	22	19	12					
4C						14	20	20	23	23

3. A concentrated vehicle load on the acute side of a span (4C).

The above three loading cases are compared in Table 5 with corresponding loading cases on similar straight and curved bridge models (10,12) tested previously.

A comparison of the vertical reactions R_W, R_F, and R_E in Table 5 (see key above Table 1) shows excellent agreement between the three bridge types for all load cases except 3C where, in the case of the skew bridge, the construction vehicle is located on the obtuse side of the span and more load is transferred directly into the end abutment and less into the center footing than for the comparable straight and curved bridge cases. The end moments M_W and M_E, which are only present for the skew bridge, clearly show the characteristics of skew bridge behavior. Considering only the loaded undiaphragmed span 2 (Figure 1) and the end moment in this span (M_E), it is found that for the case where the loads are uniformly distributed across the width (4B+5B+6B) and for the case where the span is loaded on the obtuse side (3C), the end moment M_E is positive, which means the midspan moment due to the vehicle loading is effectively reduced by this end moment. However, in the case where the acute side of the span is loaded (4C), the end moment M_E is negative and thus unfavorably increases the midspan moment due to this midspan vehicle load.

The total midspan moments at section D at the bottom of Table 5 clearly show this influence of skewness. Although straight and curved bridges show good agreement for all three load cases, the skew bridge features a lower total midspan moment when the load is applied on the obtuse side of the span and a higher total midspan moment when the load is applied on the acute side of the span.

The same phenomenon can be seen from the vertical deflections across midspan section Y. Although the skew bridge deflections are much smaller for the load on the obtuse side of the skew span (3C) than for comparable straight and curved bridge cases, significantly higher deformations are encountered in the skew bridge when the vehicle is placed on the acute side of the span.

A final comparison of results for the straight, curved, and skew bridge model is made in Table 6 for maximum live load experimental strains and stresses under truck and construction-vehicle loadings. Strains shown are the maximum values recorded at any point in the bridge model under the loadings shown. From Table 6 it can be seen that the concrete strains are very low for all three bridge types. The order of magnitude for concrete and steel strains and stresses is about the same for straight, curved, and skew bridge models.

Table 5. Comparison between straight, curved, and skew box-girder bridge models.

Item	Three-Lane Truck, 4B+5B+6B			Construction Vehicle, 3C			Construction Vehicle, 4C		
	Straight	Curved	Skew	Straight	Curved	Skew	Straight	Curved	Skew
Reactions									
R_W (kips)	-2.0	-2.1	-2.0	-3.0	-2.5	-3.2	-3.0	-3.5	-2.5
M_W (kip-ft)	0.0	0.0	1.0	0.0	0.0	18.4	0.0	0.0	-26.3
R_F (kips)	18.8	18.8	18.1	28.6	27.7	24.5	28.6	28.9	30.5
R_E (kips)	10.5	9.9	11.0	16.2	16.4	20.5	16.2	15.9	15.2
M_E kip-ft)	0.0	0.0	20.5	0.0	0.0	112.5	0.0	0.0	-51.6
Deflections (in)									
1Y	0.25	0.27	0.19	0.49	0.56	0.37	0.25	0.28	0.20
3Y	0.23	0.28	0.22	0.35	0.39	0.25	0.35	0.43	0.38
5Y	0.23	0.31	0.30	0.25	0.30	0.24	0.49	0.64	0.74
Moments, section D (kip-ft)									
1	25	19	26	30	41	43	29	21	34
2	30	32	33	49	57	48	39	39	48
3	33	30	29	44	40	32	44	42	49
4	37	34	28	39	36	27	49	52	56
5	21	24	27	29	25	25	30	36	58
Total	146	139	143	191	199	175	191	190	245

Note: 1 kip = 4.448 kN, 1 kip-ft = 1.356 kN-m, 1 in = 25.4 mm.

Table 6. Comparison of maximum live load experimental strains and stresses for straight, curved, and skew bridge models under truck and construction-vehicle loads.

Item	Concrete Sections				Steel Sections			
	A	B	C	D	A	B	C	D
Experimental strains (μ in/in)								
Two-lane truck								
Straight	59	81	83	65	276	128	133	229
Curved	110	67	70	83	221	123	125	197
Skew	116	103	88	67	233	124	123	174
Three-lane truck								
Straight	72	123	119	100	334	202	201	369
Curved	138	99	110	127	306	195	200	290
Skew	175	145	129	98	365	185	183	340
Construction vehicle								
Straight	135	176	177	115	586	352	324	448
Curved	191	154	155	178	565	303	324	450
Skew	249	175	225	230	527	249	338	519
Experimental stresses (psi)								
Two-lane truck								
Straight	207	235	241	249	8 030	3 710	3860	6 690
Curved	297	178	186	254	6 080	3 380	3440	3 420
Skew	348	309	264	201	6 450	3 440	3410	4 820
Three-lane truck								
Straight	276	351	346	383	9 980	5 850	5830	10 700
Curved	373	263	292	387	8 420	5 360	5500	7 980
Skew	525	435	387	294	10 100	5 130	5070	9 420
Construction vehicle								
Straight	516	510	514	440	17 000	10 200	9380	13 000
Curved	516	408	411	543	15 500	8 330	8910	12 400
Skew	747	525	675	690	14 600	6 900	9360	14 400

Note: 1 psi = 0.006 895 MPa.

MOVING FORKLIFT TRUCK LOADINGS

For highway bridges, the most critical live loads are moving concentrated loads (such as heavy overload construction vehicles) traveling across the bridge. Therefore, part of this investigation of vehicle loadings on a skew, continuous box-girder bridge consisted of a moving forklift truck positioned at 50 selected points on the bridge deck in order to obtain general shapes of influence lines for different important design quantities. Selected influence lines for the total vertical and moment reactions at the west end abutment, as well as vertical deflections at the exterior girders of midspan section Y, are given in Figures 7 and 8.

From the general shape of these influence lines, the overall behavior of the bridge model under moving loads can be deduced, but they should not be used to obtain numerical design quantities. Scaling factors obtained from extreme or midspan values were used on the theoretical data (shown in Figures 7 and 8) to account for stiffness deterioration due to cracking in the reinforced concrete model in order to allow a comparison of the general shape of theoretical and experimental influence lines. Scaling factors and reference locations are also indicated in Figures 7 and 8.

Influence Lines for Reactions

Influence lines for the west end reactions are depicted in Figures 7a and b. For the vertical reaction, a remarkable agreement between experimental and theoretical values can be observed. It also should be noted that the scaling factors involved are very close to unity.

Influence lines for the west end moment show close agreement for the north and center pass between experiment and theory. The south pass features larger discrepancies in both general shape and scaling factor. The influence lines for the west end moment clearly show the influence of skewness of the bridge model, since the end moment directly influences the important midspan design moment. In

Figure 7. Shapes of influence lines for west end reactions.

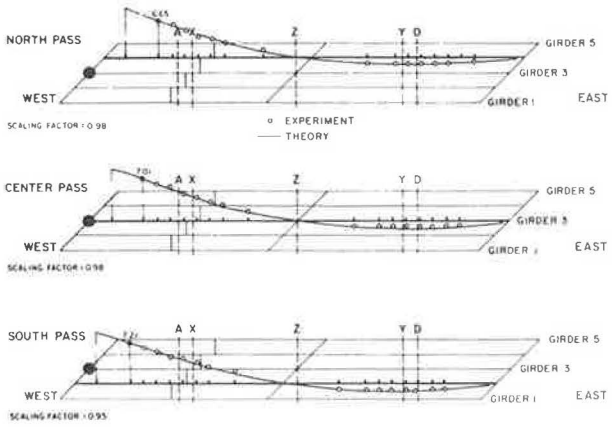

(a) TOTAL VERTICAL WEST END REACTION

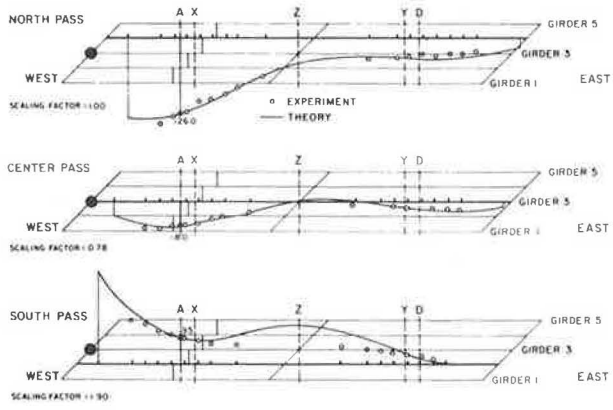

(b) TOTAL WEST END MOMENT

Figure 8. Shapes of influence lines for vertical midspan deflections.

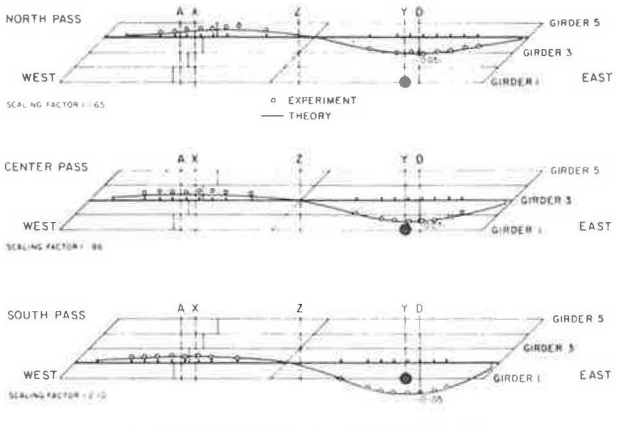

(a) DEFLECTION AT LOCATION 1Y

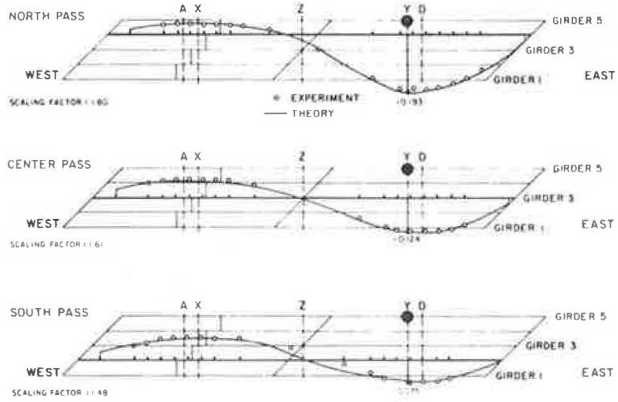

(b) DEFLECTION AT LOCATION 5Y

Figure 7b, an end moment value below the reference axis indicates a beneficial reduction in the total midspan moment, while an end moment value above the reference axis shows an unfavorable increase in the midspan moment. Thus, from Figure 7b it can be clearly seen that as long as concentrated loads move along the center of the bridge or on the obtuse side of the span, the skewness of the bridge model has a beneficial effect on the design midspan moment, while the midspan moment for a concentrated load moving along the acute side of a span will be unfavorably influenced by the skewness of the bridge.

Influence Lines for Midspan Deflections

Influence lines for midspan deflections at 1Y and 5Y in the undiaphragmed span are shown in Figures 8a and b. Again, remarkable agreement can be noticed in the general shape of the experimental and theoretical influence lines. A magnification factor between 1.5 and 2.0 is necessary to account for stiffness deterioration in the bridge model due to cracking of the concrete.

The influence of skew is seen again when comparing displacement values at the obtuse and acute side of the span in Figures 8a and b, respectively. Although the displacements on the acute side of the span are generally larger for all load positions than corresponding displacements on the obtuse side of the span, a big increase in maximum midspan displacements can be observed for loads shifting transversely across the bridge from the obtuse side to the acute side of the span.

SUMMARY AND CONCLUSIONS

The box-girder bridge model tested in this investigation clearly showed different behavior under various types of vehicle loadings than similar straight and curved bridge models, which can be attributed to the presence of skew end abutments and the skew center diaphragm. The influence of skewness depends largely on the type of loading and, more specifically, on the location of load application on the skew bridge deck.

The following conclusions can be drawn from the present investigation:

1. In addition to the vertical end reaction, a skew bridge also features an end moment that acts along an axis perpendicular to the bridge axis, which directly influences the design total midspan moments. Concentrated loads on the acute side of a span result in an end moment reaction that increases the midspan moment, while all other load positions and distributed loads across the span produce an end moment that reduces the midspan moment favorably.
2. The largest deflections under any vehicle load occurred at midspan at the acute side of the bridge loaded with a single overload class 2 con-

struction vehicle at the same location. The maximum deflection observed for this load case gives a deflection-to-span ratio of 1/580, which is still quite small but substantially larger than the comparable ratio for the similar straight bridge model of 1/870. However, the same load on the obtuse side of the span of the skew continuous bridge produced only a deflection-to-span ratio of 1/1170.

3. The transverse distribution of maximum moments to individual girders was found to be substantially different from the case where a uniform stress distribution is assumed across the section.

4. Steel and concrete stresses produced by dead load and vehicle loads are lower than allowable values for two- and three-lane AASHTO HS 20-44 trucks but slightly exceed the allowable values for one lane of proposed class 2 construction vehicles. However, all observed stresses were well below the proportional limit.

ACKNOWLEDGMENT

This investigation was sponsored by the Business and Transportation Agency, Caltrans, and the Federal Highway Administration, U.S. Department of Transportation. The opinions, findings, and conclusions expressed are ours and not necessarily those of the sponsors.

REFERENCES

1. Standard Specifications for Highway Bridges, 12th ed. AASHTO, Washington, DC, 1977.
2. K.J. Willam and A.C. Scordelis. Cellular Structures of Arbitrary Plan Geometry. Journal of the Structural Division, ASCE, Vol. 98, No. ST7, July 1972.
3. C.D. Comartin and A.C. Scordelis. Analysis and Design of Skew Box Girder Bridges. Univ. of California, Berkeley, Structural Engineering and Structural Mechanic Rept. UC SESM 72-14, Dec. 1972.
4. W.G. Godden and M. Aslam. Model Studies of Skew Multicell Girder Bridges. Journal of the Engineering Mechanics Division, ASCE, Vol. 99, No. EM1, Feb. 1973.
5. M.R. Wallace. Studies of Skewed Concrete Box Girder Bridges. TRB, Transportation Research Record 607, 1976, pp. 50-55.
6. A.C. Scordelis. Analytical Solutions for Box Girder Bridges. Proc., Conference on Modern Developments in Bridge Design and Construction, Cardiff, Great Britain, April 1971.
7. A.C. Scordelis. Analytical and Experimental Studies of Multi-Cell Concrete Box Girder Bridges. Bull., International Association for Shell and Spatial Structures, Madrid, No. 58, Aug. 1975.
8. A.C. Scordelis, J.G. Bouwkamp, and S.T. Wasti. Structural Behavior of a Two Span Reinforced Concrete Box Girder Bridge Model: Vols. 1-3. Univ. of California, Berkeley, Structural Engineering and Structural Mechanics Rept. UC SESM 71-5, 71-6, and 71-7, Oct. 1971.
9. A.C. Scordelis, J.G. Bouwkamp, and S.T. Wasti. Study of AASHO Loadings on a Concrete Box Girder Bridge. HRB, Highway Research Record 428, 1973, pp. 22-31.
10. A.C. Scordelis, J.G. Bouwkamp, and S.T. Wasti. Structural Response of a Concrete Box Girder Bridge. Journal of the Structural Division, ASCE, Vol. 99, No. ST10, Oct. 1973.
11. A.C. Scordelis, J.G. Bouwkamp, and S.T. Wasti. Ultimate Strength of a Concrete Box Girder Bridge. Journal of the Structural Division, ASCE, Vol. 100, No. ST1, Jan. 1974.
12. A.C. Scordelis, J.G. Bouwkamp, and P.K. Larsen. Structural Behavior of a Curved Two Span Reinforced Concrete Box Girder Bridge Model: Vols. 1-3. Univ. of California, Berkeley, Structural Engineering and Structural Mechanics Rept. UC SESM 74-5, 74-6, and 74-7, Sept. 1974.
13. A.C. Scordelis and P.K. Larsen. Structural Response of Curved RC Box Girder Bridge. Journal of the Structural Division, ASCE, Vol. 103, No. ST8, Aug. 1977.
14. A.C. Scordelis, P.K. Larsen, and L.G. Elfgren. Ultimate Strength of Curved RC Box Girder Bridge. Journal of the Structural Division, ASCE, Vol. 103, No. ST8, Aug. 1977.
15. A.C. Scordelis, L.G. Elfgren, and P.K. Larsen. Time Dependent Behavior of Box Girder Bridges. Journal of the American Concrete Institute, Title 76-9, Jan. 1979.
16. A.C. Scordelis, J.G. Bouwkamp, S.T. Wasti, and D. Anicic. Structural Behavior of a Skew Two Span Reinforced Concrete Box Girder Bridge Model: Vols. 1-4. Univ. of California, Berkeley, Structural Engineering and Structural Mechanics Rept. UC SESM 80-1, 80-2, 80-3, and 80-4, June 1980.
17. A.C. Scordelis, S.T. Wasti, and F. Seible. Structural Response of Skew RC Box Girder Bridge. Journal of the Structural Division, ASCE, Vol. 108, No. ST1, Jan. 1982.
18. A.C. Scordelis, J.G. Bouwkamp, S.T. Wasti, and F. Seible. Ultimate Strength of Skew RC Girder Bridge. Journal of the Structural Division, ASCE, Vol. 108, No. ST1, Jan. 1982.
19. A.C. Scordelis and F. Seible. Time-Dependent Behavior of a Skew RC Box Girder Bridge. Journal of the American Concrete Institute, Concrete International (in preparation).

Publication of this paper sponsored by Committee on Concrete Bridges.

Evaluation and Verification of Time-Dependent Deformations in Posttensioned Box-Girder Bridges

HENRY G. RUSSELL, KWOK-NAM SHIU, WILLIAM L. GAMBLE, AND VERNON L. MARSHALL

A 76.2-m (250-ft) span, constant-depth precast concrete posttensioned box-girder bridge was instrumented to measure longitudinal strain caused by applied loads, posttensioning, creep, and shrinkage. Material properties of the concrete used in the instrumented span were obtained. Variation of compressive strength, elastic modulus, coefficient of thermal expansion, creep, and shrinkage with age of concrete were measured for specimens cured indoors and outdoors. Time-dependent deformations were calculated by using a step-by-step numerical procedure that used detailed construction records and material properties. Comparisons between measured and calculated deformations showed best agreement when concrete properties were based on specimens cured in an outdoor environment. However, good agreement was also obtained when concrete data from laboratory specimens were used. This indicates that time-dependent deformations of box girders can be predicted by using the step-by-step numerical procedure with the physical properties of laboratory specimens.

Three posttensioned box-girder bridges have been instrumented by the Construction Technology Laboratories of the Portland Cement Association to measure long-term deformations. The three bridges are Denny Creek Bridge in Washington, Kishwaukee River Bridge in Illinois, and Linn Cove Viaduct in North Carolina. Although the specific objectives of each project have been different, the overall objective has been to obtain information to verify design and analysis procedures for time-dependent effects in posttensioned box-girder bridges. This paper concentrates on the research program that was performed in connection with the Kishwaukee River Bridge. The specific objective of the project was to verify a step-by-step numerical procedure for calculating time-dependent deformations in segmental box-girder bridges constructed by the cantilever method.

HIGHLIGHTS

Kishwaukee River Bridge, which is located near Rockford, Illinois, consists of twin constant-depth precast concrete posttensioned box-girder bridges. Each bridge has five spans that measure 51.8 m (170 ft) for the end spans and 76.2 m (250 ft) for the three interior spans. The bridge was constructed by using the balanced-cantilever method with a launching girder. A cast-in-place section was used to complete each span.

Three cross sections of one bridge span were instrumented during construction. Instrumentation was installed to measure longitudinal strains caused by applied loads, posttensioning, creep, and shrinkage. Instrumentation was installed before the precast segments were cast.

In parallel with the field investigation, properties of the concrete used in the instrumented segments were measured from concrete cylinders obtained in the field. Variation of compressive strength, elastic modulus, coefficient of thermal expansion, creep, and shrinkage with time were measured. Specimens were cured under both constant temperature and humidity and under field conditions.

Deformations of the instrumented segments were calculated by using a step-by-step numerical procedure developed at the University of Illinois, Urbana. The procedure accounted for important parameters that influence the time-dependent behavior of segmental bridges.

Comparisons were made between calculated deformations and those measured on the structure. Good agreement was obtained for calculations that used properties of the concrete that was stored outside.

KISHWAUKEE RIVER BRIDGE

The Kishwaukee River Bridge, shown in Figure 1, is located in Winnebago County, about four miles south of Rockford, Illinois. When completed, it will carry four lanes of US-51, which serves as a major north-south highway. The Kishwaukee River Bridge consists of two identical parallel bridges spanning about 30 m (100 ft) above the heavily wooded Kishwaukee River Valley. Each bridge has three main spans of 76.2 m (250 ft) and two end spans of 51.8 m (170 ft) for a total length of 332 m (1090 ft). Arrangement and elevation of the spans are shown in Figure 2.

The Kishwaukee River Bridge is a continuous single-cell box girder made with precast concrete segments. Overall cross-sectional dimensions of a midspan segment are shown in Figure 3. Except for those over the piers, each segment has a length of 2.1 m (7 ft). Pier segments have a diaphragm, a thicker soffit, and are shorter in length. Each main 76.2-m span is made up of 34 precast segments with 1 cast-in-place closure segment at midspan.

Posttensioning ducts are located in the top and bottom slab of the box section. The top slab is prestressed both transversely and longitudinally. Matching alignment keys are located in the webs and the top slab to facilitate erection.

Threaded 32-mm (1.25-in) diameter posttensioning bars were used as longitudinal tendons. Mechanical couplers were used to connect bars. Each span was constructed by cantilevering out from the main piers. A launching girder was used to position the segments. Temporary longitudinal posttensioning was applied to hold segments together during construction. A cast-in-place segment closed each span so that all spans were continuous for live load.

FIELD MEASUREMENTS

Three segments in the southbound lane bridge of a

Figure 1. Kishwaukee River Bridge.

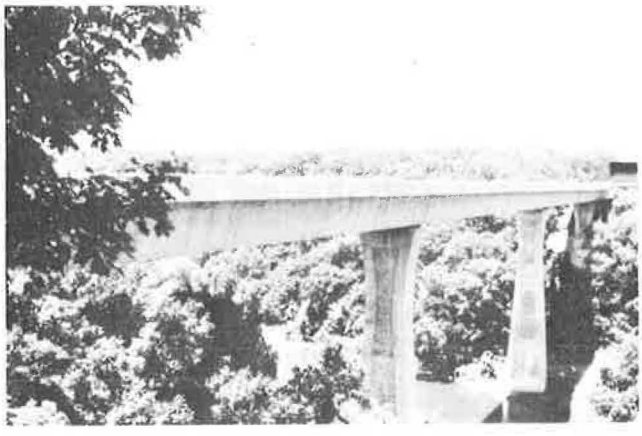

Figure 2. Elevation and plan of Kishwaukee River Bridge.

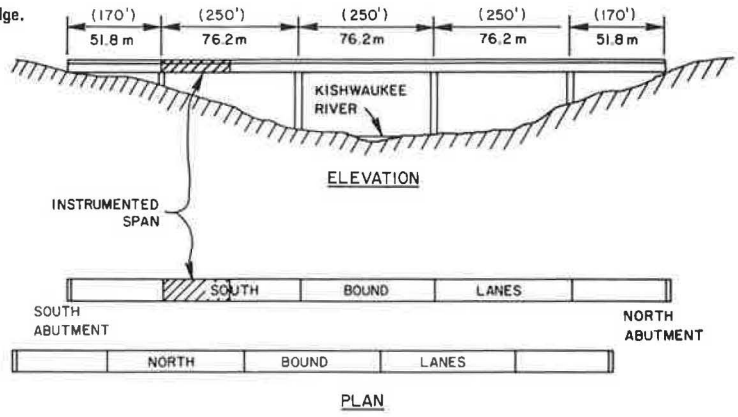

Figure 3. Segment dimensions and locations of strain measurements.

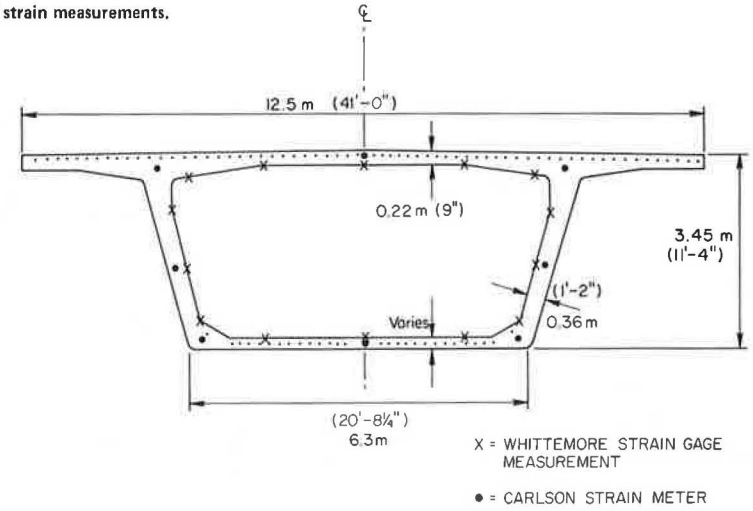

Figure 4. Location of instrumented segments.

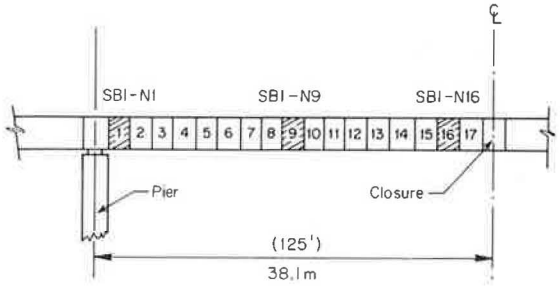

76.2-m span (shown in Figure 2) were instrumented. Segments were designated as SB1-N1, SB1-N9, and SB1-N16. The segments were located next to the pier support, at quarter span, and near the center of the span, respectively. Locations of instrumented segments are shown in Figure 4.

Measurements of longitudinal strains, vertical deflections relative to the pier, and surface temperature of concrete were made in each instrumented segment. Installation of field instrumentation was completed in 1978.

Longitudinal strains were measured with a Whittemore mechanical strain gage (1) and 24 Carlson strain meters. Locations of Whittemore gage measurements and installed Carlson strain meters are indicated in Figure 3. The Whittemore strain gage measured the surface strain of concrete. The Carlson meter readings gave internal concrete strains and temperatures. Both Carlson strain meters and Whittemore strain gage readings yielded consistent and similar results. In this paper, only data from the Carlson strain meters are discussed.

MATERIAL PROPERTIES

Properties of the concrete used in the instrumented segments were determined from tests of concrete cylinders made at the precasting plant. Thirty-five 152x305-mm (6x12-in) concrete cylinders were used for each bridge segment. Cylinders were steam-cured alongside the segments before shipping to Construction Technology Laboratories for tests. After arrival, the cylinders were cured either under a constant temperature of 23°C (73°F) and 50 percent relative humidity or under outdoor conditions.

Physical property tests were conducted to determine the variation of compressive strength (ASTM C39-72), modulus of elasticity, Poisson's ratio, and coefficient of thermal expansion with time. Physical properties of the concrete at different ages are summarized in Table 1.

Creep tests of cylinders cured under a constant temperature of 23°C and 50 percent relative humidity were initiated at three different concrete ages. All creep cylinders were subjected to a constant stress of 13.8 MPa (2000 psi). Tests were conducted according to ASTM C512-74. Similar creep tests for cylinders cured outside were started at a concrete age of 28 days. Whenever creep readings were made,

Table 1. Concrete properties.

Segment	Curing Environment	Age (days)	Compressive Strength, f'_c (MPa)	Modulus of Elasticity, E (MPa)	Poisson's Ratio	Coefficient of Thermal Expansion (millionths/°C)
SB1-N1	Controlled	28	39.2	29 800	0.15	9.63
		180	43.0	31 000	0.15	9.86
		360	40.9	30 400	0.13	-
	Outdoor	28	39.6	29 000	0.15	-
		180	44.5	31 200	0.15	-
SB1-N9	Controlled	28	42.7	30 800	0.16	9.86
		90	41.9	31 900	0.15	10.26
		180	44.5	32 800	0.15	10.13
		360	41.1	31 200	0.14	-
	Outdoor	28	41.9	31 800	0.14	-
		90	44.9	32 500	0.15	-
		180	44.5	31 600	0.14	-
SB1-N16	Controlled	28	39.6	30 500	0.15	10.17
		90	42.3	32 800	0.15	10.53
		180	43.4	30 400	0.15	10.49
		360	41.9	31 200	0.14	-
	Outdoor	28	32.2	28 900	0.14	-
		180	42.8	29 200	0.15	-

Note: 1 MPa = 145 psi, $t°C = (t°F - 32)/1.8$.

Figure 5. Specific creep versus time.

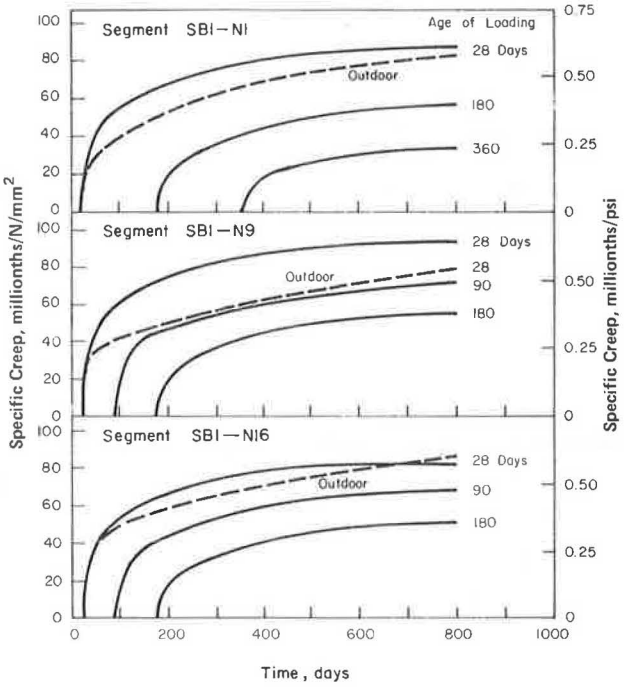

Figure 6. Shrinkage versus time.

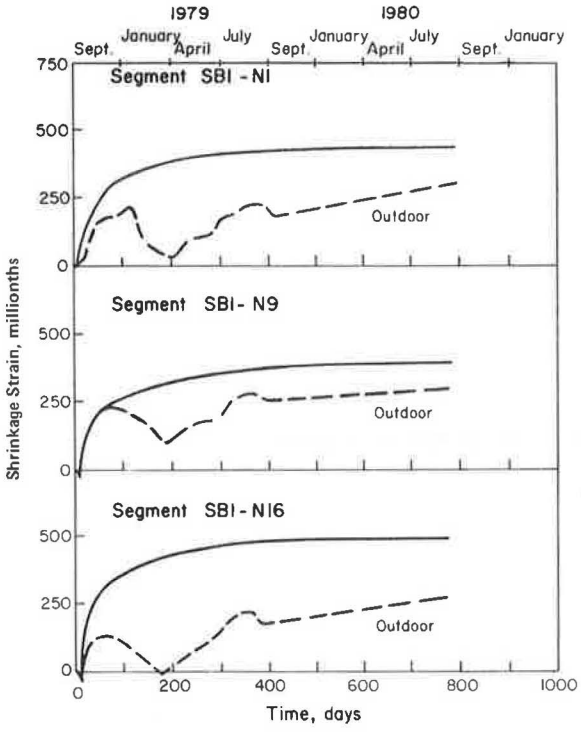

companion shrinkage readings of concrete were taken.

Variation of specific creep of concrete with time for each segment is shown in Figure 5. Specific creep is defined as the amount of creep strain under unit stress in millionths per newton per square millimeter. Concrete shrinkage was excluded from the creep strain readings. Different curves in the figure represent specific creep of concrete loaded at different ages. For outdoor specimens, creep readings were adjusted back to 23°C for comparison. Specific creep of outdoor specimens was found to be lower than for those cured under the controlled environment. This relation is shown in Figure 5.

Shrinkage measurements of concrete cylinders began seven days after casting. A comparison of the data for specimens cured at constant temperature and under the outdoor environment is shown in Figure 6.

CALCULATED DEFORMATIONS

The time-dependent deformations of the bridge were calculated by using a step-by-step numerical procedure (2). Total shortening was considered to include instantaneous deformation, shrinkage deformation, and creep deformation. The analysis accounted for effects of concrete material properties, relaxation of prestressing steel, member thickness, elastic recovery, age of loading, and creep of concrete under a variable stress history. Size correction factors were based on Comite Europeen du Benton (CEB) recommendations (3). The actual casting and erection schedule of the segments was followed. Further details are given elsewhere (2).

Analyses were performed for three different sets of material properties. In analysis 1, experimen-

Figure 7. Comparison of measured and calculated strains for segment SB1-N1.

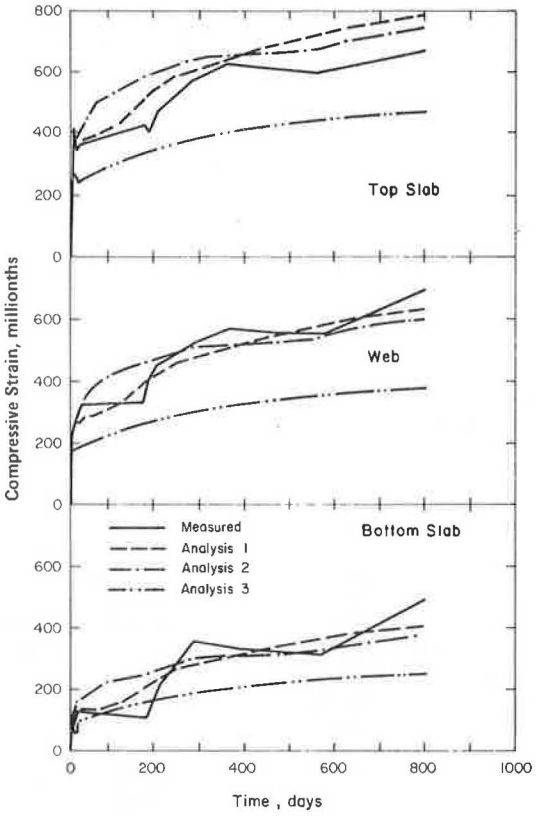

Figure 8. Comparison of measured and calculated strains.

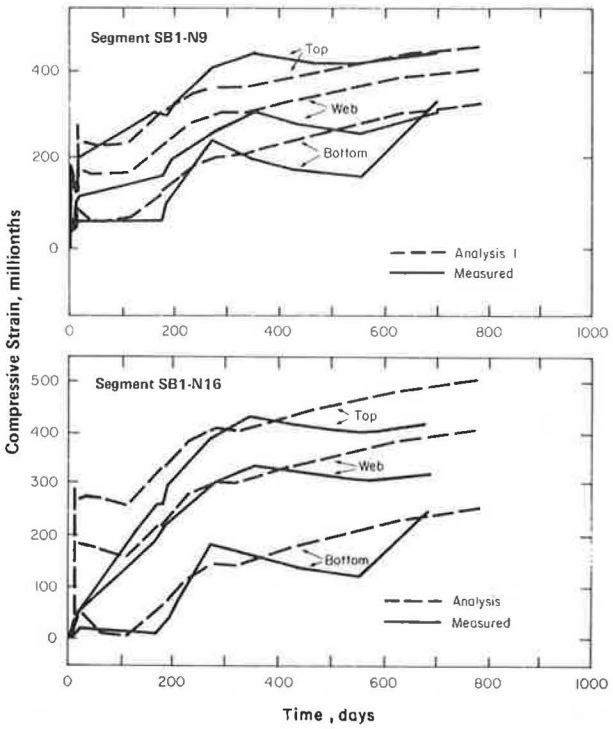

tally determined properties of the concrete specimens stored outdoors were used. Analysis 2 was performed by using material properties determined from the laboratory-cured specimens. For analysis 3, the recommendations of CEB (3) were used to generate material properties. Relative humidity was assumed to be 50 and 80 percent for creep and shrinkage, respectively (4).

COMPARISON OF RESULTS

Calculated strains were compared with measured strains to determine the effectiveness of the analytical procedure. Detailed comparisons are presented elsewhere (2). Comparisons of measured strains with strains calculated from the three analyses for segment SB1-N1 are shown in Figure 7. The best agreement was obtained with analysis 1, which used the concrete material properties of specimens stored outdoors. Good comparison was obtained with analysis 2, which used material properties of laboratory-cured concrete cylinders. In analysis 3, calculated strains were consistently smaller than the measured values.

The comparison of measured and calculated strains by using analysis 1 for segments SB1-N9 and SB1-N16 is shown in Figure 8. Good agreement was obtained. Similarly, good agreement between measured and calculated strains was obtained for analysis 2. This shows that time-dependent deformation of the box girder can be adequately estimated by using material properties obtained from laboratory-cured concrete cylinders.

CONCLUSIONS

Comparisons of calculated and measured deformations on the Kishwaukee River Bridge were made. Excellent agreement was obtained when concrete material properties were based on specimens stored outdoors. Reasonable comparison was also obtained when material properties based on laboratory-cured specimens were used. The analytical procedure therefore provides a suitable method for predicting time-dependent deformations in posttensioned box-girder bridges. Time-dependent behavior of box girders can be estimated by using standard laboratory data.

ACKNOWLEDGMENT

Work described in this paper was performed as part of an agreement between the Portland Cement Association and the Illinois Department of Transportation (DOT) in cooperation with the Federal Highway Administration (FHWA). The analytical work was performed at the University of Illinois, Urbana, under an agreement with the Portland Cement Association. Richard Taylor of the Illinois DOT coordinated the project for the State of Illinois. Members of the advisory committee who reviewed the progress of the project were Robert Appleman, Gayle Lane, Richard Scarr, Donald R. Schwartz, Colin Strang, Richard Taylor, and John Ross. Their contributions to the project are appreciated.

The contents of this report reflect our views, and we are responsible for the facts and the accuracy of the data presented herein. The contents do not necessarily reflect the official views or policies of the Illinois DOT or FHWA. This report does not constitute a standard, specification, or regulation.

REFERENCES

1. N.W. Hanson, T.T.C. Hsu, O.A. Kurvits, and A.H. Mattock. Facilities and Test Methods of PCA Structural Laboratory--Improvements 1960-65. Portland Cement Association, Skokie, IL, PCA Development Bull. D91, July 1965, p. 38.
2. V. Marshall and W.L. Gamble. Time-Dependent De-

formations in Segmental Prestressed Concrete Bridges. Civil Engineering Studies, Univ. of Illinois, Urbana, Structural Research Series 495, Oct. 1981, 242 pp.
3. International Recommendations for the Design and Construction of Concrete Structures: Principles and Recommendations. Comite Europeen du Benton (European Committee on Concrete), Paris, June 1970.
4. H.D. Hernandez and W.L. Gamble. Time-Dependent Prestress Losses in Pretensioned Concrete Construction. Civil Engineering Studies, Univ. of Illinois, Urbana, Structural Research Series 417, May 1975.

Publication of this paper sponsored by Committee on Concrete Bridges.

Abridgment

Load Capacity of Concrete Bridge Decks

DAVID B. BEAL

The behavior of two reduced-scale concrete bridge decks subjected to simulated wheel loads was evaluated in a series of tests. One slab was reinforced in accordance with American Association of State Highway and Transportation Officials requirements and the other had three areas with varying amounts of isotropic reinforcement. Results show that with either reinforcement pattern, service load bending moments are from 40 to 65 percent of those predicted by flexural theory. Failures were by punching shear rather than flexure and occurred at loads at least six times larger than design.

The need to determine the influence of heavily loaded, closely spaced wheels and axles on reinforced concrete bridge decks prompted the New York State Department of Transportation (NYSDOT) to initiate an analytical study of bridge deck behavior in 1977. The products of this study were charts that permitted the determination of the induced bending moment in decks due to any pattern of wheel loads (1). During the course of the research, more evidence became available [which culminated in the publication of the Ontario Highway Bridge Design Code (2)] that the failure mode of reinforced concrete bridge decks was punching shear and not flexure as assumed in design. Because of this evidence, the study reported here was started to investigate the ultimate capacity of bridge decks.

The Ontario bridge deck design resulted from extensive physical and analytical research (3). This work demonstrated that not only is the failure mode of reinforced bridge decks different from that historically assumed, but that the load capacity is substantially greater than necessary for safety. The enhanced behavior of bridge decks is explained by hypothesizing large in-plant compressive forces that result from the restraint of deck expansion under load. These compressive forces form an internal couple that enhances the flexural capacity of the deck to a level such that punching shear failure controls. Subject to certain restrictions on span length, slab thickness, and detailing of diaphragms and shear connectors, Ontario permits an empirical slab design that has a minimum of 0.3 percent isotropic reinforcement in each face. For a 9-ft slab span, this represents a reduction in reinforcement of 43 percent from that now required by New York State standards (4).

In addition to the savings that result from the reduction of steel, benefits may accrue from this empirical design by reducing fabrication costs and deck deterioration due to reinforcement corrosion. The reinforcement can be standardized over the normal range of girder spacings and has the potential benefit of modular prefabrication. Reinforcement corrosion is alleviated because the cover on the top steel can be increased without an increase in slab thickness. In addition, the reduction in bar size increases the important cover-diameter ratio (5).

The objective of the work described in this paper was to collect data on bridge slab capacity with different reinforcement schemes. This work was accomplished with several reduced-scale models that are described in detail in the complete report (6).

EXPERIMENTAL WORK

Two reinforced concrete bridge decks were constructed to study behavior under working loads and at failure. Model 1, which represents the current standard bridge deck design (4), was included to demonstrate the great reserve capacity of that design and to provide a standard of comparison with alternative designs. The 8.5-in-thick slab was reinforced with No. 5 bars in the longitudinal and transverse directions. Longitudinally, the top layer of bars was spaced at 18 in and had the bottom layer spaced at 7.75 in in the middle half of the slab span and at 18 in elsewhere. Both layers of transverse steel were spaced at 5.25 in.

Model 2 represented an 8-in-thick deck that has three different isotropic reinforcement patterns comprised of No. 4 bars. Two layers at 8-in spacing represented current Ontario practice (3). A single layer at 8 in was used because of the construction benefits to be gained if this pattern could be adopted. Two layers at 12-in spacing were used to represent the minimum reinforcement now permitted (7). In addition, an unreinforced section was included to demonstrate the inherent strength of confined concrete slabs. Both models were constructed to a linear scale factor of 5.9 and were based on a five-girder, 72-ft simple-span bridge, which is representative of composite highway structures now being built. Details of model materials and construction details are given in the full report (6). Electrical-resistance strain gages were mounted on the rebars and deflection at the center of the slab was measured.

TEST RESULTS

Each instrumented section of the model slabs was subjected to test loads for two distinct purposes: (a) determination of the distribution of bending

Figure 1. Model 1 transverse moment coefficients.

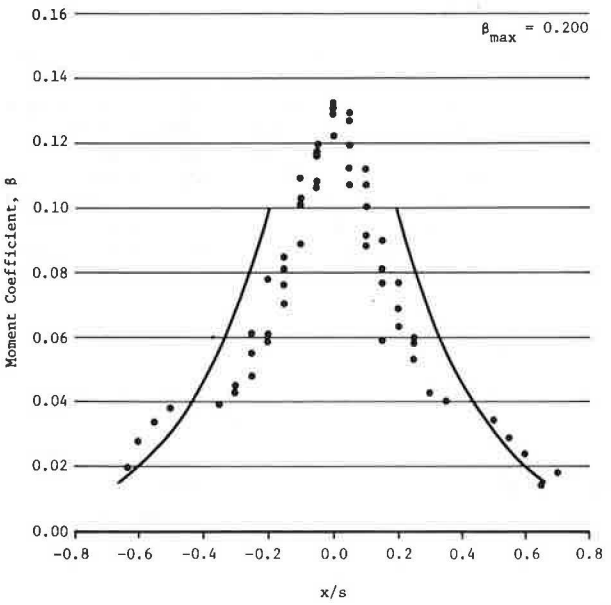

Figure 2. Model 2 interior-panel transverse moment coefficients.

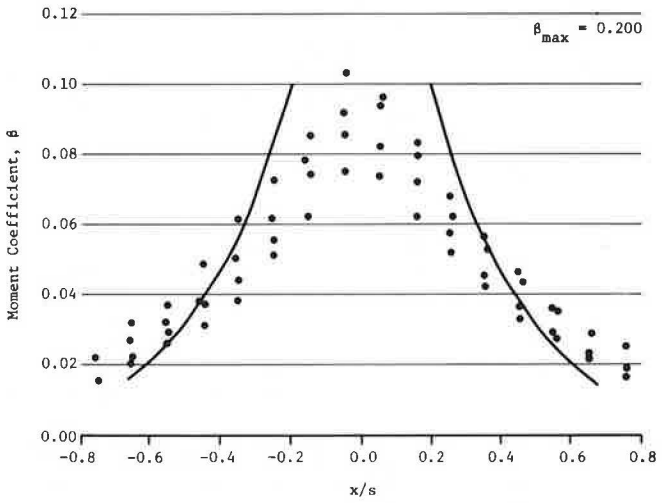

moment and (b) determination of failure load.

Uncracked- and cracked-slab testing was performed. The uncracked-slab testing of model 1 provided data for comparison with results from a test on a prototype structure. The transverse rebar stresses determined in these tests showed good correspondence in trends. The absolute magnitudes differed because of physical differences between model and prototype.

The cracked-slab testing was considered more important, since steel strains are more sensitive to bending moment, and the slab would be in this condition under overloaded vehicles. The slabs were cracked by loading repeatedly at points surrounding the instrumented section until a linear load-strain response was obtained in the transverse rebars. Loads of 5000 and 3000 lb were required on models 1 and 2, respectively, to achieve a nominal rebar strain of 1400 μin/in.

Figures 1 and 2 show typical responses for models 1 and 2, respectively [curves and β_{max} values from Beal (1)]. These results are compared with the

Figure 3. Punching failure on model 1.

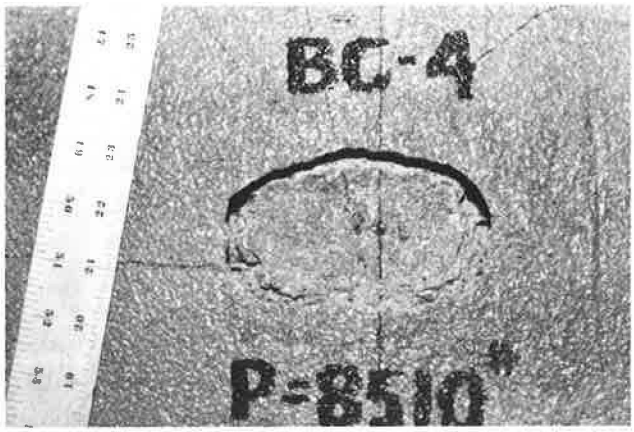

results from an elastic analysis (1). The experimental values of moment coefficients are generally less than the theoretical values. The maximum predicted value is 0.2 compared with average experimental results of 0.126 and 0.074, respectively. Under service load, the maximum stress in the transverse rebars was less than 8.3 ksi for conventionally reinforced slabs and less than 11.7 ksi with isotropic reinforcement.

Failure loads were applied through either a 1.69x4.07-in or 1.69x1.69-in pad. The smaller pad was used more frequently because load levels controlled by yield strength of the steel beams were generally reached before slab failure with the larger pad. For some tests, auxiliary supports were used to control beam stresses.

In general, the failure mode at all locations bounded by longitudinal girders was punching shear (Figure 3). The intersection of the failure surface with the tension face of the slab was elliptical and had average major and minor axes of 14 and 12 in, respectively; this face was extensively cracked. The failure at the top surface was only slightly larger than the load pad. Slab deflection at failure never exceeded 10 percent of the slab thickness.

A total of 15 failures were produced in the model 1 deck and 13 failures in model 2. Excluding tests with oversized load pads, the average equivalent prototype failure loads are 260 and 300 kips for the fascia and interior panels of model 1, respectively. For model 2, the failure loads varied, depending on the type of reinforcement and slab boundary conditions. The failure load exceeded 130 kips (six times the design wheel load) in all cases.

In addition to the tests on the reinforced section, the unreinforced section was tested and sustained an equivalent prototype load of 175 kips before loading was stopped because the cracking was propagating toward the reinforced section. In later tests, other load points on the unreinforced slab sustained loads of 70 and 100 kips, respectively.

ANALYTICAL PREDICTIONS

An analytical procedure to predict the punching shear capacity of reinforced concrete bridge decks has been developed by Hewitt and Batchelor (8) based on a theory of punching shear behavior proposed by Kinnunen and Nylander (9). A computer program was prepared based on this procedure.

Kinnunen and Nylander (9) predicted the capacity of circular slabs by hypothesizing the existence of a conical shell of concrete extending from the

loaded surface of the slab to the bottom of the shear crack. Hewitt and Batchelor (8) extended this theory to include boundary restraining forces and moments in the plane of the slab. Results from the computer program prepared for this work were satisfactorily compared with their results.

The capacity of the three reinforcement patterns for model 2 interior panels was predicted by this theory. A restraint factor of 0.5 was assumed. In all cases the analytical value was less than the average test load. The analysis does not include the boundary force contribution of compression reinforcement, and thus single and double mats are predicted to have the same strength. A 1000-lb difference in test capacities of the single and double mats indicates that compression reinforcement does make a significant contribution to load capacity.

PRACTICAL APPLICATIONS

Before implementation of a bridge deck design that incorporates reduced reinforcement, many questions must be resolved. First, strength criteria must be established to ensure safety. Because of the suddenness of the punching failures, load factors must be more conservative than values selected when yielding failures are expected. Second, the minimum acceptable reinforcement amount that satisfies both strength and serviceability (i.e., temperature and shrinkage) must be determined. Third, the behavior of the new design under common but nonstandard conditions must be determined. For example, Is adequate performance achieved without shear connectors or in negative-moment regions where the slab is in longitudinal tension? Finally, reinforcement details for the fascia overhang must be developed to ensure adequate performance.

Three important benefits could accrue if an isotropic deck reinforcement pattern were adopted. First, average reduction in steel quantities over current design requirements is estimated at 53 percent for double-mat reinforcement (No. 4 at 12 in). Second, savings in fabrication costs can be expected due to standardization of the reinforcement pattern and reduction in the number of bars. Third, rebar corrosion will be alleviated due to smaller bar diameter and increased cover.

SUMMARY AND CONCLUSION

Tests on reduced-scale reinforced concrete bridge decks have demonstrated that the service load stress levels predicted by existing design procedures and methods based on elastic isotropic thin plates do not develop in bridge decks of ordinary proportions. The maximum induced stress in a conventionally reinforced deck subjected to the design load of 20.8 kips was only 8.3 ksi. Tests on model bridge decks that have substantially less reinforcement than is ordinary caused stresses no greater than 11.7 ksi at the design load. Comparison of induced moments also showed that measured values are less than predicted. The maximum ratios of measured to theoretical induced moment were 0.65 and 0.62 for the conventional and lightly reinforced decks, respectively. Based on these results, it is concluded that even a 100 percent increase in the weight of wheel loads would not overstress the deck reinforcement and, accordingly, no methodology is needed to predict induced stress that results from the passage of occasional overload permit vehicles.

Tests to failure resulted in capacities always larger than six times the design wheel load for slabs bounded by girders, regardless of the reinforcement pattern. In addition, with the exception of two locations where the reinforcement was misplaced, all failures were by punching. Thus, reductions in total reinforcement of 30 to 53 percent had no effect on failure mode and did not reduce the strength below a safe level.

ACKNOWLEDGMENT

The research leading to this paper was sponsored by NYSDOT and the Federal Highway Administration, U.S. Department of Transportation. The preliminary planning for this work was done by Robert J. McDermott, who also supervised the construction and testing of model 1. Laboratory work was performed under the direction of Everett W. Dillon with the assistance of R.L. Morgan.

REFERENCES

1. D.B. Beal. Bending Moment in Bridge Slabs Due to Wheel Loads. Engineering Research and Development Bureau, New York State Department of Transportation, Albany, Res. Rept. 63, Aug. 1978.
2. Ontario Highway Bridge Design Code. Ontario Ministry of Transportation and Communications, Ottawa, Ontario, Canada, 1979, Section 7.
3. P. Csagoly, M. Holowka, and R. Dorton. The True Behavior of Thin Concrete Bridge Slabs. TRB, Transportation Research Record 664, 1978, pp. 171-179.
4. Standard Details for Highway Bridges. Structures Design and Construction Subdivision, New York State Department of Transportation, Albany, May 1977, Section 23.1.3.
5. J.T. Houston, E. Atimay, and P.M. Ferguson. Corrosion of Reinforcing Steel Embedded in Structural Concrete. Center for Highway Research, Univ. of Texas, Austin, Rept. CFHR-3-5-68-112-1F, 1972.
6. D.B. Beal. Strength of Concrete Bridge Decks. Engineering Research and Development Bureau, New York State Department of Transportation, Albany, Res. Rept. 89, July 1981.
7. Standard Specifications for Highway Bridges, 12th ed. AASHTO, Washington, DC, 1977, Section 1.5.7, p. 76.
8. B.E. Hewitt and B. Batchelor. Punching Shear Strength of Restrained Slabs. Journal of the Structural Division, ASCE, Vol. 101, No. ST9, Proc. Paper 11548, Sept. 1975, pp. 1837-1853.
9. S. Kinnunen and H. Nylander. Punching of Concrete Slabs Without Shear Reinforcement. Trans., Royal Institute of Technology, Stockholm, No. 158, 1960.

Publication of this paper sponsored by Committee on Concrete Bridges.

Fatigue Reliability Analysis of Highway Bridges

PEDRO ALBRECHT

A method of calculating the expected fatigue failure probability of a structural detail, given the distribution of resistance and load, is presented. The resistance data, in terms of cycles to failure, come from previous laboratory tests. The load data come either from stress-range histograms recorded on bridges or from loadometer surveys. The proposed method replaces each histogram by an equivalent stress range and converts the latter into a distribution in terms of number of cycles. The problem is thus cast into the standard format for reliability analysis and allows one to calculate failure probabilities. Application of the method to designs in accordance with American Association of State Highway and Transportation Officials specifications showed that fatigue failure probabilities for redundant load-path (RLP) structures are inconsistent and vary greatly from $P_F = 9.2 \times 10^{-2}$ for category B to $P_F = 9.2 \times 10^{-10}$ for category E' and for nonredundant load-path (NRLP) structures from $P_F = 5.1 \times 10^{-2}$ for category A to $P_F = 2.1 \times 10^{-22}$ for category E. It is proposed that the specifications be revised to include (a) allowable stress ranges for RLP and NRLP structures with uniform failure probabilities; (b) explicit formulation of the specifications in terms of the actual number of single fatigue trucks, each causing an equivalent stress range; and (c) continuous definition of allowable stress range versus truck traffic volume. An example illustrates the design of a bridge not covered by the specifications to a specified failure probability.

Design methods based on statistical reliability concepts have recently been developed for many areas of static design of members and connections. Code-writing bodies are now incorporating them into their specifications to ensure consistent reliability throughout the structure. Still lacking is a reliability method for fatigue that can then be used as a basis for a load and resistance factor approach to fatigue design. The present study addresses this need.

This paper briefly reviews the equivalent stress range and the reliability concepts needed herein. Thereafter, the load and resistance curves are constructed and transformed in a manner suitable for writing the governing equations. The failure probability of designs to American Association of State Highway and Transportation Officials (AASHTO) fatigue specifications are assessed, and an illustrative design example is presented for a special bridge not covered by the AASHTO specifications (1). The previous work (2) is extended to cover designs for over 2 million cycles and nonredundant load-path (NRLP) structures.

EQUIVALENT STRESS RANGE

Recent studies have employed, with good success, the concept of an equivalent stress range to correlate data from variable amplitude cyclic-load tests with data from constant-amplitude tests. The concept states that, for an equal number of cycles, the equivalent (constant-amplitude) stress range will cause the same fatigue damage as the sequence of variable-amplitude stress ranges it replaces. For convenience of applying the concept later in the paper, the equivalent stress range (f_{re}) is expressed in the following form (2):

$$f_{re} = [\Sigma\gamma_i(\phi_i \alpha f_{rd})^m]^{1/m} \quad (1)$$

where

γ_i = frequency of occurrence of ith stress range;
ϕ_i = ratio of an individual load to the design load, or ratio of corresponding stress ranges;
α = ratio of measured to computed stress range for the design load;
f_{rd} = computed stress range that corresponds to the design load; and
m = slope of S-N curve

Figure 1 illustrates the meaning of the parameters in Equation 1 for a typical stress-range histogram (note for Figure 1 that if detail is designed to the allowable stress range, then $f_{rd} = F_{sr}$).

Because f_{rd} and α are constant for a given stress-range histogram, taking them out of the summation in Equation 1 gives

$$f_{re} = (\Sigma\gamma_i\phi_i^m)^{1/m} \alpha f_{rd} \quad (2)$$

or

$$f_{re} = \rho\alpha f_{rd} \quad (3)$$

where ρ is defined in this paper as

$$\rho = (\Sigma\gamma_i\phi_i^m)^{1/m} \quad (4)$$

The equivalent stress-range concept is needed in calculations of the fatigue failure probability of structures subjected to variable amplitude stress cycling.

BASIC RELIABILITY CONCEPTS

The reliability concepts employed in this paper are well documented in the literature (3). Structural reliability can be defined as the probability that a structural component will not fail within its design life. In other words, it is the probability that a member's resistance to load is higher than the applied load. In deterministic design, one assumes a high value of load and a low value of resistance and specifies that the distance between the two shall not be less than a preselected safety factor. In probabilistic design, one recognizes that neither the resistance (R) nor the load (Q) are single valued; both have a mean and a distribution. The objective is then to compute the probability of failure, i.e., the likelihood of the undesirable cases where a high value of load will exceed a low value of resistance. Conversely, for purposes of

Figure 1. Illustration of terms in Equations 1 and 3.

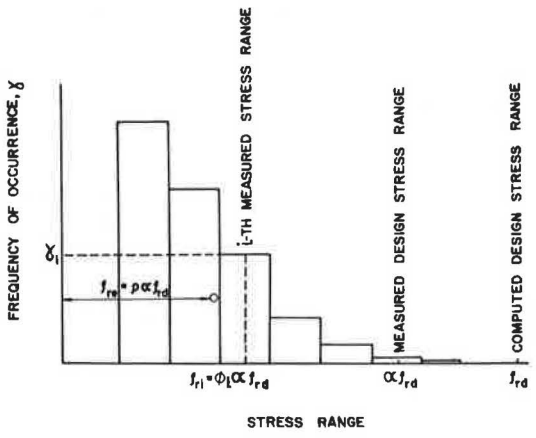

writing fatigue design specifications, one wishes to determine the distance between the mean resistance and the mean load ($\tau = \bar{R} - \bar{Q}$), so that the failure probability (P_F) does not exceed a specified value. This is done with the equation for the safety index (β):

$$\beta = (\tau/s_\tau) = (\bar{R} - \bar{Q})/\sqrt{s_R^2 + s_Q^2} \quad (5)$$

where the difference (τ) between mean load and mean resistance is equal to a number (β) of standard deviations of that difference (s_τ). If load and resistance are normally distributed, so is their difference, and the value of β that corresponds to a specified failure probability can be read from tables for the standard normal variable.

Note that increasing the safety index (β) will decrease the failure probability. This can be achieved either by moving the mean load ($\bar{Q}$) farther away from the mean resistance ($\bar{R}$) or by reducing the standard deviation. The second option is usually not available in most designs.

When applying Equation 5 to fatigue design, the resistance is given by the number of cycles to failure and the load is given by the applied stress-range history. This leads to two difficulties. One is the need to find a mean and standard deviation of many stress-range histograms, each of which describes in itself a distribution of stress ranges. Second, the resistance data, which consist of the number of cycles to failure, are distributed along a horizontal line in a S-N plot, but the stress-range data are distributed along a vertical line. The following solution to the two difficulties is proposed:

1. Replace each histogram by one equivalent constant-amplitude stress range,
2. Calculate the mean and standard deviation of all equivalent stress ranges, and
3. Convert the resulting distribution of equivalent stress ranges into one given in terms of number of cycles.

The problem is then reduced to the form to which Equation 5 applies.

Figure 2. Construction of equivalent stress-range distribution.

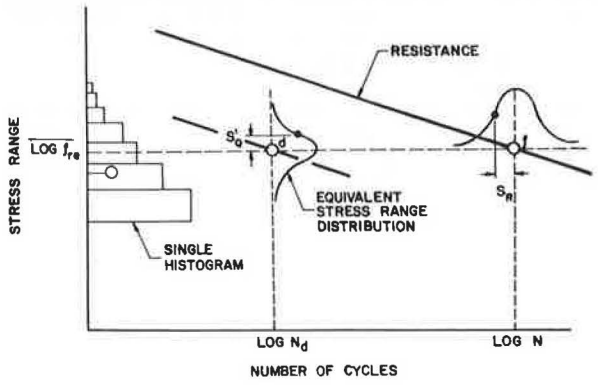

RESISTANCE CURVE

The AASHTO fatigue specifications (1) are based on constant-amplitude fatigue test data for steel beams (4,5). The statistical analysis of the S-N data has shown that the mean regression line with the best fit was of the log-log linear form:

$$\log N = b - m \log f_r \quad (6)$$

with the intercept {b[at f_r = 1 ksi (7 MPa)]}, and the slope (m) as the regression coefficients. The log-log plot of Equation 6 gives a straight S-N line, which is labeled resistance in Figure 2. The data points were found to be log-normally distributed about the mean regression line with about equal standard deviation at all stress-range levels. This held true for all details. Thus, one may assume that for any point (f) on the mean regression line, the fatigue life of replicate specimens tested at the same stress range would be log-normally distributed about that point with mean $\bar{R}$ = log N and standard deviation, i.e.,

$$s_R = s_{\log N} \quad (7)$$

The mean and the standard deviation of the number of cycles to failure define the resistance.

The regression coefficients (b and m) and the standard deviation (s_R) for the six categories A through E' are summarized in Table 1 (4-7). They provide the resistance curve parameters needed in Equation 5. The data listed under categories C and E' require some explanation. In the AASHTO specifications, category C covers both transverse stiffeners and 2-in (50-mm) attachments. The mean regression line of the former falls higher than that of the latter, thereby making it appear that the 2-in attachment data would govern. In reality, one must also consider the standard deviation, which is about 2.5 times larger for stiffeners than for 2-in attachments. This creates a peculiar situation. If one moves to the left of each mean by up to 2.56 standard deviations, the 2-in attachment governs. Beyond that, however, the transverse stiffener data become critical. Accordingly, this study employs that data for category C that governs at the value of β being considered. In contrast, the AASHTO fatigue specifications are solely based on the 2-in attachment data, although safety indices for category C reach a value of 7.12 for NRLP structures (6).

Table 1. Resistance curve parameters.

Category	Type of Detail Tested	No. of Data Points		Regression Coefficients		Standard Deviation (s_R)
		Included	Excluded	Intercept[a] (b)	Slope (m)	
A	Rolled beam	28	16	11.121	3.178	0.221
B	Welded beam	55	1	10.870	3.372	0.147
C*	Stiffeners	135	5	10.085	3.097	0.158
C	2-in attachments	14	0	10.0384	3.25	0.0628
D	4-in attachments	44	8	9.603	3.071	0.108
E	Cover plate end	193	0	9.2916	3.095	0.1006
E′	Cover plate end, t > 0.8 in	18		9.1664	3.2	0.1943

Note: 1 in = 25 mm.

[a]Values of f_r substituted in units of ksi.

Table 1 also has an entry for category E', although no regression analysis was reported (7), presumably because of a lack of data at various stress-range levels in the finite life region of the S-N plot. For the purpose of this study, the finite life region for category E' details was defined by the 18 data points at the 8-ksi (55-MPa) stress range for which the mean life was 1 890 000 cycles, and it had a standard deviation of log of life of s_R = 0.1943 (6). Assuming a slope (m = 3.2) equal to the mean of the six other slopes in Table 1, the intercept is then given from Equation 6 as

$$b = \log(1.89 \times 10^6) + 3.2 \log(8.0) = 9.1664 \quad (8)$$

LOAD CURVE

The load-curve data can come either from field measurements of stress-range histograms or from loadometer surveys. In the former case, the strain ranges caused by the applications of a live load are obtained from a strain gage mounted at a suitable point on the bridge. In the latter, the trucks are weighed. In both cases, the results are usually reported as a histogram of stress range or truck weight versus frequency of occurrence.

The proposed construction of the load curve is illustrated below for a class of comparable structures, all of which are subjected to the same design load. For example, the fatigue design of short-span highway bridges is governed by the number of single truck crossings. Each application of the design load induces one stress-range cycle. It is assumed that one has available the stress-range histograms recorded on several bridges.

The construction of the load curve begins with a single stress-range histogram, such as the one plotted along the ordinate in Figure 2. The bar width in a histogram is usually constant; it varies in Figure 2 because the S-N plot scales are logarithmic. The equivalent stress range (f_{re}) of the single histogram is then calculated. It replaces the histogram in subsequent calculations and provides one point for the desired load curve. Plotting the distribution of all equivalent stress ranges on a vertical line through the design point (d) gives the load curve. To define its distribution, one needs the mean and the standard deviation. Assuming that the ratio of measured to computed stress range (α) is constant implies that αf_{rd} is also constant. Therefore, the computation of the log mean of all equivalent stress ranges is reduced to evaluating the log-mean of ρ for all histograms (see Equation 3):

$$\overline{\log \rho} = (1/h) \Sigma \log(f_{re}/\alpha f_{rd}) \quad (9)$$

where h is the number of histograms. The standard deviation of the load is then given by the standard deviation of the log ρ values:

$$s'_Q = s_{\log \rho} \quad (10)$$

The prime added to s_Q' and to any other symbol indicates a quantity measured along a vertical line. The line through the design point (d) drawn parallel to the resistance and the standard deviation of the equivalent stress ranges define the load. The load curve could be derived in analogous fashion from the results of loadometer surveys if one assumes that loads are proportional to stresses.

Estimation of the load curve is less certain when the structure is one of a kind and few data are available. In that case, one must construct an expected load histogram over the design life, compute the equivalent stress range for that histogram, and estimate the standard deviation.

TRANSFORMATION OF LOAD AND RESISTANCE

Equation 5 applies only if the load and resistance curves are plotted side by side with the same base line. The load is distributed along a vertical line through the design point (d) shown in Figure 2, whereas the resistance is distributed along a horizontal line through the failure point (f). One of the two curves must, therefore, be transformed.

Albrecht (2) presented the transformation of the load curve, whereas this paper explains instead the transformation of the resistance curve in terms of self-evident geometrical relations. Figure 3 shows the solid resistance line and two dashed lines shifted above and below the mean resistance by a specified number of standard deviations, so that the survival probability (assuming a single-valued load) would be, say, 5 percent and 95 percent, respectively. The distribution of the resistance is drawn along a horizontal line through point f and also along a vertical line through point g. In both cases, the points with the same survival probability must lie on the same line parallel to the mean resistance. Because the slope is 1:m, it follows for reasons of geometry that

$$s'_R = s_R/m \quad (11)$$

where s_R and s_R' are the standard deviations of the resistance when its distribution is drawn about a horizontal and a vertical line, respectively. For the same geometrical reasons, the distance between the mean resistance and the mean load, measured along the vertical line g-d, is given by

$$\bar{R}' - \bar{Q}' = (1/m)(\bar{R} - \bar{Q}) \quad (12)$$

Rewriting Equation 5 for the distance g-d and substituting Equations 11 and 12 gives

$$\beta = (\bar{R}' - \bar{Q}')/\sqrt{(s'_R)^2 + (s'_Q)^2} = (1/m)(\bar{R} - \bar{Q})/\sqrt{(s_R/m)^2 + (s'_Q)^2} \quad (13)$$

or, after simplifying

$$\beta = (\bar{R} - \bar{Q})/\sqrt{(s_R)^2 + (ms'_Q)^2} \quad (14)$$

Equation 13 applies to distributions of load and resistance along a vertical line through points d and g, respectively. It requires a 90-degree rotation of the resistance distribution, which decreases the standard deviation by a factor (m) in accordance with Equation 11. The load remains unchanged.

Figure 3. Transformation of load and resistance.

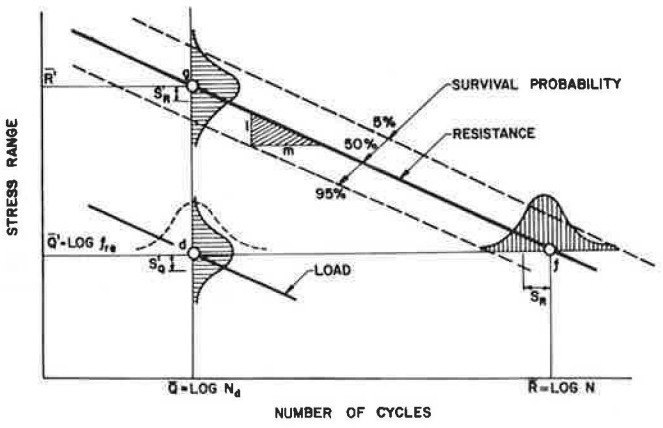

Equation 14 applies to distributions along a horizontal line through points d and f. In this case, the load distribution is rotated by 90 degrees, thus increasing its standard deviation to $s_Q = ms_Q'$, which is compatible with the geometrical condition stated in Equation 11. The resistance remains unchanged. Both equations give the same result for β.

Finally, substituting the identities $\bar{R} \equiv \log N$ and $\bar{Q} \equiv \log N_d$ into Equation 14 and using the abbreviation for the standard deviation of the difference between the resistance and the load:

$$s_\tau = \sqrt{(s_R)^2 + (ms_Q')^2} \tag{15}$$

Using the above equation yields the safety index for fatigue design:

$$\beta = (1/s_\tau)(\log N - \log N_d) \tag{16}$$

The terms s_R and s_Q' are given by Equations 7 and 10, respectively. The failure probability that corresponds to any numerical value of β can be read from tables for the normal distribution.

Equation 16 addresses the problem of computing the failure probability for a given design. The solution to the reverse problem, that of computing the design life (N_d) for a desired failure probability, follows from the same equation:

$$\log N_d = \log N - \beta s_\tau \tag{17}$$

On substitution of N from Equation 6 with $f_r = F_{re}$, one gets

$$\log N_d = (b - \beta s_\tau) - m \log F_{re} \tag{18}$$

or, taking the antilog:

$$N_d = 10^{(b-\beta s_\tau)}/F_{re}^m \tag{19}$$

The mean safety factor (F.S.) on life is, from Equation 17:

$$(F.S.)_N = N/N_d = 10^{\beta s_\tau} \tag{20}$$

and that on stress range:

$$(F.S.)_{f_r} = (F.S.)_N^{1/m} = 10^{\beta s_\tau/m} \tag{21}$$

For a fixed value of β, the safety factors vary with type of detail because the standard deviation of the resistance (s_R) varies.

In summary, Equations 16 and 19 yield the safety index and the allowable number of cycles, respectively, for a given design or a desired failure probability.

ASSUMPTIONS

Summarized below are the principal assumptions made in the development of the load and resistance. Many are based on data from previous studies and are referenced accordingly; others rely on engineering judgment when little or no data exist to support them.

Assumptions pertaining to the resistance curve are as follows:

1. The log-log linear S-N curve for constant-amplitude fatigue test data is extended below the constant-amplitude fatigue limit (F_L) downwards to a point where the equivalent stress range meets the variable-amplitude fatigue limit (8) at

$$F_{Le} = \rho F_L \tag{22}$$

2. Calculations that pertain to a specific type of detail employ the exponent m, which corresponds to the slope of the S-N curve for that detail. Calculations of equivalent stress range are insensitive to small changes in m. Therefore, a rounded value m = 3 is used, thereby lending to Equation 1 the meaning of a root-mean-cube (RMC) stress range (9).

3. Load interaction effects in high-low stress-range sequences are neglected because, in most civil engineering structures, the random nature of loading does not provide enough low-load cycles following a high-load excursion to retard crack growth (10).

4. The fabrication quality of the test specimens, from which the resistance data of Table 1 originate (4,5,7), is representative of all structures in service.

5. Except for thick cover plates, which are now covered by the newly adopted category E' (11), any effect of specimen size and plate thickness on the fatigue life is neglected.

6. Loss of life due to corrosion fatigue (all steels) and weathering (A588 steel) is neglected, although it can be large for high-fatigue strength details (12).

7. The resistance data are log-normally distributed (4,5).

Assumptions pertaining to the load curve are as follows:

1. The maximum stress range in a recorded histogram is caused by the design load.

2. The measured-to-computed stress-range ratio (α) has a single value with no distribution.

3. Available loadometer surveys and stress-range histograms describe typical load variability for highway bridges.

4. The load data are log-normally distributed (13).

It should be emphasized that the safety index and failure probability computed from Equation 16 apply to one detail. Because all structures have more than one detail, the probability that the first detail will fail is about equal to the sum of the failure probabilities of all details. Finally, failure of the first detail does not necessarily induce collapse. This depends on the redundancy of the load path.

The user must evaluate the assumptions listed above and the remarks on failure probabilities when applying the proposed method to a specific problem.

APPLICATION TO AASHTO SPECIFICATIONS

This section illustrates the first type of application, namely, to compute with Equation 16 the failure probability of a detail that was designed to a specified design line.

Background

The current fatigue specifications for highway bridges, railway bridges, buildings, and weldments state in identical tables the allowable stress range (F_{sr}) as a function of type of detail and number of loading cycles, N_d (1, Table 1.7.2A1). The listed pairs of stress range versus number of loading cycles are coordinates of points on the allowable S-N lines for each type of detail. For redundant load-path (RLP) structures, these lines were set at two standard deviations ($2s_R$) to the left of the resistance (14). They are loosely called in the literature the 95 percent confidence limit for 95 percent survival, although a design to those allowable S-N lines will not give a failure prob-

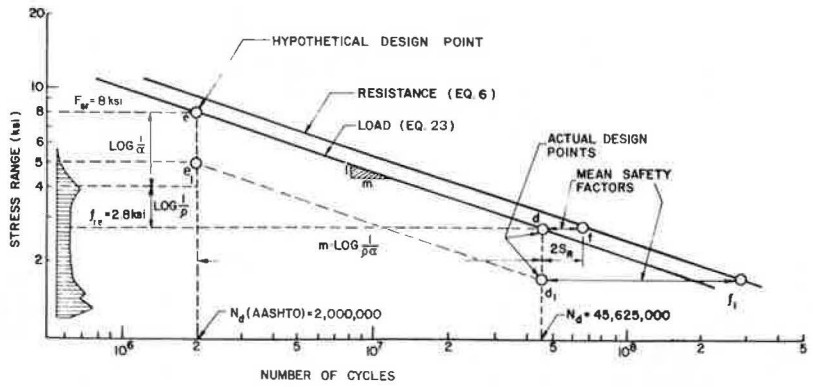

Figure 4. Illustration of AASHTO fatigue specification requirements for category E and ADTT = 2500.

ability of P_F = 5 percent (95 percent survival) for reasons that will become apparent in the following. It should also be noted that the current specification makes no allowance for load variability. Substituting $s_Q' = 0$ and $\beta = 2$ into Equation 17 and computing log N for $f_r = F_{sr}$ from Equation 6 gives, indeed, the AASHTO fatigue design lines for RLP structures:

$$\log N_d = \log N - 2s_R = (b - 2s_R) - m \log F_{sr} \quad (23)$$

The tabulated values of F_{sr} and N_d are approximate coordinates of points on those lines. Equations 6 and 23 for category E details are plotted in Figure 4.

RLP Structures

Equation 16 is applied to loading case 1 for which the average daily truck traffic (ADTT) equals 2500 (or more). It cannot be applied to case 2 and case 3 without assuming a frequency of loading, because AASHTO does not specify the value of ADTT for those cases.

Consider, for example, a category E cover-plate end detail on an RLP structure designed to point e on the allowable S-N line shown in Figure 4. Its coordinates are F_{sr} = 8 ksi (55 MPa) and N_d (AASHTO) = 2 000 000 cycles. To locate the actual design point (d), one must find the equivalent stress range (f_{re}) and the actual number of loading cycles (N_d).

The equivalent stress range was extracted from the information reported in Fisher (14). In that report, a linear relation was assumed between gross vehicle weight and stress range. Accordingly, the coefficients ρ and α that relate the equivalent stress range (f_{re}) to the design stress range (F_{sr}) can be obtained from gross vehicle weight data. The gross vehicle weight distribution from the 1970 Federal Highway Administration (FHWA) nationwide loadometer survey yielded a summation of $\gamma_i \phi_i^3 = 0.35$ (14). This gives, in the manner of Equation 4, $\rho = 0.705$. The ratio of the actual stress range due to the passage of a design vehicle and the design stress range is $\alpha = 0.5$. It is obtained from Equation 6 in Fisher (14) for a 50-year design life. Note that F_{sr} is based on a distribution factor for wheel loads to girders on a bridge designed for two or more traffic lanes (s/5.5), where s is the girder spacing. The combination of s/5.5 with $\alpha = 0.5$ gives s/11, a plausible value for the distribution factor for bridges designed for one traffic lane. The equivalent stress range is then

$$f_{re} = 0.5 \times 0.705 \times 8 = 2.8 \text{ ksi (19 MPa)} \quad (24)$$

For purposes of illustration, a stress-range histogram proportional to the gross vehicle weight histogram from the nationwide loadometer survey, as used in Fisher (14), is shown along the ordinate of Figure 4 [see also Fisher (14), Figure 25)]. For loading case 1 and ADTT = 2500, AASHTO specifies that a category E detail be designed to the hypothetical point e in Figure 4 and for N_d (AASHTO) = 2 000 000 cycles of the allowable stress range F_{sr} = 8 ksi (55 MPa). The αF_{sr} = 4 ksi (28 MPa) stress range corresponds to one 72 000-lbf (320-kN) truck on a bridge designed for one traffic lane. The $f_{re} = \alpha\rho F_{sr}$ = 2.8 ksi (19 MPa) stress range corresponds to one (ρ • 72 000) = 50 760-lbf (226-kN) fatigue truck on a bridge designed for one traffic lane (15, Table 5). The actual number of cycles for a 50-year design life is N_d = 2500 trucks/day x 365 days x 50 years = 45 625 000 cycles. The actual design point (d) has therefore the coordinates f_{re} = 2.8 ksi and N_d = 45 625 000 cycles. That the actual design point (d) also lies on the load curve at $2s_R$ to the left of the resistance follows from the identities:

$$(F_{sr}/f_{re})^m = [1/(0.5 \times 0.705)]^3 = 22.83 \quad (25)$$

$$N_d/[N_d(\text{AASHTO})] = 45\,625\,000/2\,000\,000 = 22.81 \quad (26)$$

Equations 25 and 26 reflect the geometrical relation that the slope times the rise must equal the flat of the log-log linear design S-N line.

Evidently, the intentional mismatch between the AASHTO number or cycles of F_{sr} stress range and the actual number of cycles of f_{re} stress range means that the AASHTO specifications apply, in reality, to one traffic lane loaded by a single fatigue truck. The fatigue design to the hypothetical point e is mathematically identical to a design to the actual point d. This conclusion is illustrated in Figure 4 for a category E detail, but it holds equally true for all other categories.

The horizontal distance between the failure point (f) and the actual point (d) is therefore $2s_R$. Substituting this value into Equation 16 gives the safety index for main longitudinal load-carrying members in RLP structures designed for ADTT = 2 500, i.e.,

$$\beta = 2s_R/s_r \quad (27)$$

Note again that neglecting load variability implies that $s_Q' = 0$ and leads to $\beta = 2$, as in Equation 23. AASHTO requires that "members shall also be investigated for over 2 million stress cycles produced by placing a single truck on the bridge distributed to the girders as designated in Article 1.3.1(B) for one traffic lane loading" (1). (The distribution factor for one traffic lane loading is

S/7.) This requirement lowers the hypothetical design point in Figure 4 from e to e_1 and the actual design point from d to d_1. It increases the numerator of Equation 27 from the distance d-f to d_1-f_1. The safety index for more than 2 million cycles is then given by

$$\beta = (1/s_T)\left\{2s_R + m \cdot \log [F_{sr}(2 \times 10^6)/F_{sr}(\text{over } 2 \times 10^6)]\right\} \quad (28)$$

in which the allowable stress ranges for 2 million cycles and over 2 million cycles are read from AASHTO Table 1.7.2A1 (1) for RLP structures. There is really no need to check both loading conditions for every design, since the one that governs can be determined a priori. The condition for 2 million cycles of loading always governs for categories A, B, and C* because $[F_{sr}(2x10^6)/F_{sr}(\text{over } 2x10^6)] < [(S/5.5)/(S/7)]$. The condition for over 2 million cycles always governs for categories C, D, E, and E' because $[F_{sr}(2x10^6)/F_{sr}(\text{over } 2x10^6)] > [(S/5.5)/(S/7)]$. Hence, Equation 27 always applies to categories A, B, and C*, and Equation 28 applies to categories C, D, E, and E'. Both are in reality for single truck loading; the former with a distribution factor $\alpha(S/5.5) = S/11$, as shown previously, and the latter with $\alpha(S/7) = S/14$. The double-check requirement is superfluous and leads to inconsistent failure probabilities.

The numerical evaluation of Equations 27 and 28 was carried out for all categories. The values of s_R and m needed to calculate s_T with Equation 15 are listed in Table 1. Lacking variability information for fatigue truck weights, the standard deviation of the load was set equal to the standard deviation of the equivalent stress ranges that were obtained from 104 histograms recorded on 29 bridges in eight states [s_Q' = 0.0492 (13)]. The allowable stress ranges for main longitudinal load-carrying members in RLP structures were taken from AASHTO Table 1.7.2A1 (1). The calculated safety indices and failure probabilities are shown in the left part of Table 2. The results reveal extreme variations in failure probability, which range from a high of $P_F = 9.2x10^{-2}$ for category B to a low of $P_F = 9.2x10^{-8}$ for category E'.

NRLP Structures

Failure probabilities of main longitudinal load-carrying members in NRLP structures can be calculated in a similar manner. Again, the condition for 2 million cycles of loading always governs for categories A, B, and C*, for which the safety index is as follows:

$$\beta = (1/s_T)\left\{2s_R + m \cdot \log [F_{sr}(2 \times 10^6; \text{RLP})/F_{sr}(2 \times 10^6; \text{NRLP})]\right\} \quad (29)$$

The condition for over 2 million cycles of loading always governs for categories C, D, and E that have a safety index of

$$\beta = (1/s_T)\left\{2s_R + m \cdot \log [F_{sr}(2 \times 10^6; \text{RLP}) \div F_{sr}(\text{over } 2 \times 10^6; \text{NRLP})]\right\} \quad (30)$$

The results, shown to the right in Table 2, reveal once more extreme variations in failure probability, from a high of $P_F = 5.1x10^{-2}$ for category A to a low of $P_F = 2.1x10^{-22}$ for category E. Note also that the failure probabilities for category A, B, and C* details on NRLP structures exceed the failure probabilities for category C, D, E, and E' details on RLP structures. The original intent of adding a table of F_{sr} values for NRLP structures had been to lower failure probabilities to less than those for RLP structures.

DESIGN EXAMPLE

This section illustrates with one example the second type of application, namely, the fatigue design of a detail for a desired failure probability. This type of example is not covered by the AASHTO specifications. Additional examples are presented in Albrecht (2).

Problem

A one-lane bridge consists of two plate girders and a concrete deck. It is located on a private access road from an ore concentrating plant to the mine. The trucks cross the bridge empty on the way to the mine and full on the way back to the plant. The net vehicle weight (NVW) and gross vehicle weight (GVW) are NVW = 40 kips (178 kN) and GVW = 140 kips (625 kN). Because all other vehicles weigh much less than the empty ore truck, their contribution to fatigue damage is neglected. About 150 daily round trips will keep the plant working at full capacity. At that rate, all ore will be mined in 12 years. Because the bridge has low clearance, crosses a shallow river, and serves no public roads, a low safety index of $\beta = 3$ ($P_F = 1.35x10^{-3}$) is assumed. Compute the allowable stress range for the category B flange-to-web weld.

Solution

The load- and resistance-curve data are determined and substituted into Equation 18. Its solution yields the allowable stress range for the specified number of loading cycles (see Figure 5).

1. The load-curve data for vehicle weights and frequencies are as follows:

$\phi_{NVW} = 40/140 = 0.286$; $\gamma_{NVW} = 0.5$.

Table 2. Fatigue failure probabilities for main longitudinal load-carrying members designed for ADTT = 2500.

		RLP Structures				NRLP Structures			
	Standard Deviation of $\bar{R} - \bar{Q}$[a]	2 Million Cycles		Over 2 Million Cycles		2 Million Cycles		Over 2 Million Cycles	
Category	(s_T)	β[b]	P_F	β[c]	P_F	β[d]	P_F	β[e]	P_F
A	0.2707	1.633	5.1×10^{-2}	-	-	1.633	5.1×10^{-2}	-	-
B	0.2217	1.326	9.2×10^{-2}	-	-	2.104	1.8×10^{-2}	-	-
C*	0.2195	1.440	7.5×10^{-2}	-	-	1.930	2.7×10^{-2}	-	-
C	0.1718	-	-	2.887	1.9×10^{-3}	-	-	3.752	8.8×10^{-5}
D	0.1857	-	-	3.725	9.5×10^{-5}	-	-	6.141	4.1×10^{-10}
E	0.1825	-	-	4.564	2.5×10^{-6}	-	-	9.669	2.1×10^{-22}
E'	0.2501	-	-	6.012	9.2×10^{-10}	-	-	-	-

[a] Equation 15. [b] Equation 27. [c] Equation 28. [d] Equation 29. [e] Equation 30.

Figure 5. Design example.

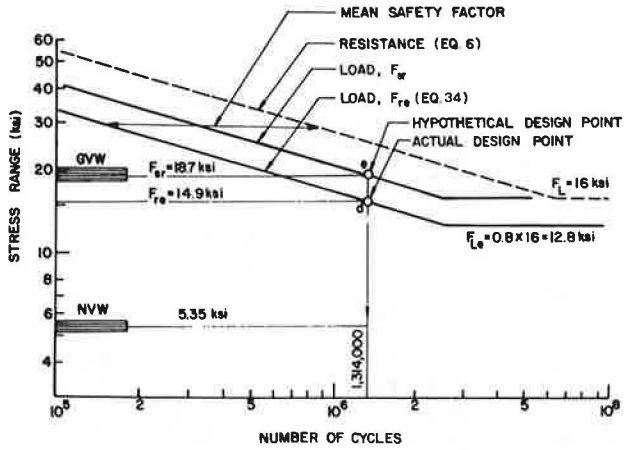

$\phi_{GVW} = 140/140 = 1.0$; $\gamma_{GVW} = 0.5$.

Then substitute into Equation 4; i.e.,

$$\rho = [0.5(0.286)^3 + 0.5(1.0)^3]^{1/3} = 0.80 \quad (31)$$

For a one-lane bridge assume that $\alpha = 1.0$. A 15 percent coefficient of variation (C = 0.15) is estimated for the equivalent truck weight, so that

$$s'_Q = \sqrt{0.4343 \log_{10}(1 + C^2)} = 0.0648 \quad (32)$$

2. Resistance-curve data for category B, which are taken from Table 1, are as follows: b = 10.870, m = 3.372, and $s_R = 0.147$.

3. The design equations (Equations 15 and 19) are as follows:

$$s_r = \sqrt{(0.147)^2 + (3.372 \times 0.0648)^2} = 0.2634 \quad (33)$$

$$N_d = 10^{(10.870-3\times0.2634)}/F_{re}^{3.372} = (12.0 \times 10^9)/F_{re}^{3.372} \quad (34)$$

4. The number of loading cycles is as follows:

$$N_d = (2 \times 150 \text{ trips})(365 \text{ days})(12 \text{ years}) = 1\,314\,000 \text{ cycles} \quad (35)$$

5. The allowable stress range for a design based on equivalent truck weight is

$$F_{re} = [(12.0 \times 10^9)/(1.314 \times 10^6)]^{1/3.372} = 14.9 \text{ ksi (103 MPa)} \quad (36)$$

and for a design based on GVW is

$$F_{sr} = F_{re}/\rho\alpha = 14.9/(0.80 \times 1.0) = 18.7 \text{ ksi (129 MPa)} \quad (37)$$

6. Check the fatigue limit; i.e.,

$$f_r(\text{GVW}) = 18.7 \text{ ksi} > F_L = 16 \text{ ksi (110 MPa)} \quad (38)$$

Therefore, fatigue must be checked.

7. The safety factor on life, which is taken from Equation 20, is as follows:

$$(\text{F.S.})_{N_d} = 10^{(3\times0.2634)} = 6.2 \quad (39)$$

The results of the previous calculations are shown in Figure 5. The histogram is plotted along the ordinate. The upper and lower load lines are for designs to F_{sr} and F_{re}, respectively. Both give analogous results, since the two lines are shifted by the ratio $\alpha\rho = F_{re}/F_{sr}$. The safety factor on life is the horizontal distance between the resistance curve and the F_{re} load curve.

CONCLUSIONS AND RECOMMENDATIONS

A method of calculating fatigue failure probabilities based on the S-N approach was presented in a form suitable for examining designs to current fatigue specifications and for performing designs to any desired level of risk. The method is general. It was illustrated here in detail for highway bridges. The main findings were as follows:

1. The design for the AASHTO number of cycles of maximum stress range (F_{sr}) calculated for multiple HS-20 trucks with a distribution factor for two or more traffic lane loadings (S/5.5) is mathematically identical to the design for the actual number of single fatigue trucks with a distribution factor of S/11.

2. The dual requirement to check all case 1 designs for 2 million cycles with S/5.5 and for over 2 million cycles with S/7 is superfluous because the former always governs for categories A, B, and C*, and the latter always governs for categories C, D, E, and E'. It is also inconsistent because both are, in reality, for single fatigue truck loading. But the former is for a higher stress range with an actual distribution factor α(S/5.5) = S/11, while the latter is for the fatigue limit with an actual distribution factor α(S/7) = S/14.

3. The failure probabilities lack uniformity. For RLP structures, they vary from a high of $P_F = 9.2\text{x}10^{-2}$ for category B to a low of $P_F = 9.2\text{x}10^{-10}$ for category E'. For NRLP structures they vary from a high of $P_F = 5.1\text{x}10^{-2}$ for category A to a low of $P_F = 2.1\text{x}10^{-22}$ for category E.

4. The failure probabilities for category A, B, and C* details on NRLP structures are higher than those for category C, D, E, and E' details on RLP structures. This violates the intent of the requirements for NRLP structures.

There are dangers of either giving too much credence to the accuracy of calculated failure probabilities or of dismissing the results out of hand because of unavoidable uncertainties and a lack of data. The most important benefit is the ability to compare the values relative to each other.

The pressing need for specifications that are based on uniform failure probabilities mandates that AASHTO choose two values, one for RLP and one for NRLP structures. Thereafter, allowable stress ranges can be derived with methods such as the one outlined here. This need alone calls for a revision of the current specifications. In addition, AASHTO should consider the following points, which have also been made by other investigators in the past:

1. Define the allowable stress range as a continuous function of truck traffic volume instead of the step function approach by loading case in Table 1.7.2B (1).

2. Explicitly formulate the fatigue specifications in terms of the actual number of single fatigue trucks, each of which cause an equivalent stress range, instead of a hypothetical number of HS-20 design trucks that cause the maximum stress range.

3. Examine what impact the distribution factors would have on the fatigue specifications if they were expressed in terms of number of girders and lanes instead of girder spacing.

REFERENCES

1. Standard Specifications for Highway Bridges, 12th ed. AASHTO, Washington, DC, 1977.

2. P. Albrecht. Analysis of Fatigue Reliability. Univ. of Maryland, College Park, Civil Engineering Rept., Jan. 1981.
3. T.V. Galambos. Proposed Criteria for Load and Resistance Factor Design of Steel Building Structures. Civil Engineering Department, Washington Univ., St. Louis, Res. Rept. 45, May 1976.
4. J.W. Fisher, K.H. Frank, M.A. Hirt, and B.M. McNamee. Effect of Weldments on the Fatigue Strength of Steel Beams. NCHRP, Rept. 102, 1970.
5. J.W. Fisher, P.A. Albrecht, B.T. Yen, D.J. Klingerman, and B.M. McNamee. Fatigue Strength of Steel Beams with Welded Stiffeners and Attachments. NCHRP, Rept. 147, 1974.
6. P. Albrecht and S. Simon. Fatigue Notch Factors for Structural Details. Journal of the Structural Division, ASCE, July 1981.
7. J.W. Fisher, H. Hausammann, and A.W. Pense. Retrofitting Procedures for Fatigue Damaged Full-Scale Welded Bridge Beams. Fritz Engineering Laboratory, Lehigh Univ., Bethlehem, PA, Rept. 417-3(79), Jan. 1979.
8. P.A. Albrecht and I.M. Friedland. Effect of Fatigue Limit on Variable Amplitude Cyclic Behavior of Stiffeners. Journal of the Structural Division, ASCE, Dec. 1979.
9. K. Yamada and P. Albrecht. Fatigue Design of Welded Bridge Details for Service Stresses. TRB, Transportation Research Record 607, 1977, pp. 25-30.
10. P. Albrecht and K. Yamada. Simulation of Service Fatigue Loads for Short-Span Highway Bridges. In Service Fatigue Loads Monitoring, Simulations, and Analysis, ASTM, Philadelphia, Special Tech. Publ. 671, 1979.
11. Interim Specifications--Bridges. AASHTO, Washington, DC, 1980.
12. P. Albrecht. Fatigue Behavior of 4-Year Weathered A588 Steel Specimens with Stiffeners and Attachments. Department of Civil Engineering, Univ. of Maryland, College Park, Rept. FHWA/MD-81/02, July 1981.
13. K. Duerling. Guidelines for Variable Amplitude Fatigue Design Based on Reliability. Univ. of Maryland, College Park, M.Sc. thesis, 1978.
14. J.W. Fisher. Bridge Fatigue Guide. American Institute of Steel Construction, New York, 1977.
15. Recommended Design Loads for Bridges. Journal of the Structural Division, ASCE, July 1981.

Publication of this paper sponsored by Committee on Concrete Bridges.